UNIVERSITY OF
BIRMINGHAM

Investigation of Functional-Dependencies Between PG Hydrolases and The Bifunctional Class A PBPs Across Stress Conditions in *E. coli*

By

DEMA ALODAINI

A thesis submitted to the University of Birmingham for the degree of

DOCTOR OF PHILOSOPHY

Institute of Microbiology and Infection School of Biosciences

College of Life and Environmental Sciences

University of Birmingham

September 2023

Abstract.

Gram-negative bacteria possess a slender peptidoglycan layer, known as sacculus, positioned between the cytoplasmic and outer membrane. This layer serves as protection against osmotic challenges. Peptidoglycan hydrolases play a crucial role in breaking bonds within the sacculus to facilitate the insertion of newly synthesized peptidoglycan strands. The precise regulation of peptidoglycan synthases and hydrolases is essential to prevent cell lysis, but to date we do not know the detailed molecular mechanism how PG synthases and hydrolases coordinate their activities. To study this, we investigated the genetic interactions of the two PG synthases *mrcA* (encodes PBP1A) and *mrcB* (encodes PBP1B) with genes encoding for peptidoglycan amidases and endopeptidases under various envelope stress conditions. Our comprehensive analysis of the genetic interaction network revealed only a limited number of hydrolase gene deletions that led to reduced fitness in the absence of PBP1A or PBP1B. This suggests that none of the amidases or endopeptidases is strictly indispensable for the functioning of class A PBPs, highlighting the robustness of the peptidoglycan growth mechanism. Notably, we observed a significant decrease in the fitness of Δ*mrcB* cells under high salt stress. This reduction was attributed to the diminished peptidoglycan synthesis activity of PBP1A at elevated salt concentrations, underscoring the impact of environmental conditions on bacterial cell fitness.

We also present an approach that utilizes peptidoglycan sacculi labelled with fluorescein-5-isothiocyanate (FITC) to analyze PG hydrolases under controlled laboratory conditions. Within this procedure, we isolate soluble hydrolytic byproducts released by PG hydrolases from the non-soluble FITC-PG sacculi. These byproducts are then measured and set in relation to the total available substrate. This method allows to assay PG hydrolase activity through end-point or

time-course assays. Here we assess the amount of fluorescence released from covalently-linked FITC-PG as a result of amidases hydrolytic activity in the presence of two distinct proteins (NlpI and DolP) using optimized FITC release assay to accommodate a 96-well format and compare their activity to a control Lysozyme. However, our analysis suggests that NlpI indirectly impacts AmiA/AmiC activation via amidases regulators EnvC and NlpD, meanwhile DolP is likely not to be NlpD upstream regulator but might function indirectly through yet undiscovered mechanism.

Dedication.

I would like to dedicate this thesis to my parents, husband, and siblings, who supported me all the way during this journey.

To my son, who made each day brighter since his arrival.

And to friends I found along the way.

Acknowledgements.

I would like to acknowledge my supervisor, Dr. Manuel Banzhaf, and his efforts to provide a great environment for personal and professional growth. Can not thank you enough for your patience and guidance during this journey.

Thanks to every member of Banzhaf group, Dr. Patrick Moynihan group, and Prof Waldemar Vollmer for helping me in different ways during our collaborations.

Thanks to my sponsors, Imam Abdulrahman Bin Faisal University and the Saudi Arabian Cultural Mission (SACM) for their generous support along this journey.

Thanks to my country, Kingdom of Saudi Arabia.

Table of contents **Page**

List of figures **Page**

List of tables.

List of abbreviations.

APC - ATP-binding cassettes.

BAM - β-barrel-assembly machinery.

CPase – carboxypeptidase.

Dcw - division and cell wall.

EPase - endopeptidase.

FRET - fluorescence resonance energy transfer.

Fts - filament temperature sensitive.

GTase - glycosyltransferase.

HMW - high molecular weight.

IF - intermediate filament.

IM - Inner membrane.

LTA - lipoteichoic acids.

LPS – lipopolysaccharides.

LMW - low molecular weight.

LT - lytic transglycosylase.

MIC - minimal inhibitory concentration.

MST - MicroScale Thermophoresis.

OM - Outer membrane.

OMP - Outer membrane protein.

PBP - penicillin-binding proteins.

PCR - Polymerase Chain Reaction.

PG - Peptidoglycan.

SDS - sodium dodecyl sulphate.

SDS-PAGE - SDS-polyacrylamide gel electrophoresis.

SEDS - shape, elongation, division and sporulation.

TA - teichoic acids.

TEMED - tetramethyl-ethylenediamine.

TPase – transpeptidase.

WTA - wall teichoic acid.

WT - wild-type.

Chapter 1. General Introduction.

1.1 Why do we study bacterial growth?

In 1684, Leeuwenhoek became interested in observing the cilia of Vorticella using a microscope of his own creation. Shortly afterwards Winogradsky and his colleagues studied the chemical changes in the environment caused by microbial activities. In the early 20th century, the physiology of microbes was an essential contributor to the biochemistry field, playing a major role in understanding the central metabolism of life. Many scientists focused on the microbial ability to grow, like Raulin (1869), who carried out endless experiments on the mold *Aspergillus niger* (Zervosen et al., 2004). His work revealed its ability to simply grow in media supplemented with just sugar and mineral salts. Even Pasteur believed that microbial morphology/activities are conditioned by the surrounding environment. Later, two other scientists who were referred to as the "fathers of molecular biology", Alfred Hershey (1930's) and Jacques Monod (1940's), who were interested in understanding the dynamics and molecular mechanisms of microbial growth. Experiments of Hershey (Hershey, 1939) reported the use of bacterial culture growing in the log phase as an inoculum to initiate a new culture. Monod (Monod, 1958) redefined the growth response of entire cultures by associating it with enzyme kinetics (growth rate was dependent on substrate concentration) (Schaechter, 2015).

Bacterial cells were classified by Hans Christian Gram in 1884 into two groups, Gram-positives and Gram-negatives (based on their reaction to crystal violet, also referred to as Gram stain). To date, it remains an essential classification, as it provides information about the bacterial cell walls gross structure (Amir et al., 2019).

Despite the huge impact of microbes for our planets ecology we still do not understand all aspects of bacterial growth. Therefore, research into the physiology of microbial growth still continues and is guided by the continuous development of new experimental tools and mathematical analysis. In the past, these methods helped clarify and answer questions, such as how microbes grow and divide, or to describe the needed cellular components needed for bacterial growth. In my thesis, I aim to utilize molecular biological tools to study how bacterial peptidoglycan hydrolases and synthases work together to enable Gram-negative bacteria to grow without lysing.

1.2 The bacterial cell envelope.

Bacterial cells are faced with an unpredictable hostile environment. To survive, bacteria evolved a sophisticated mesh-like cell envelope. Bacteria are classified into two large groups, Gram-positive and Gram-negative, based on how their cell walls can be stained by Gram stain crystal violet (Gram, 1884).

Gram-positive bacteria consist of two layers (thick PG cell wall and cytoplasmic membrane) and they lack an OM. To withstand the environmental pressure, Gram-positive bacteria are surrounded by layers of PG many times thicker than Gram-negative organisms (Neuhaus & Baddiley, 2003). Threading through PG layers are long anionic polymers named teichoic acids (TAs), composed of glucosyl phosphate, glycerol phosphate, or ribitol phosphate repeats. Two classes of these polymers are the wall teichoic acids (WTA) and Lipoteichoic acids (LTA).

The wall teichoic acids are attached covalently to peptidoglycan, whereas the lipoteichoic acids are attached to glycolipids embedded within the cell membrane (Dramsi et al., 2008; Neuhaus & Baddiley, 2003; Vollmer et al., 2008). Collectively, all these polymers can make up to 60% of Gram-positive cell wall mass and generate a polyanionic matrix (network) that contributes to functions related to cell elasticity, porosity, and more. The chemical structure of Gram-positive PG is composed of disaccharide-peptide repeats attached via glycosidic bonds forming linear glycan stands, that are crosslinked into mesh-like structure via peptide stems connected to the disaccharide repeats (Vollmer et al., 2008).

The envelope structure of Gram-negative bacteria is a cell-shape key determinant that confers the necessary protection to withstand environmental stresses and occupying a position between the cell and its surrounding environment. Gram-negative envelope possess the inner (cytoplasmic) membrane (IM), the outer membrane (OM), and peptidoglycan cell wall in the periplasmic space sandwiched between the IM and the OM (**Figure 1**) (Fivenson et al., 2023). All the following sections from now on will focus on Gram-negatives bacteria.

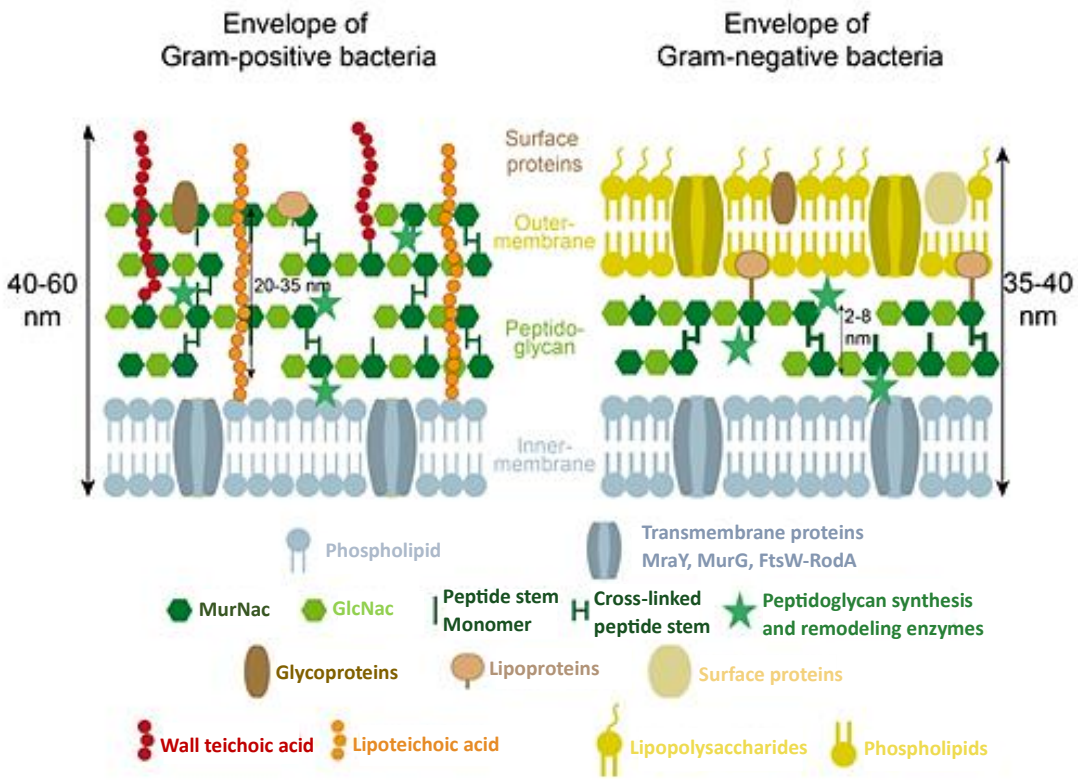

Figure 1: Schematic organization of bacterial cell envelope main components (Silhavy et al., 2010). Cell envelope compositions in Gram-positive bacteria (PG thickness: multilayered 20-80 nm, teichoic acid: present, lipoteichoic acid: present, LPS: absent, periplasmic space: absent, lipoprotein & lipid cell envelope contents: low) are different from Gram-negative bacteria (PG thickness: single layered 5-10 nm, teichoic acid: absent, lipoteichoic acid: absent, LPS: present, periplasmic space: present, lipoprotein & lipid cell envelope contents: high).

1.2.1 The outer membrane.

The OM bilayer is a feature of Gram-negative bacteria (not found in Gram-positive bacteria. This membrane's inner leaflet contains phospholipids (phosphatidylglycerol, phosphatidylethanolamine, and cardiolipin) and an outer leaflet composed of

lipopolysaccharide (LPS) (Amir et al., 2019; Fivenson et al., 2023). LPS is classified as an endotoxin which elicits individual's immune response (endotoxic shock) due to septicaemia as result of a Gram-negative infection. Along with providing a protective barrier, the OM can help bacterial cells to resist internal turgor pressure (Fivenson et al., 2023).

The OM possesses lipoproteins and β-barrel proteins (Silhavy et al., 2010). Lipoproteins help staple the OM to the underlying peptidoglycan. Many chromosomally encoded OM lipoproteins were identified in *E. coli,* and despite their differences, they share the common feature of attachment to the outer or inner membrane. This attachment is governed by a common signal sequence, the "lipobox" (Leu(Ala, Val)$_{-4}$-Leu$_{-3}$-Ala(Ser)$_{-2}$-Gly(Ala)$_{-1}$-Cys$_{+1}$ (Waxman & Strominger, 1983). The lipobox contains a cysteine residue, the signature component of bacterial lipoproteins responsible for lipid attachment.

The β-barrel proteins form a structure that is inserted into the OM layer through a periplasmic-chaperone BAM system (Booth et al., 2021). The β-barrel-assembly machinery (BAM) is required for the assembly of outer-membrane-proteins (OMPs) found in the outer membrane of Gram-negatives. OMPs is one type of the integral membrane proteins, along with the α-helical membrane proteins (Onufryk et al., 2005). BAM consists of a five-protein complex, responsible for the proper folding and accurate insertion of nascent OMPs in cell's outer membrane (Fleming, 2015). The first step of OMP biogenesis is the synthesis of OMP substrates in the cytoplasm (Mamou et al., 2021; Wu, 2022). Next, these substrates are translocated via the Sec translocon across the cytoplasmic membrane. With the help of chaperones, OMP substrates are escorted to the inner side of the outer membrane by BAM

complex (Danese & Silhavy, 1998; Wu et al., 2005). The complex comprises of BamA (an integral OMP) and four lipoproteins (BamB, BamC, BamD, and BamE) (Gu et al., 2016; Han et al., 2016; Noinaj et al., 2015).

In addition, the OM layer is punctuated by porins that act as highly selective channels to facilitate the entrance of specific size hydrophilic substrates into the periplasm (Alva et al., 2020). For instance, these channels regulate permeability of the β-lactam antibiotics (more details are found in section **1.3**). As one of main mechanisms, bacterial β-lactam resistance is usually observed to decrease influx through porins (Benz, 2006).

1.2.2 Inner membrane.

The bacterial inner membrane is composed of proteins and a phospholipid bilayer. The phospholipid bilayer is very rich in phosphatidylglycerol, phosphatidylethanolamine, and cardiolipin (Corey et al., 2021). Cytoplasmic membrane is hydrophobic by nature, and it functions as a barrier to enclose the cellular contents and prevents leakage of cellular components and nutrients (Hughes et al., 2019).

In order to survive, bacteria need effective and constant communication within their environment. For that, the bacterial cell evolved various mechanisms to respond to external effector/stimuli and has different transport proteins to import essential nutrient (Luirink et al., 2005). Hereby the cytoplasmic membrane serves in several crucial functions, like electron transport, translocation of proteins across the membrane, chemotaxis, motility, lipid

synthesis, chromosome segregation, and cell division. It is semi-permeable and allows the passage of molecules like oxygen and water (but not electrolytes) across the membrane. One of the well-studied mechanisms to translocate proteins over the cytoplasmic membrane is the *sec* system (Hughes et al., 2019), which involves SecB chaperone, SecA (the ATPase), and membrane channel consisting of SecYEG and supporting proteins such as SecDE (De Gier & Luirink, 2001). The system utilizes ATP for proteins translocation through the membrane by ratchet-like mechanism (Crane & Randall, 2017; Sanganna Gari et al., 2019). The recruited proteins are; I) addresses to this pathway by a signal sequence at the N-terminus, II) traverse the membrane in an unfolded state, and then III) the leader peptide will be cleaved by peptidase (Auclair et al., 2012; Luirink et al., 2005).

1.2.3 Peptidoglycan cell wall.

The PG cell wall is located in the periplasmic space between the inner and outer membranes and serves to uphold an outstanding amount of osmotic pressure created by cytoplasmic solutes (Lutkenhaus et al., 2012). The periplasmic space is almost 15 nm wide and is a multipurpose compartment heavily packed with hydrolytic enzymes, chaperon-like molecules (function in envelop biogenesis), chemoreceptor for chemotaxis, and the periplasmic binding proteins (participates in the transport of sugar and amino acid through the ATP-binding cassette system) (Booth et al., 2021). PG is composed of long rigid strands of glycans crosslinked by peptides, forming a mesh-like sacculus. Electron micrograph of rod-shaped bacteria sacculi suggested that these strands are arranged in 'hoops' that extend

perpendicular to the cell's longitudinal axis (Höltje, 1998; Meeske et al., 2016; Rohs et al., 2018). The linear glycan strands are composed of rigid polymers of β-1,4-linked N-acetylglucosamine (GlcNAc) and N- acetylmuramic acid (MurNAc) disaccharide units in which the D- lactoyl of each MurNAc is attached covalently to the first amino acid of the peptide chain. Peptide chains in *E. coli* are made up of five amino acids (pentapeptides) that has a sequence as follows: L-Ala-D-Glu-*m*-Dap-D-Ala-D-Ala (*m*-Dap, *meso*-diaminopimelic acid) (Schleifer & Kandler, 1972).

Peptidoglycan synthesis takes place in two different cellular compartments: first, in the cytosol, and then, in the periplasm. In the cytosol, the UDP-MurNAc-pentapeptide is synthesized by a series of enzymatic reactions (MurA, -B, -C, -D, -E, and –F) to generate lipid I (**Figure 2**). After that, by adding an UDP-GlcNAc molecule, lipid II is formed and ready to flip across the cell inner membrane to reach the periplasm (more details are found in **1.5** section), where other PG synthases will act (Egan et al., 2015; Typas et al., 2010).

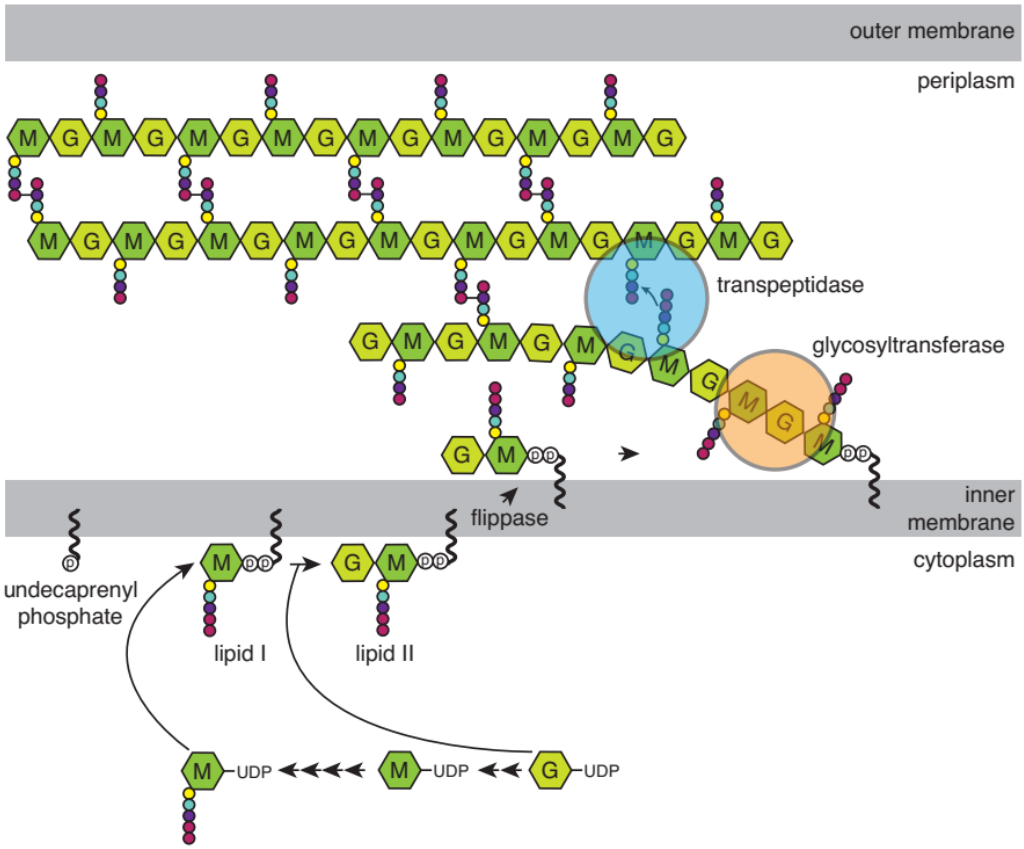

Figure 2. Illustrating model of peptidoglycan synthesis in *E. coli* (Truong, 2020). PG synthesis needs the coordination of a number of proteins and begins with synthesizing PG precursors within the cytoplasm. G = N-acetylglucosamine; M = N-acetylmuramic acid. The UDP-G will be converted to UDP-M by MurAB. An amino acid side chain will then be added to UDP-M catalyzed by MurCEDF (sequential addition of the colored peptide stem: L-Ala, D-Glu, *meso-Dap*, and two D-Ala). The newly formed UDP-M-pentapeptide will be anchored to the IM by MraY to create Lipid I. A UDP-G moiety will bind to Lipid I (glycosidic bond) by MurG to form Lipid II (the building block of PG). Lipid II flips across the IM to reach the periplasm by MurJ and will be incorporated into the newly synthesized PG chain by PBP transglycosylase activity. PBP transpeptidases will then crosslink D-Ala of one pentapeptide to *meso*-Dap of an opposing pentapeptide.

1.2.3.1 Peptidoglycan synthases.

1.2.3.1.1 Penicillin-binding proteins (PBP).

Peptidoglycan synthases are periplasmic enzymes that synthesize new peptidoglycan strands to be attached later to the existing peptidoglycan sacculus. Sacculus growth regulated by a repertoire of these synthases, including the glycosyltransferases (GTase) to polymerize glycan strand from lipid II, and transpeptidases (TPase) for peptide cross-linking between adjoining glycan strands (Typas et al., 2010).

A group of synthases called penicillin-binding proteins (**Table 1**), a set of IM proteins defined by their affinity to bind β-lactam antibiotic penicillin (more details are found in **1.3** section) and involved in latter stages of PG synthesis (Sauvage et al., 2008). PBPs polymerize glycan strands based on two machines of cell wall synthesis. First, the elongasome (the Rod complex) (more details are found in **1.5.1** section) polymerizes PG across the cell cylinder to direct cell elongation. Second, the divisome (**1.5.2** section) during cytokinesis synthesizes PG to generate the cell poles (Matteï et al., 2010) *E. coli* possesses high-molecular weight (HMW) PBPs (> 45 kDa) with either bifunctional (Class A: have both GTase and TPase, e.g., PBP1A, PBP1B, and PBP1c) or monofunctional (Class B: have TPase, e.g. PBP2 and PBP3) activities (Sauvage et al., 2008; Spratt, 1975).

HMW are multi-modular PBPs involved in PG polymerization, as well as insertion into cell wall (Born et al., 2006; Goffin & Ghuysen, 1998). Depending on HMW N-terminal domain structure and catalytic activity, HMW can be classified as either class A or B PBPs. The C-terminal of both classes possesses a TPases activity, to incorporate nascent strands into PG existing meshwork.

N-terminal domain of class A is responsible for catalyzing elongation of uncross linked glycan strand by GTase activity (**Figure 3**).

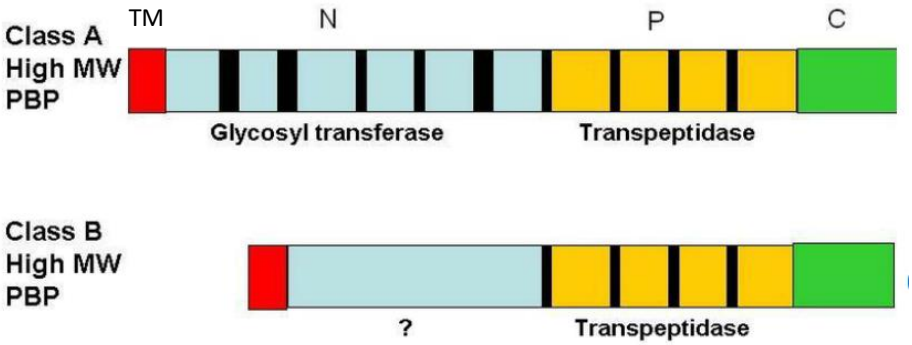

Figure 3. The structural compositions of high molecular weight PBPs in class A and class B (Xue, 2008). Class A and B high MW PBPs consist of TM (transmembrane anchor, depicted in red), N (blue), P (orange), and C (green) domains. The N domain encodes glycosyl transferase, while the P domain serves as a transpeptidase. The functional role of the N-terminal domain in class B PBPs remains unexplored. In contrast, low MW PBPs feature a singular P domain, which houses either carboxypeptidase or endopeptidase activity. The conserved sequences (depicted in black) within the P domain across all PBPs play a critical role in the active sites of each enzymatic activity, as well as serving as the target for penicillin.

There are also the monofunctional GTase (MtgA), which catalyze uncross-linked glycan strand formation in *E. coli*, but they are less well understood (Terrak & Nguyen-Disteche, 2006). The monofunctional GTase domain shares high sequence similarities with class A PBPs GTase domain (Derouaux et al., 2008).

The two major class A PBPs are PBP1A and PBP1B, that participate in elongation and division, respectively. Likewise, the two major class B PBPs are PBP2 and PBP3, that are important for the elongasome (more details are found in **1.5.1** section) and the divisome (**1.5.2** section), respectively (Banzhaf et al., 2012; Typas et al., 2010). In *E. coli*, class A PBPs require interactions with LpoA (YraM) and LpoB (YcfM) (for lipoprotein activator of PBP from the OM A and B) to activate their GTases and TPases by affecting distinct domains. Interestingly, Lpo activation of one domain of PBP1A/1b enhances the activation of the other domain (Tania J Lupoli et al., 2014), indicating that domains activities are coupled. Domain coupling/activation could provide alternative strategies to disable PG synthesis machinery.

Protein	Gene	Function	Enzymatic action	Reference
PBP1a	*mrcA*	D,D transpeptidase and transglycosylase	Addition of lipid II to newly synthesized stands and crosslinking into existing PG	(Paradis-Bleau et al., 2010; Typas et al., 2010) (Boes et al., 2019)
PBP1b	*mrcB*			
PBP2	*mrdA*	D, D transpeptidase	Crosslinks nascent PG strands into existing PG during cell elongation	(Özbaykal et al., 2020; Rohs et al., 2018)
PBP3	*FtsI*		Crosslinks nascent PG strands into existing PG during cell division	(Meeske et al., 2016; Spratt, 1975)
PBP4	*dacB*	D, D endopeptidases / carboxypeptidase	Involves in cell separation	(Heidrich et al. 2002, Priyadarshini et al. 2006)
PBP5	*dacA*	D, D carboxypeptidases	Maintain the uniform shape of *E. coli*	(Choi et al., 2023; Spratt, 1975)
PBP6	*dacC*	D, D carboxypeptidases	Maintain the uniform shape of *E. coli* in acidic pH	(Amanuma & Strominger, 1980; Choi et al., 2023)
PBP7	*pbpG*	D, D endopeptidases	Maintain the rod shape of PG sacculus in *E. coli*	(Nelson & Young, 2001; Romeis & Höltje, 1994)

Table 1. *E. coli* PG penicillin-binding proteins (PBPs) important for this thesis.

The bifunctional PG synthase PBP1A (encoded by *mrcA* gene) requires LpoA to stimulate its GTase activity *in vivo* (Sardis et al., 2021) and/or its TPases activity *in vitro* (Tania J Lupoli et al., 2014; Typas et al., 2010). Also, it was found that PBP1A has a small region between its GTase and TPase domain named the "outer membrane PBP1A docking domain" (ODD, the LpoA docking domain). LpoA has N-terminal domain adopts TPR- (tetratricopeptide repeat) -like fold, and a C-terminal domain involved in binding/activating PBP1A (Jean et al., 2014).

PBP1B (encoded by *mrcB* gene) also requires LpoB for its GTases activity (Paradis-Bleau et al., 2010) and/or TPases activity (Typas et al., 2010) *in vitro*. In addition to the TPase and GTase domains, PBP1B has a non-catalytic small UvrB domain two homolog (Pfam 14814) domain (UB2H, the LpoB docking domain) (Egan et al., 2015; Typas et al., 2010). LpoB has a flexible N-terminal domain followed by globular domain (binds with purified UB2H domain) (Sung et al., 2009). LpoB binding to PBP1B through large interface that includes multiple amino acids within both proteins (Egan et al., 2015) PBP1B-LpoB can support cell growth in the PBP1A-LpoA absence (Typas et al., 2010). Notably, PBP1B is also stimulated by FtsN (septal ring component) to subsequently facilitate the synchronization between PG synthesis and invagination of OM (Gray et al., 2015).

Independently of PBP1A/1b, LpoA and LpoB localize at sidewall of elongation cells, but might depend on FtsI (PBP3) and/or FtsZ (Typas et al., 2010). Deletion of one class A PBP is not lethal to bacterial cells (Denome et al., 1999; Meberg et al., 2001).

In addition to HMW, *E. coli* possesses seven LMW PBPs with endopeptidase (Epases)/carboxypeptidases (CPases) activities (**Table 1**). These LMW PBPs are involved in PG maturation, cell separation, and PG recycling (Typas et al., 2010; Vollmer & Holtje, 2004). PBP4 and PBP7 possess EPases to cleave cross-linked glycan strands and should be considered as hydrolases (more details are found in **1.2.3.2.2** section). The major CPases PBP5, is highly abundant enzyme and it only cleaves the D-Ala-D-Ala terminal bond, rendering the stem peptide inaccessible for transpeptidation (Spratt & Strominger, 1976). Also, both PBP6 and PBP6b are homologous to PBP5 and have similar activity by possessing a strict CPase. Lastly, AmpH is a PBP that catalyzes both DD-CPases and DD-Epases activities and associated with PG

recycling (González-Leiza et al., 2011; Vega & Ayala, 2006). The historic PBPs numbering is based on SDS-PAGE (sodium-dodecyl-sulfate-polyacrylamide gel electrophoresis) migration.

1.2.3.1.2 Shape, Elongation, Division, and Sporulation proteins (SEDS).

There are PG synthases that are essential to maintain growth that do not bind penicillin. The integral membrane proteins SEDS (Shape, Elongation, Division, and Sporulation) family is important for rod-shaped cells (Mueller et al., 2019; Taguchi et al., 2019; Vermassen et al., 2019) as they are PG polymerases play critical roles during cell elongation and division (more details are found in **1.5 – 1.5.2** sections) (Den Blaauwen et al., 2008; Emami et al., 2017; White et al., 2010). Both SEDS and PBPs are reported to work together generating different-purpose subcomplexes (Fraipont et al., 2011; Mercer & Weiss, 2002), and they are genetically-linked in different bacteria (Meeske et al., 2016). Many rod-shaped bacteria recruit two distinct multi-protein complexes, organized by cytoskeletal filaments, to orchestrate PG synthesis during their growth and division. The elongasome, also known as the Rod complex, facilitates cell elongation and is organized by the actin-like MreB protein (more details in **1.4**) (Li et al., 2022). This complex of SEDS-bPBP pair, consisting of RodA and PBP2, which collaborates to insert new glycan strands into the PG layer perpendicular to the cell's long axis (Fivenson et al., 2023). On the other hand, the divisome, or septal ring, utilizes a SEDS-bPBP pair formed by FtsW and FtsI (PBP3) to synthesize septal PG during cytokinesis. This process is organized by the Z ring, created by filaments of the tubulin-like FtsZ protein (Li et al., 2022). A comprehensive

understanding of the regulatory mechanisms governing the activities of RodA-PBP2 and FtsW-FtsI is imperative for unraveling the intricacies that control bacterial cell elongation and division.

1.2.3.2 Peptidoglycan hydrolases.

PG hydrolases are responsible for cleaving the existing sacculus to allow the newly synthesized peptidoglycan strands to be inserted without increasing the cell wall thickness (Egan et al., 2015), and achieving cell division by separation of the two daughter cells. The first hydrolase was discovered by the bacteriologist Sir Alexander Fleming in 1921 when he observed an “astonishing bacteriolytic elements” that caused cell lysis on a culture agar plate, in which he named “lysozyme” in 1922 (Fleming, 1929). This hydrolytic enzyme works on PG to cleave the β-(1-4)-glycosidic bond between N-acetylmuramic acid (MurNAc) and N-acetylglucosamine (GlcNAc) (Chipman et al., 1967). Lysozyme has been a model in protein biochemistry with well-recognized contribution in antimicrobial defense. In *E. coli*, there are at least 35 peptidoglycan hydrolases that have been identified and classified into 12 different families (van Heijenoort, 2011) (β-*N*-Acetylglucosaminidase NagZ, lytic transglycosylases, DD-carboxypeptidases, LD- carboxypeptidases, DD-peptidases, LD-transpeptidases, DD-endopeptidases, LD-endopeptidases, endoamidase MpaA, MurNAc-L-Ala amidases, L-Ala-D/L-Glu epimerase YcjG, D-Ala-D-Ala dipeptidase DdpX) based on their substrate specificity as described by van Heijenoort (van Heijenoort, 2011). The redundancy of hydrolases in *E. coli* led to questioning their respective roles in different aspects of PG metabolism. Studies up to 1995 have been reviewed (Höltje, 1995; Höltje & Schwarz, 1985;

Höltje & Tuomanen, 1991), and more recent works have focused on specific hydrolase families (Höltje, 1998; Nelson & Young, 2000; Park & Uehara, 2008; Scheurwater et al., 2008; Vollmer et al., 2008).

We focused our attention on some of *E. coli* hydrolases (MurNAc-L-Ala amidases, LD/DD-endopeptidases, DD-peptidases, and DD-carboxypeptidases) and their series of action (**Figure 4**) (Fenton et al., 2010; Rigden et al., 2003; Rios-Szwed et al., 2020; Vermassen et al., 2019). The classification of PG hydrolases is associated with the existence of conserved catalytic domains specific to these distinct enzymatic activities (Alcorlo et al., 2017).

A)

Function	Enzymatic action	Known Genes/Proteins in *E. coli*	Reference
Amidases	Peptide stem cleavage from glycan strand	AmiA, AmiB, AmiC	(Meisel et al., 2003; Vermassen et al., 2019; Vollmer, 2006)
D, D Endopeptidases	D-Ala-mDAP crosslink 3-4 cleavage	DacB, PbpG, MepS, MepM, MepH, MepA	(Park et al., 2020; Sjodt et al., 2020)
D, D Carboxypeptidase	D-Ala D-Ala 4-5 cleavage	DacA, DacC, AmpD	(Amanuma & Strominger, 1980; Choi et al., 2023; Spratt, 1975)
L, D Endo/ Carboxypeptidase	mDAP mDAP 3-3 cleavage	MepA	(Chodisetti & Reddy, 2019; Marcyjaniak et al., 2004; Voedts et al., 2021).
Lytic transglycosylase	Glycan stand breaking at GlucNac-MurNac (endo-lytic)	Slt70, MltA – MltE, MltG	(Höltje et al., 1975; Uehara et al., 2009; Dik et al., 2017; Heidrich et al., 2001)

B)

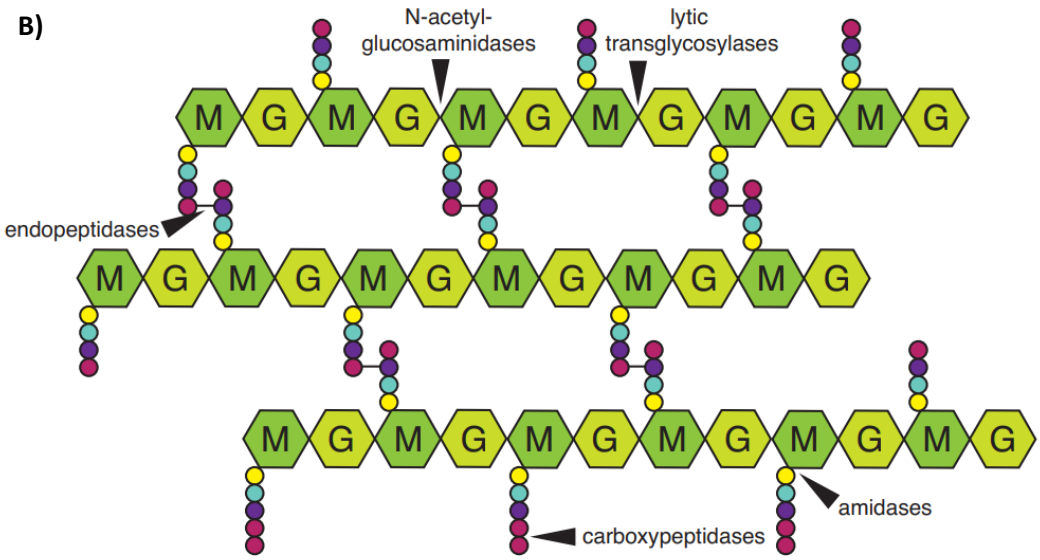

Figure 4. *E. coli* PG hydrolases and their linkage cleaving-site (Truong, 2020). *E. coli* has a repertoire of > 20 periplasmic hydrolases that show specificity to almost all PG bonds. **A)** Brief characterizations of PG Hydrolases in *E. coli*. We focused our attention on some of *E. coli* hydrolases and their series of action: **MurNAc-L-Ala amidases**: AmiABC, **DD-endopeptidases**: MepA, MepS, MepM, MepH, PBP7, and **DD-endopeptidase/DD-carboxypeptidase**: PBP4. **B)** action sites of different hydrolases in PG.

1.2.3.2.1 Amidases.

Amidases are Zn^{++}-metallo-enzymes that hydrolyze the amide bond between L-alanine and MurNAc residues to separate glycan strands from peptide stem during cell separation (**Figure 4**) (Höltje, 1995; Vollmer et al., 2008). *E. coli* has three periplasmic amidases important for septation, AmiA, AmiB, and AmiC, of which at least one of them is required for cell division (Priyadarshini et al., 2007; Tsang et al., 2017). Cells lacking all amidases create a septum with a defective geometry resulting in connected cells growing in long chains (Heidrich et al., 2001); and chaining, which bacterial cells are stick together post division with more than two septa (Vejborg & Klemm, 2009). AmiABC amidases are auto-inhibited and need to be activated by interaction partners. In *E. coli*, the two most characterized regulators are NlpD and EnvC (Peters et al., 2013; Tsang et al., 2017; Uehara et al., 2009; Uehara et al., 2010; Yang et al., 2012).

Periplasmic AmiA (encoded by *amiA*) and AmiB amidases (encoded by *amiB*) are activated by EnvC (IM-anchored). EnvC (encoded by *envC*) has 3 functional domains: a C-terminal LytM domain, a central-regulatory-domain, and N-terminal FtsEX-Coiled Coil (CC) domain (Cook et al., 2023; Hara et al., 2002). For EnvC to activate amidases, it is regulated and recruited to septation ring and by FtsEX (ABC-transporter-like complex) where it binds to EnvC CC domain (Cook et al., 2020; Pichoff et al., 2019; Yang et al., 2012). The interaction of EnvC with FtsEX may cause conformational changes that result in amidases activation. EnvC possesses a structural element called the “restraining-arm” that is involved in self-inhibition system (Cook et al., 2020). Meanwhile, AmiC (encoded by *amiC*) is activated by NlpD (OM-localized lipoprotein) (Rocaboy et al., 2013). NlpD (encoded by *nlpD*) possesses a lipoprotein signal-

sequence, a LysM domain, and a LytM domain (Buist et al., 2008; Mesnage et al., 2014; Uehara et al., 2009). NlpD LysM domain is required for proper septal ring localization, whereas LytM domain is necessary for amidase activation, and subsequently cell separation *in vivo*. Based on genetic interaction analysis (Tsang et al., 2017), it was found that Tol-Pal system and DolP (OM lipoprotein) are involved in NlpD-mediated AmiC activation.

In addition, ActS (activator during stress) is the third LytM-family protein that contributes to cell separation by activating amidases ABC for PG digestion *in vitro* (Gurnani Serrano et al., 2021). ActS has LytM domain that shares 34%, 35%, and 65% sequence Identity with MepM, EnvC, and NlpD, respectively. However, ActS function has not been recognized until recently. Some independent works concluded that ActS preferentially activates AmiB in acidic conditions (Mueller et al., 2021), and AmiC in OM stress (Gurnani Serrano et al., 2021). The cells with defected or deleted *ΔactS* formed abnormally long cell chains when *ΔnlpD* or *ΔenvC* are not present (Priyadarshini et al., 2007; Uehara et al., 2009).

In the presence of PG-synthesis inhibitors, amidases are powerful autolysins -along with endopeptidases and lytic transglycosylases- that can act in the un-restricted dissolution of PG sacculus that take place when antibiotics block insertion of new PG subunits into bacterial sacculus (Kohlrausch & Höltje, 1991).

1.2.3.2.2 Endopeptidases.

Endopeptidases (Epases) and carboxypeptidases (Cpases) (**Figure 4**) are highly redundant in different bacterial species, where cells lacking single/multiple hydrolases usually have no significant morphological defects (Vollmer et al., 2008). Epases and Cpases can be differentiated depending on the substrate-specificity. Epases cleave within PG peptides, while Cpases detach the C-terminal of amino acid. D,D-peptides cut between two D-amino acids, while L,D- and D,L-peptides cut between D- and L-amino acids (Smith et al., 2000). In one study, they presented at least ten different types of domains for PG peptidases (Vermassen et al., 2019). In *E. coli*, several enzymes possess DD-endopeptidase activity such as MepS, MepA, MepH, MepM, DacB, and PbpG. *In vitro* laboratory experiment showed that MepM, MepA, MepS, MepH, and PbpG have only Epase activity, whereas DacB have both Epases and Cpases activities (Park et al., 2020; van Heijenoort, 2011). Cpases have an important role as cell shape regulators during growth, and PBP5 seems to be the most important one. Cells lacking PBP5 will cause alteration in morphology, resulting in bent cells (Typas et al., 2012).

The periplasmic MepA (coded by *mepA*) of *E. coli* is a penicillin-insensitive murein DD-endopeptidase that plays a role in murein removal from bacterial sacculus and integrate nascent murein strands withing the sacculus. mepA belongs to LAS (lysostaphin, D-Ala-D-Ala and sonic) metallopeptidase family (dependent on the Zn^{2+} presence) that hydrolyses the LD (*meso*-A_2pm-*meso*-A_2pm) and DD (*meso*-A_2pm-D-Ala) bonds within Gram-negative peptidoglycan cell wall (Chodisetti & Reddy, 2019; Marcyjaniak et al., 2004; Voedts et al., 2021).

Another metallopeptidase is MepM (formerly yebA). It has dual selectivity murein endopeptidase that cleaves D-ala-m-DAP and m-DAP-mDAP cross-links and does not exhibit LD-Cpases activity. In addition, it plays a role in cell elongation by incorporating murein during cell growth. MepM is paralogous to NlpD, EnvC, and ActS (Uehara et al., 2009). Increased activity levels of MepM interferes with peptidoglycan septal biogenesis, while its deletion cripple membrane invagination (Goodall et al., 2018; Voedts et al., 2021). MepH (formerly ydhO) is also a murein DD-endopeptidase specific for D-ala-m-DAP cross links that does not exhibit LD-Cpases activity. A little is known about mepH, but its overproduction can compensate for the MepM absence (Voedts et al., 2021)

The bifunctional, class C penicillin-sensitive protein PBP4 (coded by *dacB* gene) has peptidoglycan DD-endopeptidase with a specificity for D-ala-m-DAP that catalyzes the hydrolysis peptide bonds, along with DD-carboxypeptidase activity (Korat et al., 1991). PBP4 activity has been involved in cell separation. It has been reported to show chaining phenotype in double gene deletion with *amiC* (Banzhaf et al., 2019).

Another penicillin-binding-protein is PBP7 (coded by *pbpG*), a DD-endopeptidase that hydrolyzes D-alanyl-DAP amide bonds within peptidoglycan crosslinks (Spratt, 1977). It is one of the rod-shape maintaining factors of the murein sacculus. Both deletion and overexpression of *pbpG* has no obvious growth defect (Banzhaf et al., 2020; Voedts et al., 2021).

MepS (formerly spr) is a murein DD-endopeptidase associated with incorporating murein during cell growth with a specificity for D-ala-m-DAP cross links. The C-terminal domain

showed hydrolase activity on intact PG sacculi and affects cell division process. It also appeared that MepS has a weak activity of LD-carboxypeptidase (cleavage of (L)-mDAP−D-ala peptide bond) (Singh et al., 2012). One published study aiming to find new potential targets for antibacterial development (Goodall et al., 2018), predicted *mepS* to be non-essential. Mutants of *E. coli* lacking four Epases (*ΔmepS, ΔmepA, ΔdacB, ΔpbpG*) were not significantly defective, as multiple copies of *mepM* (*yebA*) or *mepH* (*ydhO*) suppress the *ΔmepS* growth phenotypes at high temperature (Singh et al., 2012). A triple deletion mutant (*ΔmepS, ΔmepM, ΔmepH*) grew fine when multiple copies of only one (MepS, MepM, or MepH) was provided, emphasizing their redundant essential functions *in vivo*. During exponential phase of cell growth, MepS is extremely abundant throughout the exponential phase, until the stationary phase begins and MepS levels fall steeply. At the onset of stationary phase, MepS is targeted for proteolytic degradation by an OM lipoprotein called NlpI, and the periplasmic tail-specific protease Prc (Singh et al., 2015; Su et al., 2017). Increased MepS activity hinders septal peptidoglycan biogenesis activation (Voedts et al., 2021).

1.2.3.2.3 Lytic peptidoglycan transglycosylase.

Removal of PG material in every generation requires the action of lytic transglycosylases (LTs) to hydrolyze the glycan backbone (Scheurwater et al., 2008). Bacteria rely on a diverse range of cellular functions carried out by LTs, and they encode a seemingly corresponding variety of LTs to fulfill these functions. While it is assumed that each LT member performs specialized tasks, extensive research points towards functional redundancy, compensating for the loss of

any single member. Gram-negative bacteria exhibit unique LTs categorized into six distinct families (Herlihey & Clarke, 2016) based on the identification of distinct sets of consensus motifs (Blackburn & Clarke, 2001). In *E. coli*, a minimum of six distinct LTs has been recognized (Jorgenson et al., 2014; van Heijenoort, 2011) to cleaving the β-1,4 glycosidic linkage between MurNAc and GlcNAc in PG, producing 1,6-anhydromuramyl disaccharide muropeptides (Scheurwater et al., 2008). *E. coli* LTs consisting of one soluble variant (Slt70) and five anchored in the outer membrane (MltA-MltE). Slt70, MltC, MltD, and MltE are LTs of family 1 that facilitate the cleavage of the beta-1,4-glycosidic bond between N-acetylmuramic acid (MurNAc) and N-acetyl-D-glucosamine (GlcNAc) for PG recycling during cell elongation and/or division (Scheurwater et al., 2008). MltA represents family 2, which is an integral membrane-bound enzyme involved in the degradation of PG, playing a significant role in the regulated growth of the stress-bearing sacculus in *E. coli* (van Straaten et al., 2007). The family 3 LT, MltB, also facilitates the cleavage of glycosidic bonds between N-acetylmuramic acid and N-acetylglucosamine residues in peptidoglycan. Although the physiological role remains unclear, as evidenced by the lack of an obvious phenotype upon gene deletion (Ehlert et al., 1995), there is a suggestion that it may be involved in the recycling of PG during processes like cell elongation and/or cell division (van Asselt & Dijkstra, 2000; Lee et al., 2013). The fourth LT family predominantly includes enzymes encoded by λ bacteriophages, believed to play a role in secretion system assembly that enhances host-cell pathogenicity (Walmagh et al., 2013). The recently identified Family 5 LTs represent the first LT family present in both Gram-negative and Gram-positive bacteria, denoted as MltG, presumed to be involved in termination of glycan chains during the

peptidoglycan biosynthesis of the cell wall (Yunck et al., 2016). Family 6 LTs were thought to participate in catalysis, mirroring the characteristics of MltA from the Family 2 LTs (Herlihey & Clarke, 2016).

Additionally, LTs can be further classified based on their substrate preference for either exolytic or endolytic strand cleavage. Exolytic LT activity involves cleaving a terminal NAG-NAM disaccharide from the end of the glycan strand, while endolytic LT activity cleaves chains internally, resulting in products of at least four saccharides in length (Lee et al., 2013; 2017). These dual characteristics serve as the foundation for organizing LTs and, consequently, offer insights into their respective cellular functions (Scheurwater & Clarke, 2008; Herlihey & Clarke, 2016; Lee et al., 2013; 2017). Also, LTs cleave the PG glycosidic bonds creating appropriate space to allow the assembly of membrane molecular machines, such as pili, flagella, and secretion systems (Scheurwater et al., 2008). *E. coli* cells growing in normal environment with a single or multiple knockouts are viable, whereas deletion in all LT genes is lethal, suggesting an overlapping functions within LTs array of *E. Coli* (Dik et al., 2017; Heidrich et al., 2001).

1.3 β-lactam antibiotics and PG synthesis.

As PBPs are crucial for survival of bacteria, the discovery of penicillin in the 1940s showed to be a ground-breaking mechanism to tackle bacterial infection (Fleming, 1944). PG synthesis is a target of different classes of antibiotics, including glycopeptide (e.g. vancomycin) and β-

lactam (e.g. penicillin) (Mueller et al., 2019). One of these major targets is the PBPs, a group of enzymes important for peptidoglycan synthesis and were named after their affinity to penicillin and other β-lactam class antibiotics (Tipper & Strominger, 1965). All β-lactam antibiotics have a common core possessing a four-member- β-lactam ring (**Figure 5**). B-lactam antibiotics primarily target the Tpase domain of PBPs restrict its action by mimicking the same structure of the terminal D-Ala-D-Ala motif as in PG stem peptide, sequestering the active site serine covalently, rendering PBP's transpeptidase domain inactive (Cho et al., 2014)

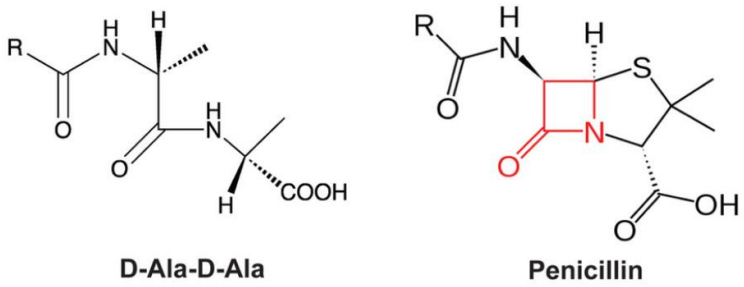

Figure 5. β-lactam antibiotic mimicry to D-Ala-D-Ala (Zeng & Lin, 2013). Lactam ring, highlighted in red, reacts on PBPs side chain of an active site serine (CH2OH).

In the presence of β-lactam in Gram-negative bacteria, inhibition of class A PBPs results in uncontrolled hydrolytic activities leading to cell lysis, inhibition of PBP2 causes cell division cessation and rod-shape loss, and inhibition of PBP3 shows cell division arrests leading to

filamentation formation (Bush & Bradford, 2016). The process of cell division begins through an ordered assembly of the divisome (more details are found in section **1.5.2**) that contains the FtsI (PBP3) protein, a β-lactam target. FtsI is an essential PBP needed for division and β-lactam antibiotics targeting FtsI (e.g. cephalexin and piperacillin) are among world's massive-selling β-lactams. Cephalexin induces filamentation as a result of its ability to block FtsI activity (Chung et al., 2009; Hedge & Spratt, 1985).

Gram-negative bacteria evolved strategies to evade the bactericidal impact of β-lactam antibiotics, such as β-lactamase production (Jacoby, 2009), β-lactam entry reduction via mutations in porins, novel PBPs production with less affinity to β-lactams (Fuda et al., 2004), and using drug efflux pumps to expel β-lactam out of cells. Among these mechanisms, β-lactamases is the most efficient strategy (Jacoby & Munoz-Price, 2005) that can open up the β-lactam ring to make products that do not inhibit PBPs (Magnet et al., 2007; Mainardi et al., 2005).

1.4 Bacterial cytoskeleton.

The term 'cytoskeleton' was used after discovering a network of thin, long, cell-shape-determinant structures in eukaryotic cells' cytoplasm (Shih & Rothfield, 2006). In bacteria, these network structures were found to be made of at least four polymeric filaments: 1) actin homologs, 2) tubulin homologs, 3) the Min system, 4) and intermediate filament (IF) proteins (Pilhofer & Jensen, 2013). They are able to assemble, disassemble, and rearrange within the cell into extended polymeric filaments. Filament's rearrangement is in response to the signals that

balance between cellular functions (e.g., intracellular organelle transport, cell shape, motility, cell cycle progression) (Celler et al., 2013). The proteins involved in the organization of these filamentous polymers interact with the cytoplasmic membrane and create supportive structures along the cell (Cabeen & Jacobs-Wagner, 2007).

In bacteria such as *E. coli*, actin homologs interact directly with tubulin homologs to coordinate cell growth and division. They both contribute to bacterial cytokinesis, which involves accurate placement, assembly, and the activity of the 'divisome'. The actin-like cytoskeletal MreB protein present in bacteria plays essential roles in bacteria, including cell elongation and membranous organelles arrangement (van den Ent et al., 2001). The gene coding for the MreB protein was found in rod-shaped, helical, and filamentous species (absent in cocci-shaped ones). Different bacteria possess different numbers of MreB paralogs. In *E. coli* cells, a single MreB protein was found, whereas in *Bacillus subtilis* (*B. subtilis*) there are several MreB-related proteins (MreB, Mbl (*MreB-like*), and MreBH (*MreB homolog*) protein) (Meeske et al., 2016). Cells with depleted or with drug-induced inactivated MreB will grow as spheres (Van Teeffelen & Gitai, 2011). Also, the divisome is regulated by polymerizing tubulin homologs. One of the major cytoskeletal proteins involved is the FtsZ (Filament Temperature Sensitive) protein. FtsZ is a tubulin homolog, citing the existence of a signature amino acid sequence of a tubulin and the FtsZ (Bi & Lutkenhaus, 1991) ability to bind to GTP and hydrolyze it (Busiek & Margolin, 2015). FtsZ is an essential protein of cell division machinery in almost all bacteria. The idea of considering FtsZ as a cytoskeletal protein originated from an immunoelectron microscopy picture of *E. coli* cell showing FtsZ proteins tightly bundled and encircling the mid cell forming a ring ('Z-ring') (Busiek & Margolin, 2015) . These rings establish a scaffold for the latter assembly of the recruited

divisome proteins. Also, they are important to provide the driving force to constrict the inner membrane upon cell division. When scientists discovered Fts in the 1960's, they found that *E. coli* cells in the absence of Fts genes could not divide at high temperatures and grew as long filaments instead. Elongation in bacteria have two known types: filamentation, which can be defined as bacterial cell continue to grow but fail to divide, creating connected and un-septated cellular compartments (Wehrens et al., 2018). During the normal division cycle, positive and negative effector proteins -spatially and temporally- regulate Z-ring's assembly, function, and stability. Spatial regulation limits Z-ring formation at any desired location in preparation for septum formation. This is accomplished by the Min system. It controls and prevents bacterial septation at unwanted sites through three proteins, MinC, MinD, and MinE (**Figure 6**) (Godino et al., 2022; Rothfield et al., 2005). Unlike actin filaments and microtubules, intermediate filaments do not participate directly in cell movements. Instead, their primary function seems to be providing structural support to cells, contributing to mechanical strength (Cooper, 2000).

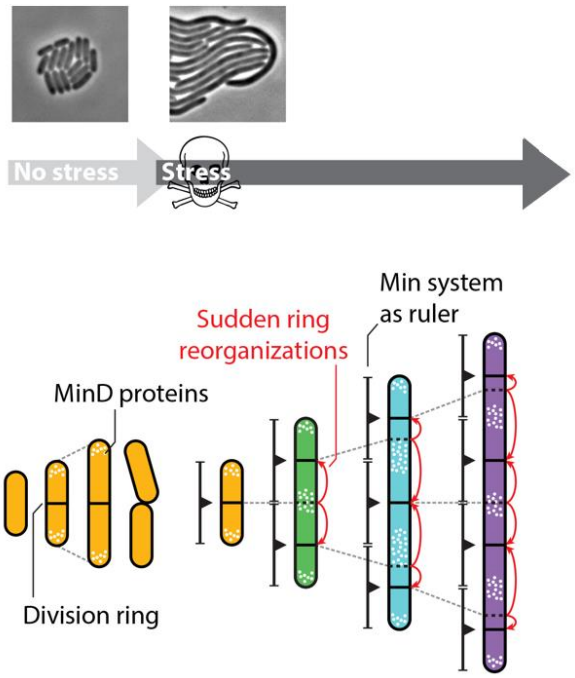

Figure 6. Role of the Min system in *E. coli* in ensuring cells divide at appropriate sites under normal conditions (Truong, 2020). During periods of stress, E. coli cells undergo filamentation, and the Min system assumes the role of a regulator, preventing division in areas where Min proteins are active and determining the spacing of division rings.

1.5 Bacterial morphogenesis and cell division.

Bacterial morphogenesis is the process of how bacteria develop their shape to ultimately grow. This shape development is a mechanical process involving forces that create mechanical stresses. The bacterial shape is determined by its surface-to-volume ratio. In rod-shaped bacteria, this ratio increases with growth (Harold, 2007). Division and Cell Wall cluster genes (*dcw*) are a bacterial group of genes (16 in *E. coli*) responsible for the synthesis of peptidoglycan precursors and cell division: *mraZ-mraW-ftsL-ftsI-murE-murF-mraY-murD-ftsW-murG-murC-*

ddlB-ftsQ-ftsA-ftsZ—murB. Phylogenetic analysis tools revealed that there is a strong relationship between the organization of this gene cluster and cell growth, morphology, and division (Mingorance et al., 2004). The cluster was identified in *E. coli* as a region of genes related to murein precursors synthesis and was referred to as 'mra Region/Operon'. There are four promoters found in the 5' end of the cluster and six in the 3' end. *MraZ* gene acts as transcriptional repressor controlling around 100 cell-wall genes involved in cell division process. The next gene*, mraW*, was recently found to function as DNA methylase possessing wide-ranging effects on virulence and motility of *E. coli* (Xu et al., 2019). The *mraY, ddlB,* and *mur* genes all code enzymes (D-alanine:D-alanine ligase) that regulate the synthesis of murein precursors. Also, the *ddlB* has another copy in *E. coli* chromosome, *ddlA*, and both are essentials for the activity of the enzyme for cell wall synthesis. In addition, the cluster has six *Fts* genes (*ftsL, ftsI, ftsW, ftsQ, ftsA,* and *ftsZ),* which are critical for cell septation. These genes code for their designated proteins, which are all found localized to division site during septation (Mingorance et al., 2004).

Conceptually, there are two main modes for peptidoglycan synthesis whose combination will yield the majority of bacterial shape: growth and division (or cytokinesis). The two modes are accomplished by multiprotein complexes within the cell. These complexes are formed when two or more proteins interact noncovalently to form a cluster. Proteins clustering may enhance/reduce the complex stability, catalytic activity, diffusion of substrates, and the regulation of several proteins. Most rod-shaped organisms employ two multiprotein complexes to guide peptidoglycan synthesis, the elongasome and the divisome, during cell lateral growth and division, respectively (Jiang et al., 2015).

1.5.1 Elongasome complex.

Cell wall lateral synthesis is achieved by a protein complex named the “Elongasome”. The proteins include: MreB, MreC, MreD, MraY, MurG, RodA, RodZ, PBP2, and one of the class A PBPs (PBP1A or PBP1B). This complex is recruited mainly by MreB, the actin-like protein essential for length growth (Van der Ploeg et al., 2013). MreB first attaches to the inner side of the cytoplasmic membrane via its N-terminal amphipathic helix (**Figure 7**). Then, it is associated with critical cell elongation proteins to form the elongasome. Following the synthesis of UDP-N-acetylmuramyl-pentapeptide (UDP-MurNAc-pentapeptide) from UDPN-acetyl-glucosamine (UDP-GlcNAc) by MurA through MurF enzymes (the first step of peptidoglycan biosynthesis described above in **1.5** section), the second step will occur within the inner side of cytoplasmic membrane, includes the activity of MraY and MurG. MraY is an integral membrane protein that catalyzes and transfer phosphor-MurNAc-pentapeptide (the motif of UDP=MurNAc-pentapeptides) to undecaprenyl phosphate (a lipid carrier) to form Lipid I (Emami et al., 2017; Typas et al., 2010; Van der Ploeg et al., 2013). The next step involves the link between Lipid I and GlcNAc molecule by the MurG (membrane-associated enzyme) to generate Lipid II. After synthesizing Lipid II peptidoglycan precursors in the cytoplasm, they will cross to the periplasmic side to provide the substrate needed for PBP1A and PBP2 (Egan et al., 2015; Laddomada et al., 2016; Typas et al., 2010). PBP1A (bifunctional class A PBP) (see section **1.2.3.1.1**) has a glycosyltransferase activity that polymerizes the glycan strands, along with transpeptidases to cross link peptides between glycans. While PBP2 (monofunctional class B PBP) has a transpeptidases activity crucial for cell elongation. MreB will interact with PBP, the bi-topic membrane protein, while RodZ interacts with both MreB and MreC to maintain bacterial cell

morphology (Ago & Shiomi, 2019; Emami et al., 2017). After that, RodA and PBP2 will form a stable complex providing Gtase and Tpase activity, respectively. The bifunctional Gtase-Tpase PBP1A will then interact with PBP2 to stimulate its activity. MreC and MreD are needed to modulate the interaction between RodA and PBP2. Through glycosylation and transpeptidation reactions, PBPs will incorporate the GlcNAc-MurNAc-pentapeptide into cell's peptidoglycan layer (Emami et al., 2017; Liu et al., 2020).

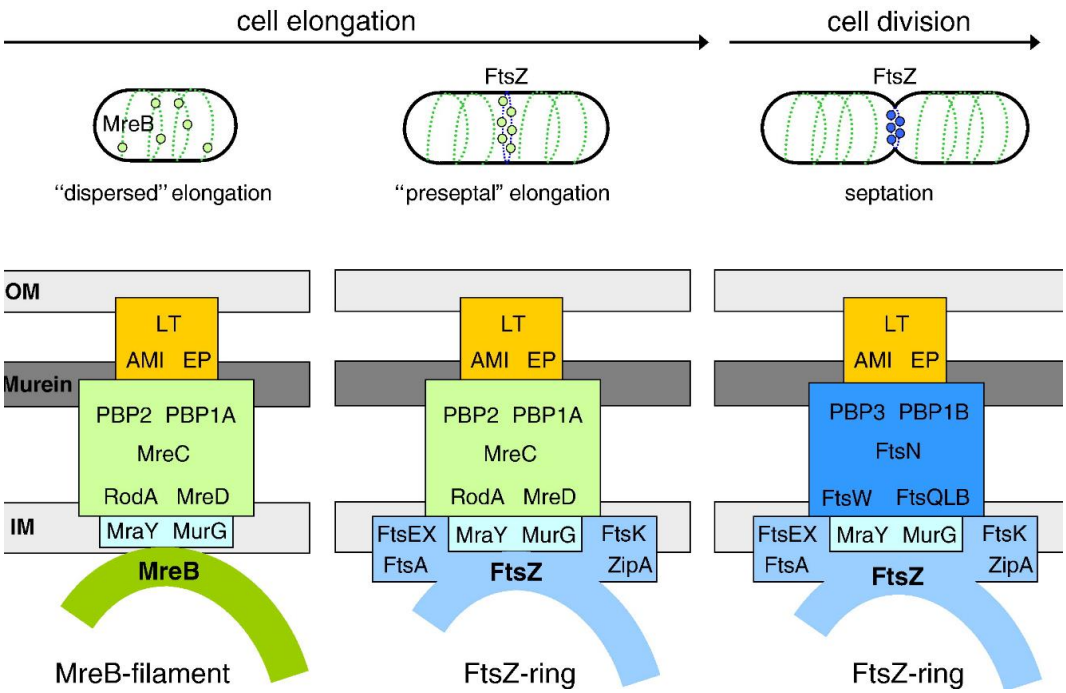

Figure 7. Organization model of cytoskeletal elements and synthesis of PG complexes during bacterial cell cycle (Vollmer & Bertsche, 2008). Upper Section: Young cells undergo elongation through the 'dispersed' integration of precursors by elongation-specific murein synthesis complexes (depicted as green circles) along filaments of the actin-like MreB (illustrated as a green dotted line). The emergence of the FtsZ-ring (along with other early cell division proteins, shown as a blue dotted line) redirects the elongation complexes to the mid-cell, resulting in pre-septal elongation at the mid-cell. Constriction initiates once the elongation complexes have been replaced from the FtsZ ring by the cell division-specific murein synthesis complexes (depicted as blue circles). The lower section illustrates the composition of the sub-complexes for the various modes of growth.

1.5.2 Divisome complex.

When the bacterial cell initiates the division process, FtsZ molecules polymerize in a GTP-dependent manner ("treadmilling") into filaments, to form the Z-ring (Busiek & Margolin, 2015).

The proper ring formation process requires the action of FtsA and/or ZipA to regulate the tethering of FtsZ to the cytoplasmic membrane; however, no such homolog is found in Gram-positive bacteria (instead, SepF proposed to fulfil this function). FtsA is an ATP hydrolyzing enzyme important to deliver energy during cell division, while ZipA helps anchoring FtsZ to the cytoplasmic membrane (**Figure 7**) (Godino et al., 2022). Along with FtsZ, there are other essential proteins for divisome assembly (**Figure 8**), including: FtsEX, FtsK, FtsQ, FtsL, FtsB, FtsW, FtsI, and FtsN. Soon after the Z ring forms, the ATP-binding cassette (ABC) transporter-like complex FtsEX will join (FtsE is the ATPases and FtsX is the inner membrane component)(Du et al., 2018; Schmit & Nick, 2008). Also, the FtsEX complex interacts with the periplasmic EnvC during cell division to coordinate both cell wall synthesis and hydrolysis. Next, FtsK, a linker/DNA translocase needed to resolve chromosome dimers and discards DNA from constricting septum (Kleckner et al., 2014). FtsQLB are bitopic membrane proteins that act as a scaffolding complex for the next recruited downstream proteins and thereby regulate divisome activity at some level (Käshammer et al., 2023). FtsWI complex is next recruited, where FtsW is a SEDS protein (see section **1.2.3.1.2**) possesses a peptidoglycan glycosyltransferase, and FtsI is a peptidoglycan transpeptidase working with its partner FtsW as a division's septal-peptidoglycan-synthase (Dubarry et al., 2010). The last to join the divisome is FtsN, the protein which acts on FtsA (in the cytoplasm) and perhaps on FtsQLB (in the periplasm) to trigger cell constriction and activate septal peptidoglycan synthesis (**Figure 8**) (Käshammer et al., 2023; Van der Ploeg et al., 2013).

Additionally, FtsN links the Tol-Pal system to the divisome by recruiting the proteins of Tol-Pal system to the constriction site. Tol-Pal system proteins connect the cytoplasmic membrane with

the OM. It was suggested that Tol-Pal system along with other OM proteins (e.g. hydrolases) can possibly form a division sub-complex at the OM side (Hale et al., 2022; Petiti et al., 2019).

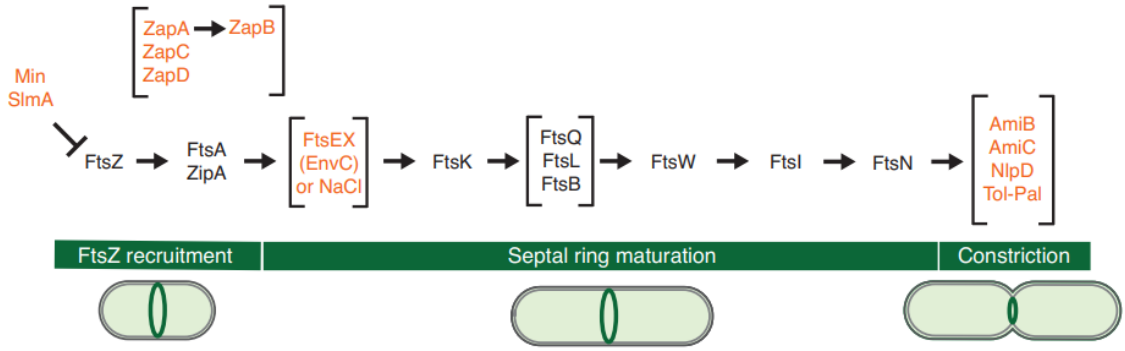

Figure 8. Pathway of *E. coli* cell septal ring assembly (Truong, 2020). The recruitment of the specified division proteins follows a linear and hierarchical process. Initially, FtsZ is recruited, guided to the midcell by the inhibitory actions of the Min system and SlmA. Zap proteins serve as auxiliary factors, enhancing the stability of the Z-ring. The subsequent stage involves the maturation of the septal ring, leading to the accumulation of FtsN and the activation of peptidoglycan synthesis facilitated by FtsW and FtsI. FtsN initiates the final stage of constriction, which encompasses amidases, their activators, and the Tol-Pal system. Essential proteins are depicted in black, while nonessential or conditionally essential proteins are shown in orange.

1.6 Aim of this thesis:

While the identities and functions of numerous proteins engaged in cell division and elongation have been elucidated over time, various questions persist regarding how cell envelope biogenesis proteins in Gram-negative bacteria are orchestrated to successfully grow and divide.

In Chapter 3 of this thesis work, our aim is to investigate the impact of selected stress conditions on *E. coli* mutants of single and/or double gene deletions encoding for PG hydrolases (six endopeptidases: MepA, MepS, MepM, MepH, PBP4, PBP7, three amidases: AmiA, AmiB, AmiC) and two class A penicillin-binding-proteins (PBP1A and PBP1B) during cell growth and division. Contributing to the existing knowledge, I aim to use fluorescent microscope, colony-fitness, and chemogenomic approaches to find potential dependency between our selected panel of enzymes under environmental stress to ensure cell wall integrity.

In Chapter 4, we aim to test our hypothesis if NlpI and/or DolP proteins could modulate amidases (AmiA, AmiB, and AmiC) activities. For this, I will use an optimized *in vitro* PG-labelled degradation assay to measure amidases hydrolytic activity in the presence of NlpI and DolP.

Chapter 2. Material and methods.

2.1 Microbial methods.

2.1.1 Strains used in this study.

This study used *Escherichia coli* BW25113 as the parental strain and obtained other mutants from the KEIO library (Baba *et al*., 2006) (**Table. 2**). Mutations were then transduced into parental strain by P1 transduction. Chromosomal modifications were checked by PCR to detect Kan^R, Tet^R, and Cat^R cassettes.

Table 2. Bacterial strains used in this study.

Strain ID	Genotype	Source
MB01064	BW25113	(Datsenko & Wanner, 2000)
MB01119	BW25113 Δ*amiA::kan*	(Boelter et al., 2022)
MB01120	BW25113 Δ*amiB::kan*	(Boelter, et al., 2022)
MB01121	BW25113 Δ*amiC::kan*	(Boelter et al., 2022)
MB01122	BW25113 Δ*envC::kan*	(Boelter et al., 2022)
MB01051	BW25113 Δ*nlpD::kan*	(Boelter et al., 2022)
MB01118	BW25113 Δ*amiA::kan*Δ*mrcA::tet*	This study
MB01119	BW25113 Δ*amiB::kan*Δ*mrcA::tet*	This study
MB01120	BW25113 Δ*amiC::kan*Δ*mrcA::tet*	This study
MB01121	BW25113 Δ*envC::kan*Δ*mrcA::tet*	This study
MB01122	BW25113 Δ*nlpD::kan*Δ*mrcA::tet*	This study
MB01123	BW25113 Δ*amiA::kan*Δ*mrcB::tet*	This study
MB01124	BW25113 Δ*amiB::kan*Δ*mrcB::tet*	This study

MB01125	BW25113 Δ*amiC::kan*Δ*mrcB::tet*	This study
MB01126	BW25113 Δ*nlpD::kan*Δ*mrcB::tet*	This study
MB10098	BW25113 Δ*pbpG*	(Banzhaf et al., 2020)
MB10502	BW25113 Δ*mepS::kan*	(Banzhaf et al., 2020)
MB10075	BW25113 Δ*mepM::kan*	(Banzhaf et al., 2020)
MB10397	BW25113 Δ*mrcA::tet*	(Banzhaf et al., 2020)
MB10398	BW25113 Δ*mrcB::tet*	(Banzhaf et al., 2020)
MB10067	BW25113 Δ*mepA::kan*	(Banzhaf et al., 2020)
MB10023	BW25113 Δ*dacB::kan*	(Banzhaf et al., 2020)
MB10020	BW25113 Δ*mepH*::kan	This study
MB10718	BW25113 Δ*mepS::kan*Δ*mrcA::tet*	This study
MB10714	BW25113 Δ*mepA::kan*Δ*mrcA::tet*	This study
MB10716	BW25113 Δ*mepH::kan*Δ*mrcA::tet*	This study
MB10715	BW25113 Δ*pbpG::cat*Δ*mrcA::tet*	This study
MB10719	BW25113 Δ*mepM::kan*Δ*mrcA::tet*	This study
MB10717	BW25113 Δ*dacB::kan*Δ*mrcA::tet*	This study
MB10724	BW25113 Δ*mepS::kan*Δ*mrcB::tet*	This study
MB10720	BW25113 Δ*mepA::kan*Δ*mrcB::tet*	This study
MB10722	BW25113 Δ*mepH::kan*Δ*mrcB::tet*	This study
MB10721	BW25113 Δ*pbpG::cat*Δ*mrcB::tet*	This study
MB10725	BW25113 Δ*mepM::kan*Δ*mrcB::tet*	This study
MB10723	BW25113 Δ*dacB::kan*Δ*mrcB::tet*	This study

2.1.2 Growth of strains.

All *E. coli* strains were cultivated on LB (Luria Bertani) agar plate (5 g/L yeast extract, 10 g/L peptone, 5 g/L NaCl, 1.5% w/v agar pH of 7.2) and incubated at 37°C, or in LB medium containing 5 g/L yeast extract, 5 g/L NaCl, 10 g/L peptone, with a pH of 7.2, and incubated at

37°C with constant agitation. Growth of strains were monitored by measuring the OD (optical density) using a spectrophotometer at a wavelength of 600 nm.

2.1.3 Strains storage and preservation.

Depending on the period of use, strains were either stored for short-term (streaked on LB agar plate with/out the appropriate antibiotic, incubated 24 hours at 37°C overnight, and stored in refrigerator (4°C), or preserved for long-term (overnight culture mixed with 50% v/v sterile glycerol to a ratio of 4:1 and kept at -80°C).

2.1.4 Competent cells.

An overnight culture (at 37°C) was diluted in 50 mL Luria-Bertani (LB) media to a ratio of 1:100 and allowed to grow to mid-exponential phase (OD_{600}= 0.4 – 0.6). The culture was centrifuged in a centrifuge tube for 10 minutes, 13,000 rpm, at 4°C. After centrifugation, the supernatant was removed and 2 mL of 0.1 M $CaCl_2$ was used to resuspend the pellet and incubated for 30 minutes on ice. The culture was again centrifuged (10 minutes, 13,000 rpm, at 4°C). The pellet was resuspended in 0.1 M $CaCl_2$ (2 mL) + 50% v/v glycerol (1 mL) and left on ice for 30 minutes. Aliquots were then made (100 µL/each).

2.1.5 Transformation of competent cells.

1 µL of plasmid was added to competent cells aliquot of 100 µL and incubated on ice for 30 minutes. Sample was heat-shocked at 42°C in water-bath for 30 seconds. The sample was placed back on ice for 2 minutes. 1 mL of LB media was added to the sample and incubated at 37°C for 1 hour with constant agitation at 180 rpm. After incubation, the sample was centrifuged at 6000 rpm for 2 minutes. The supernatant was discarded, and pellet was resuspended in 100 µL LB. Final cells resuspension was then plated on LB agar plate with the appropriate antibiotic and incubated at 37°C.

2.2 Standard DNA procedures.

2.2.1 Oligonucleotides.

Oligonucleotides with final concentration of 100 pmol/µL resuspended in water was acquired from Merck.

2.2.2 Colony PCR.

Oligonucleotides were prepared with a final concentration of 10 µM. A small portion of sample colony was picked by a sterile tip and mixed with PCR reagents in a reaction tube. PCR MyTaq Mix 2x (Bioline) was applied following manufacturer's instructions. The thermocycler was programmed as follows: 95°C for 5 minutes > 95°C for 30 seconds > 54°C 30 seconds (35 cycles) > 72°C for 1 minutes > 72°C for 5 minutes > and hold for 4°C.

PCR products and hyperladder 1 kb (Bioline) were loaded in 1% agarose gel in 1x TAE buffer (prepared from stock solution of 50x TAE buffer= 1 M acetic acid, 0.05 M EDTA in water, 2 M Tris). Samples were stained by 0.07 /mL Midori Green (Nippon Genetics) and electrophoresis current was applied at 110 V for 1 hour. Using BioRad system, the gel was visualized under UV light.

2.3 Advanced DNA procedures.

2.3.1 P1 phage isolation.

This procedure was in terms of a previously described protocol (Thomason et al., 2007). In a 50 mL flask, a donor strain culture was grown for 24 hours and diluted into 5 mL LB media (with 25 µL of 1M $CaCl_2$ + 50 µL glucose) to a ratio of 1:100. The sample flask was incubated for 40 minutes at 37°C with aeration. 100 µL of P1 phage stock was added to the sample culture and put back in the 37°C incubator until cells were lysed and suspension seemed clear (approximately 3-4 hours). 100 µL of chloroform was added to the culture and incubated again in 37°C for 5 minutes. The culture was centrifuged for 1 minute at 13,000 rpm. The supernatant was collected in a glass tube and stored at 4°C.

2.3.2 P1 transduction.

This procedure was performed according to previously described protocol (Thomason et al., 2007). The recipient strain culture was grown for 24 hours and then centrifuged for 2

minutes at 13,000 rpm. The pellet was mixed with one-half of the initial volume in P1 salt solution (5 mM $MgSO_4$; 10 mM $CaCl_2$). In a new glass tube, 100 µL of P1 lysate was mixed with 100 µL cells/P1 salt solution and tube were incubated at 37°C for 30 minutes to allow cells to absorb the phage, along with the control tube (same culture sample without phage). A 200 µL of 1 M sodium citrate and 1 mL of LB media were added and samples were incubated at 37°C for 1 hour. Samples were centrifuged for 2 minutes at 13,000 rpm, supernatant was removed, and pellets were resuspended with 50-100 µL of LB media. Samples were plated in selected agar plates supplemented with the appropriate antibiotic.

2.4 Phenotypic analysis methods.

2.4.1 Microscopy.

Cells preparation: overnight cultures were grown at 37°C and diluted to initial OD_{600} = 0.01 in normal LB. Cells in culture tubes were incubated and grown to OD_{600}= 0.4 – 0.6 at 37°C. Cells were centrifuged for 1 minute at 7000 x g and harvested.

Cells preparation in stress conditions: previously cultured overnights at 37°C in normal LB broth were diluted in LB broth supplemented or altered according to the stress induced (0.25% SDS; 0.5mM EDTA; pH 4.8; 0mM NaCl; 600mM NaCl) and incubated at 37°C until early exponential phase (OD_{600} ~0.2).

Slide preparation: 1.5% agarose pads were prepared by mixing agarose and PBS, which were then heated in microwave and 500-600 µL of liquid agarose pipetted into Gene Frames

(Thermo Scientific) attached to a clean glass slide (de Jong et al., 2011). Agarose on slide was allowed to solidify for 30 – 40 minutes before use.

Cells staining and fixation: 0.5 mL of cultured and harvested cells were stained with 5 µg/mL of the membrane stain FM1-43FX (Invitrogen) and incubated for 10 minutes at room temperature. 33 mM of sodium phosphate pH 7.4 was used to adjust cells, which then fixed with 0.04% glutaraldehyde and 2.4% formaldehyde. 10 mg/mL of DAPI (4',6-diamidino-2-phenylindole) (Stratech Scientific) stain was used to label the DNA in fluorescence microscopy.

Cells imaging and shape analysis: stained and fixed cells were applied to agarose pads, spread, and imaged by Zeiss AxioObserver supported with Plan-Apochromat 100x/Oil Ph3 objective. For phase contrast images, HXP 120V illumination was used. For FM1-43FX images, Zeiss filter set 38 was used with 560/40 nm excitation and 630/75 nm emission, and Zeiss BFP filter was used for DAPI images. Cell shape/size analysis was obtained by MicrobeJ plugin Fiji 600 as reported in Ducret (Ducret et al., 2016).

2.5. Chemical genomics.

2.5.1 LB agar plate preparation.

For agar media preparation, 2% agar LB was prepared by dissolving 20 g of LB powder (5 g of yeast, 10 g of pancreatic digest of casein, and 5 g of sodium chloride) and 20 g of agar in 1 L of distilled water (It is important to maintain a concentration of 2% agar LB during this study,

because it affects the penetration depth of the BM6-BC pins leading to unquantifiable colonies by Iris software). Sodium chloride concentration was adjusted to achieve both 0 mM and 600 mM NaCl conditioned LB agar. HCl and KOH were used to adjust the pH to 7.5 in most of the selected conditions, except for the low pH 4.8 media. The mixture was then sterilized by autoclaving at 121°C for 15 minutes. LB agar was separately induced with the required chemicals (antibiotics and nutritional supplements) to achieve the selected stress conditions. Different conditioned LB agar was then aseptically dispensed into plates (VWR single-well cell culture plate). Each plate contained 42 mL of the media by using an accurate pumping system and left to solidify until the next day at room temperature.

2.5.2 Library screening by Iris robotic system.

BM6-BC robot was used in this study to replicate cell colonies on solid agar mediums and screen multiple mutants from our gene library grown in the selected stress conditions. Single source plate was created for each probe strain and inoculated into screening plate by Biomatrix 6 pinning robot (**Figure 9**). Each screening plate has parental strain, single deletion X, single deletion Y, and double deletion XY that were arrayed, each has 96 copies/plate (Banzhaf *et al*., 2020). Plates of genetic-interaction were incubated for 12 hours at 37°C. Plated were then imaged using 18-megapixel Canon Rebel T3i (Canon) and controlled condition of lighting (splmager S&P Robotics). The integral opacity of colonies was quantified as fitness using Iris imaging analysis software. Colony size, circularity and integral opacity as fitness readout was quantified using the image analysis software ChemGAPP (H. M. Doherty et al., 2023) as described below.

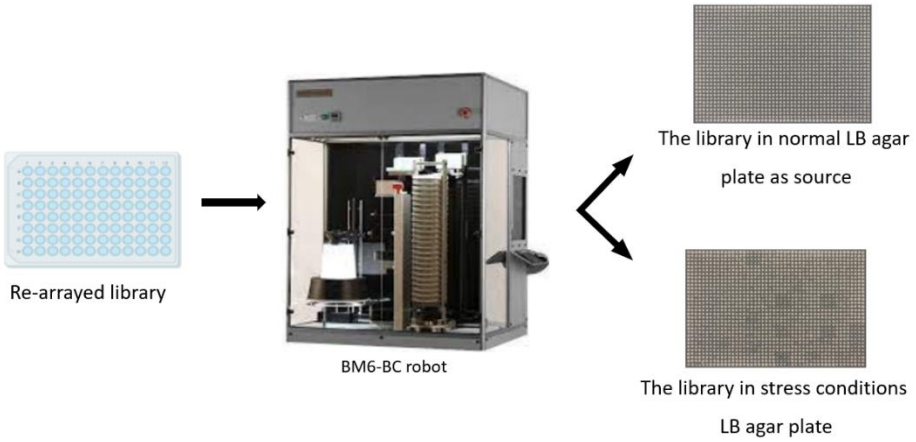

Figure 9. Scheme of re-arraying library broth culture inoculation into LB agar plates using BM6-BC robot. Source plates with all knockout mutants of interest were inoculated into stress-induced agar plates using BM6-BC robot. Plates were incubated at 37^0C for 18 hours.

2.5.3 ChemGAPP analysis.

The robot is equipped with the imaging compartment that fits a digital camera. Obtained images from the robot are then mapped by the image-analyzer software Iris. Iris can quantify multiple mutants by detecting their various colony characteristics (Hannah M Doherty et al., 2023). To start, colony size data for each plate was checked for plate effects via a Wilcoxon rank sum test between the distributions of colony sizes for the outer two edges of the plate and the centre colonies. Where $p < 0.05$ the difference in the distributions was considered as statistically significant and the outer edge colonies were scaled to the plate middle mean (PMM). The plate middle mean is defined as the mean colony size of colonies within the center of the plate, within the 40^{th} and 60^{th} percentile of size. Each plate was then scaled such that the PMM was equal to

the median colony size of all colonies within the screen. For the heatmaps, the average colony size was taken for each set of mutants within each plate and divided by the average colony size of the wildtype of the same plate to produce a fitness ratio. An ANOVA was performed between each mutant distribution of fitness ratios and the wildtype distribution of fitness ratios. A Tukey HSD analysis was then used to determine if distributions were significantly different. This was performed for each condition. Each individual fitness ratio was plotted as well as the mean fitness ratio for each mutant in each condition. Significance values between the mutant and the wildtype were denoted as such: *: 1.00e-02 < p <= 5.00e-02; **: 1.00e-03 < p <= 1.00e-02; ***: 1.00e-04 < p <= 1.00e-03; ****: p <= 1.00e-04.The average fitness ratios for each mutant in each condition was calculated between replicate plates for display. The 95% confidence intervals between replicates were calculated and displayed as error bars.

2.6 Standard protein procedures.

2.6.1. Purification of NlpI and the amidases.

NlpI was constructed using pET-28a(+) vector (soluble NlpI construct (N-terminal His-tag, Kan^R, from laboratory collection) and amplified from genomic DNA utilizing the primers 5'-GCTGCAGCACCGGAAGCTCC-3' containing the *Nde*I restriction site and 5'-GCCAGTCTACATAACTCATC-3' containing *Hind*III restriction site. Mature polypeptide with 20-294 residues, lacking the signal prosequence, was expressed in *E. coli* BL21 (Jolanda Verheul et al., 2022).

Cells were grown in 1- 2 L of LB broth at 37°C until OD_{600} = ~ 0.4 - 0.5. The culture was then induced using 1 mM IPTG and incubated for 3 – 4 hours at 30°C. Cells were centrifuged (6,000 – 7,000 x g, at 4°C, for 15 minutes) and yielded pellets were ready for purification by resuspending cell pellets using binding buffer (50 mM Tris-HCl with pH =7, 50 mM imidazole, 300 mM NaCl, and 0.5 mM TCEP) and Roche cOmplete EDTA-free protease inhibitor tablet(dilution of 1/1,000). Cells were sonicated and lysed using Avastin C3 Emulsiflex Cell disruptor. The lysate was prepared by centrifugation (16,700 rpm, at 4°C, for 1 hour). The supernatant was collected and incubated with 1 mL/L of Jena Bioscience Ni_2+ agarose beads (previously equilibrated with binding buffer) for 45 – 60 minutes with constant mixing. The sample was transferred to an elution column and washed using binding buffer, followed by protein elution using the elution buffer (50 mM Tris-HCl with pH =7, 500 mM imidazole, 0.5 mM TCEP, 300 mM NaCl). Amidases ABC and cognate activators EnvC and NlpD of *E. coli* were purified by other students as described (Uehara et al., 2010). The presence and purity of NlpI, amidases, and regulators proteins were checked by SDS-PAGE gel.

2.6.2 Sodium dodecyl sulphate-polyacrylamide gel electrophoresis (SDS-PAGE).

According to proteins molecular weights, they were separated using the discontinuous SDS-PAGE described by (Lugtenberg et al., 1975). The samples were mixed with sample-buffer (0.04 M Tris/HCl, 4% v/v glycerol, 2% w/v SDS, 0.01% w/v bromophenol blue, 2 mM β-mercaptoethanol, pH 6.8), and boiled for 10 minutes in water bath. The samples were loaded on a polymerized SDS polyacrylamide gel containing 10% or 12% polyacrylamide (w/v) according to the below table.

Table 3. Concentrations of reagents used for SDS-PAGE.

1x Running Gel Solution		
	10%	12%
Distilled water	12.3 mL	10.2 mL
Acrylamide (30% w/v)	9.9 mL	12.0 mL
20% SDS (w/v)	0.15 mL	0.15 mL
1.5 M Tris-HCl (pH 8.8)	7.5 mL	7.5 mL
10% ammonium persulfate (APS) (w/v)	0.15 mL	0.15 mL
TEMED	0.02 mL	0.02 mL
Stacking Gel solution (4% acrylamide)		
Distilled water	3.075 mL	
Acrylamide (30% w/v)	0.67 mL	
20% SDS (w/v)	0.025 mL	
0.5 M Tris-HCl (pH 6.8)	1.25 mL	
10% ammonium persulfate (APS) (w/v)	0.025 mL	
TEMED	0.005 mL	

The used gel electrophoresis system was filled with SDS running buffer (0.1% w/v SDS, 200 mM glycine, 25 mM Tris) and run at 120V. 5 µL of samples were loaded in the gel along with 2 µL of a protein ladder (New England Biolabs Color Prestained Protein Standard, Broad Range (10-25- kDa)) as a marker for molecular weight comparison.

2.6.3 SDS-PAGE gel Coomassie-staining.

The gel was stained with Coomassie dye (20% isopropanol, 0.2% Coomassie R-250, 0.4 M citric acid). Post-electrophoresis, the gel was de-stained with Coomassie-destaining solution (60% water, 10% acetic acid, 30% ethanol) until background of gel was clear.

2.6.4 Scanning and imaging of SDS-PAGE gel.

Gels were scanned with an Epson Perfection V350 Photo scanner. The professional mode of the accompanying software was used at a resolution of 400 or 600 dpi.

2.6.5 Protein concentration determination.

The concentration of a protein in solution was determined by using the BCA Microassay Reagent Kit from Pierce as described in the manufacturer's instructions. The protein determination assay was performed in a microtiter plate and scanned by a microtiter plate reader (Tecan). The measured absorption values of a BSA stock solution were plotted on a diagram to obtain the standard curve. Protein concentration was determined using the standard curve.

2.7 *In vitro* peptidoglycan degradation assay using FITC labelled sacculi.

2.7.1 *E. coli* sacculus purification and labelling with the fluorescent dye FITC.

The laboratory of Dr Patrick Moynihan purified PG from *E. coli* using a protocol by Glauner (Glauner et al., 1988) and provided the purified *E. coli* sacculi for the PG degradation assays I performed in chapter 4.

Labelling techniques have been developed and used, such as amino-acid side-chain chemical modification through covalent and/or non-covalent binding, incorporating affinity labelling such as FITC and RBBR (Remazol Brilliant Blue R) (Maeda, 1980; Glauner 1988; Uehara et al., 2010). In a round-bottom glass tube, purified PG was mixed with FITC powder using a weight ratio of 2:1. 4 mL of 0.5 M sodium bicarbonate buffer was added to the PG-FITC mix (**Figure 10**). A small magnetic stirrer was placed inside the mix tube and incubated at 37˚C on a magnetic mixer for no less than 4 hours. Mix tube was washed with sodium bicarbonate buffer and centrifuged (3,900 rpm, 4°C, 15 minutes). Supernatant was discarded and washed with sodium bicarbonate buffer by centrifugation (3,900 rpm, 4°C, 15 minutes) until excess FITC was removed. Then, the suspension was washed twice using 99.8% ethanol (centrifuged 3,900 rpm, 4°C, 15 minutes and discarded after each wash). Followed by washing twice using 99.8% acetone (centrifuged 3,900 rpm, 4°C, 15 minutes and discard after each wash). The acetone supernatant was removed without disturbing the pellet and the tube was securely placed inside a biohazard hood to evaporate overnight. The final product was stored dry and away from light. Dried and labelled PG was resuspended in sodium bicarbonate buffer to the desired concentration prior to use.

2.7.2 *In vitro* PG degradation assay using FITC labelled sacculi in 96 well format.

FITC-PG degradation assay was used to characterize soluble hydrolytic fragments released by PG hydrolases and set to measure spectrophotometrically. This protocol facilitated studying hydrolases activities in time-course or end-point experiments. The spectrophotometer will measure the released fluorescence from the degraded FITC labelled free-amines within PG sacculus. A master-mix was made by mixing 10 mg/mL PG-FITC labelled with 100 µL of reaction buffer (50 mM Tris, pH 8.0 + 150 mM NaCl) and 9 mL of distilled water (master-mix can be calculated as: [5 µL FITC-PG suspension (10 mg/mL) + 45 µL reaction buffer] x number of samples). A 100 µL of master-mix was transferred into microcentrifuge tubes and 2 µM of purified protein was added (amount of added protein can be calculated as:

$$X = \frac{\text{Protein molarity}}{2} \quad , \text{ Protein } \mu L = \frac{100}{X}$$

Lysozyme (4 µM) was used as the positive control, while a mixture of only reaction buffer and FITC-PG as the negative control. Samples and controls were placed in a 37°C heat-block and incubated for 60 minutes with maximum speed agitation. All samples and controls were transferred into a 'sample plate' of a 0.22 µm (Millipore) MultiScreen GV 96-well Filter Plate and a 96-well plate (Black Flat Bottom Microplate) was accurately positioned under 'sample plate' and secured properly. Plates were centrifuged at 4°C, 2500 rpm, for 3 minutes to stop the reaction by filtration. After centrifugation, samples and controls were filtered through the 'sample plate' into Black Flat Bottom Microplate and were added 50 µL of 0.5 M NaOH to normalize pH and reaction stopped. The Black Flat Bottom Microplate containing samples and controls was then placed in Omega plate reader (BMG Labtech) to measure the fluorescence of

soluble fraction (**Figure 10**) (FITC fluorescence intensity was measured at 485 nm excitation and 525 nm emission).

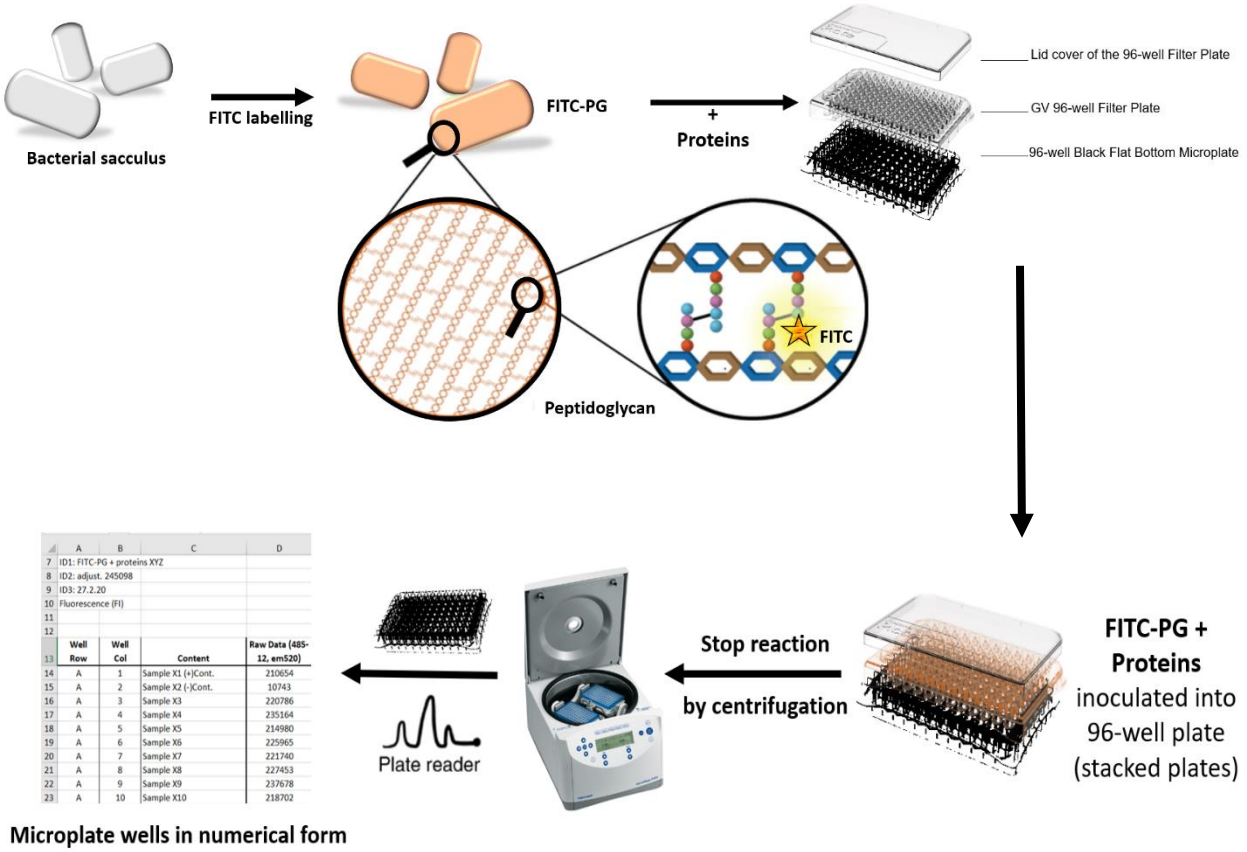

Figure 10. Schematic illustration of FITC labelling of *E. coli* sacculus and degradation assay.
Bacterial sacculus (white sacculus) is labelled by FITC (orange sacculus). The isothiocyanate group of FITC reacts with the amino group of PG peptides to form covalent amine bond. PG degradation assay starts by preparing the super mix of FITC-PG with proteins-of-interests at equal ratios (unless mentioned otherwise) and incubated in a 37°C heat-block shaker (maximum speed). After incubation, this mixture is transferred into a GV 96-well filter plate and placed between the lid cover (top lid cover) and the 96-well black plate (bottom), and centrifuged. The 96-well black plate is then placed in a plate reader to measure the fluorescence yielded from FITC-PG degradation and show microplate wells in numerical format.

Chapter 3. Investigation Of Functional-Dependencies Between PG Hydrolases and The Bifunctional Class A PBPs Across Stress Conditions In *E. coli.*

3.1 Introduction.

Gram-negative bacteria have a thin peptidoglycan (PG) layer between the cytoplasmic and outer membranes, protecting the cell against bursting due to the turgor (Vollmer & Seligman, 2010). PG is composed of glycan chains connected by peptides, forming a mesh-like sacculus. Growing and dividing cells expand their PG layer by inserting new PG into the sacculus through the combined activities of PG synthases and hydrolases (Egan *et al.*, 2015; Typas *et al.*, 2010). Most bacteria have multiple PG synthases (see **1.2.3.1**). Glycosyltransferases (GTases) polymerize PG chains from lipid II precursor and this activity is provided by shape, elongation, division, and sporulation proteins (SEDS) (see **1.2.3.1.2**) (Meeske *et al.*, 2016), monofunctional glycosyltransferases (Hara & Suzuki, 1984) and class A Penicillin-binding proteins (PBPs). DD-transpeptidases (TPases) cross-link the peptide linked to adjacent chains and this activity is provided by class A and B PBPs (Vollmer & Bertsche, 2008).

In *Escherichia coli* the class A PBP1A and PBP1B are responsible for synthesizing a major portion of the new PG (Cho *et al.*, 2016; Yang *et al.*, 2021). The depletion of both PBPs is lethal, but the absence of one of them only slightly affects cell growth or morphology, suggesting redundant roles (Kato *et al.*, 1985; Yousif *et al.*, 1985). However, both PBPs require a different outer membrane-anchored lipoprotein activator for functioning in the cell - LpoA for PBP1A and LpoB for PBP1B (Paradis-Bleu *et al.*, 2010, Typas *et al.*, 2010) - and there is evidence that both PBPs may have preferred cellular roles. PBP1A interacts with PBP2, which is needed for cell elongation (Banzhaf *et al.*, 2012a) whereas PBP1B interacts with PBP3, which is essential for cell division (Bertsche *et al.*, 2006b). In addition, both PBPs have different functionality under stress conditions. Cells lacking the *mrcB* gene (which encodes for PBP1B) are not viable at acidic pH and

cells lacking *mrcA* (which encoded for PBP1A) are sick at alkaline pH (Mueller *et al.*, 2019a). In addition, *mrcB* mutants are sensitive to osmotic stress caused by sucrose (Pepper *et al.*, 2006).

PG hydrolases (**Figure 11**) (see **1.2.3.2**) are also needed for sacculus growth, facilitating the insertion of the new PG strands during cell elongation and cleavage of septal PG for daughter cell separation during cell division (Egan *et al.*, 2015)**.** The activities of PG synthases and hydrolases need to be tightly regulated and coordinated to allow for accurate expansion of the sacculus and prevent cell lysis (Egan *et al.*, 2020; Typas *et al.*, 2012; Vollmer & Höltje, 2001). This coordination is likely achieved by protein-protein interactions of PG synthases, hydrolases and/or regulator proteins. We currently do not know whether PBP1A or PBP1B can interchangeably work with *E. coli*'s entire arsenal of periplasmic PG hydrolases (autolysins), which include 4 N-acetylmuramoyl-L-alanine amidases, 7 endopeptidases (EPases) and 8 lytic transglycosylases (Vermassen *et al.*, 2019; Vollmer *et al.*, 2008), although several protein-protein interactions have been observed (Banzhaf *et al.*, 2012, Banzhaf *et al.* 2020, Bertsche *et al.*, 2006, Pazos & Vollmer, 2021). Amidases (see **1.2.3.2.1**) remove peptides from the glycan strands and DD-EPases hydrolyse DD-cross-links. In this study, we focused on the 3 well described amidases crucial for septation, AmiA, AmiB and AmiC. Amidases are activated by EnvC (AmiA and AmiB) (Uehara *et al.*, 2009; Uehara *et al.*, 2010; Yang *et al.*, 2011), NlpD (AmiC) (Tsang *et al.*, 2017) and ActS (AmiA, AmiB and AmiC) (Gurnani Serrano *et al.*, 2021; Mueller *et al.*, 2021). We also included the main DD-EPases, MepA, MepM, MepH, MepS, PBP4 and PBP7 (Chodisetti & Reddy, 2019; Singh *et al.*, 2015; Singh *et al.*, 2012b; Voedts *et al.*, 2021).

We probed the genetic interactions of *mrcA* and *mrcB* in various envelope stresses in *E. coli*. Our analysis shows that the genetic interaction-network between the class A PBPs and the amidases

and endopeptidases lacks strongly interacting pairs and hence none of the hydrolases is specifically required for PBP1A or PBP1B function. However, we discovered that the fitness of Δ*mrcB* cells is significantly reduced under high salt stress and confirm that this phenotype is likely caused by a reduced PG synthesis activity of PBP1A at high salt concentration. This project is part of collaboration between the Dr Manuel Banzhaf group and Prof Waldemar Vollmer laboratory. Vollmer laboratory performed and provided data of the GTase/TPase and FRET activity assays (**Figure 17, Figure 18,** and **Table 5**).

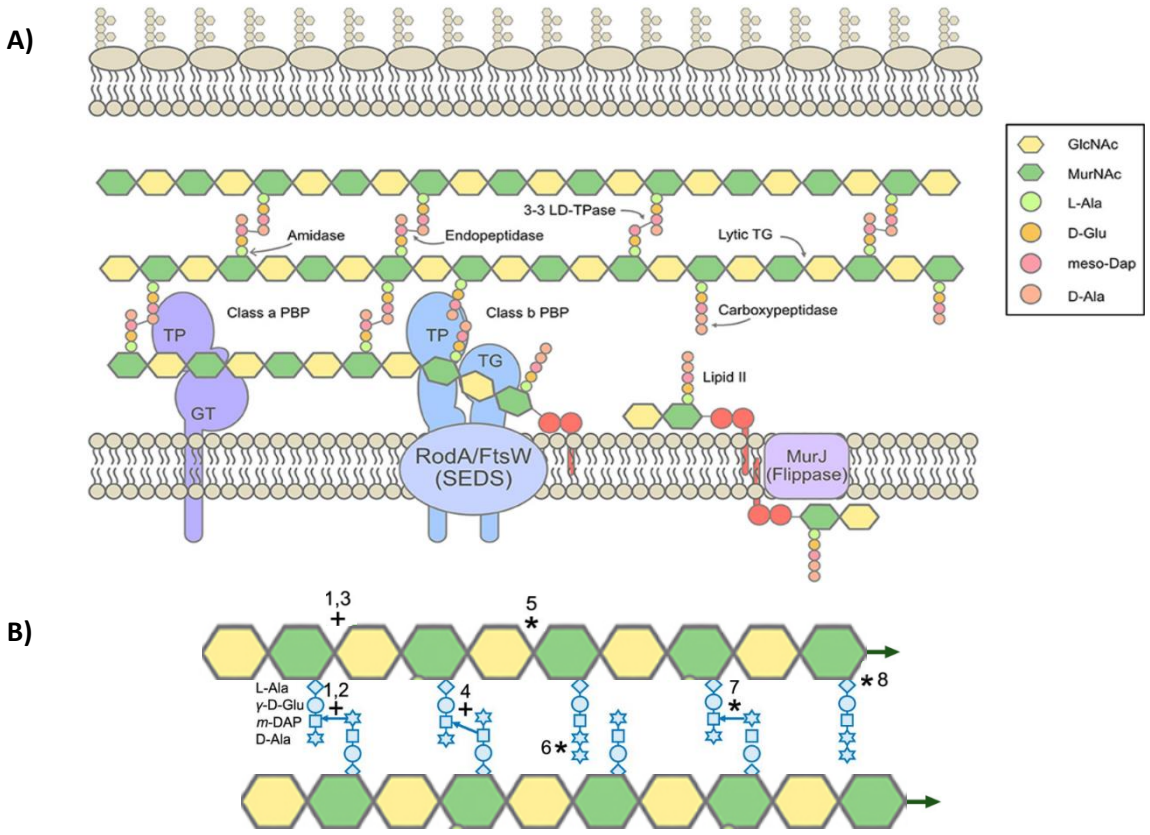

1. DD-TPases/GTases (bifunctional): PBP1A, PBP1B, PBP1C.

2. DD-TPases (monofunctional): *PBP2*, *PBP3*

3. GTases (monofunctional): *RodA*, *FtsW*, MtgA

4. LD-TPases: LdtA – LdtF

5. LTs: Slt, MltA – MltG

6. CPases: PBP4 – PBP7, AmpH

7. Epases: MepA, MepM, MepS, MepH, MepK, PBP4, PBP7

8. Amidases: AmiA, AmiB, AmiC, AmiD

Figure 11. Overview of cell wall synthases/hydrolases activities in *E. coli*. A) The PG synthesis (see **1.2.3** – **1.2.3.2.2** sections for more details) process involves three primary stages: (1) producing the crucial intermediate lipid II, which is a precursor consisting of a lipid-linked disaccharide-pentapeptide, within the cytoplasm; (2) transporting lipid II across the cytoplasmic membrane; and (3) constructing the cell wall within the periplasmic space (Delhaye et al., 2019). **B)** overview of extracellular peptidoglycan enzymes and their functions in *E. coli* illustrating key synthesis reactions (# 1 - 4 and denoted by "**+**" symbol), autolysis reactions (# 5 - 8 and denoted by "*****" symbol), along with the corresponding enzymes involved. Crucial enzymes are highlighted in italicized text. The abbreviation m-DAP stands for meso-diaminopimelic acid.

3.2 Results.

3.2.1 Salt stress reduces fitness of Δ*mrcB* mutants.

In this study, we explored whether the two major *E. coli* PG synthases PBP1A and PBP1B have preferred (genetic) interactions with or are dependent on certain PG endopeptidases and amidases, or if these PG synthases and hydrolases can function interchangeably with each other. We first tested whether double mutants lacking a PG hydrolase and either *mrcA* (PBP1A) or *mrcB* (PBP1B) had an altered cell morphology. We generated a panel of single mutants lacking amidases/regulators (*amiA, amiB, amiC* and *nlpD, envC*) or EPases (*mepA, mepS, mepM, mepH, pbpG, dacB*), and double mutants in combination with Δ*mrcA* and Δ*mrcB*, by P1 transduction into the *E. coli* BW25113 background (WT - wildtype) (**Figure 12** and **Table 4**). We were unable to generate a Δ*envC*Δ*mrcB* mutant, suggesting that the simultaneous deletion of *envC* and *mrcB* may be synthetic lethal, and we are currently exploring this observation in a separate study.

We next analysed the morphology of all mutant cells using phase contrast and fluorescence microscopy. We grew the mutants to mid-exponential phase under standard laboratory conditions for *E. coli* (37°C, LB medium, pH 6.9). Cells were stained with both, membrane dye (FM-143 FX) and DNA dye (DAPI), and the images were analysed with the MicrobeJ plugin Fiji to quantify septa, cells length and cell width.

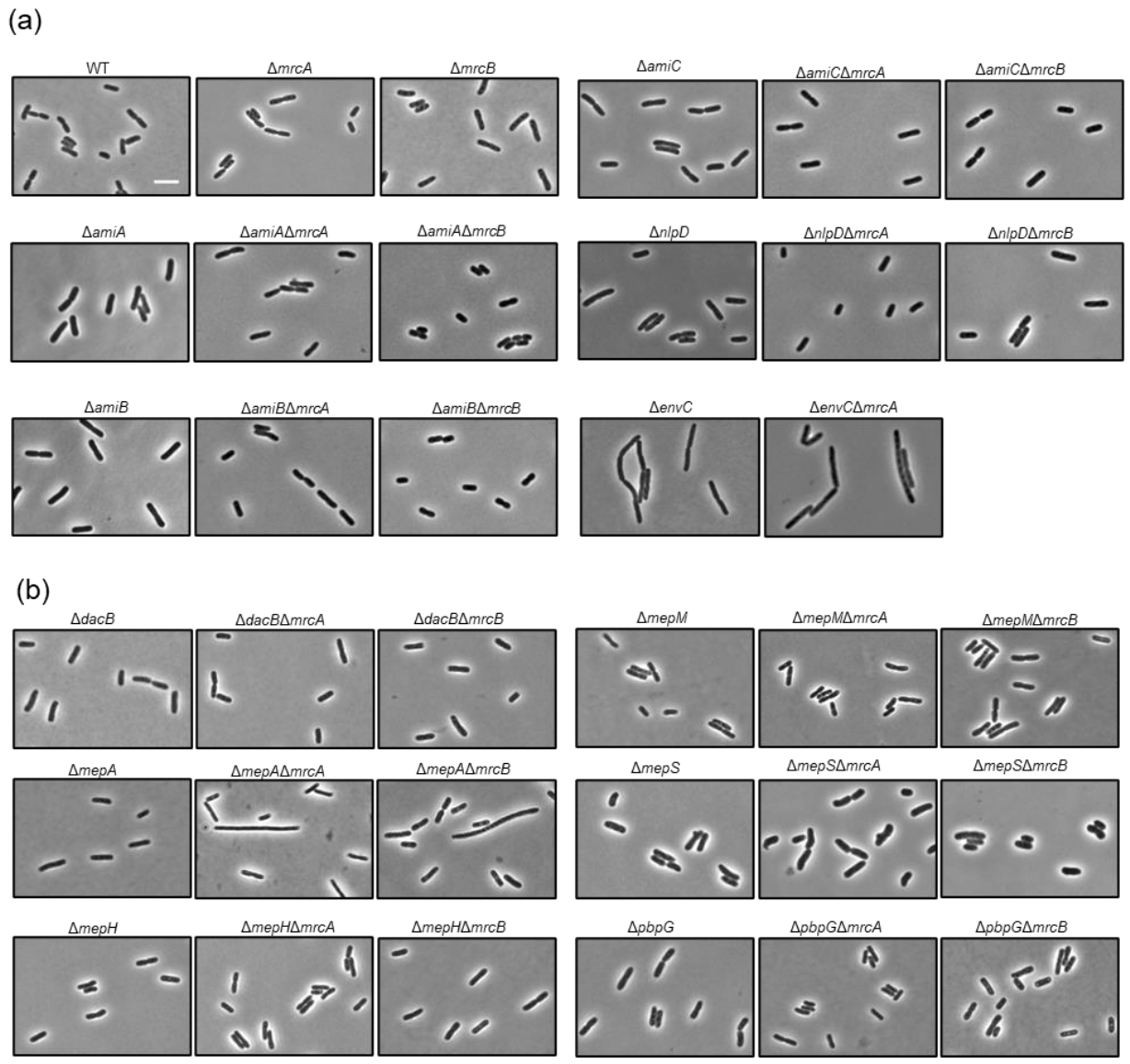

Figure 12. Absence of EPases DacB, MepM, MepA, MepS, MepH and PbpG and amidases/regulators AmiA, AmiB, AmiC, NlpD and EnvC on Δ*mrcA* and Δ*mrcB* cells causes mild changes on morphology. Phase contrast microscopy of (a) *E. coli* BW25113 WT, Δ*mrcA,* Δ*mrcB,* Δ*amiA,* Δ*amiB,* Δ*amiC,* Δ*nlpD,* Δ*envC* and respective Δ*mrcA* and Δ*mrcB* double mutants, (b) Δ*dacB,* Δ*mepA,* Δ*mepH,* Δ*mepM,* Δ*mepS,* Δ*pbpG* and respective Δ*mrcA* and Δ*mrcB* double mutants in mid-exponential phase growth (OD_{600}=0.4) in LB medium at 37°C. Scale Bar = 5 µm. Images of fluorescence microscopy in **Appendix**.

Relevant genotype	No. of cells [1]	Avg length (µm)[2]	Avg width (µm)[3]	Total no. of septa[4]	Length/ Segment (µm)[5]	No. of chaining cells[6]	% of chaining cells[7]	Phenotype observation reference
WT	445	3.6 ± 0.9	0.99 ± 0.1	179	2.6	0	0	
Δ*mrcA*	249	3.7 ± 1.0	0.90 ± 0.2	127	2.5	3	1.2	(Lam et al., 2009)
Δ*mrcB*	260	3.8 ± 1.0	0.93 ± 0.1	128	2.5	5	1.9	(Jorgenson et al., 2019)
Δ*amiA*	177	5.4 ± 1.3	1.06 ± 0.1	100	3.4	4	2.3	(Boelter et al., 2022)
Δ*amiA*Δ*mrcA*	204	3.8 ± 1.1	0.86 ± 0.1	99	2.5	3	1.5	This study
Δ*amiA*Δ*mrcB*	226	2.7 ± 0.9	0.95 ± 0.1	78	2.0	7	3.1	This study
Δ*amiB*	167	4.9 ± 1.0	1.05 ± 0.1	82.0	3.3	0	0	(Boelter et al., 2022)
Δ*amiB*Δ*mrcA*	180	3.7 ± 1.4	0.88 ± 0.1	108	2.3	8	4.4	This study
Δ*amiB*Δ*mrcB*	245	2.6 ± 0.8	0.93 ± 0.1	74	2.0	5	2.0	This study
Δ*amiC*	286	5.0 ± 1.4	1.04 ± 0.1	142	3.4	0	0	(Boelter et al., 2022)
Δ*amiC*Δ*mrcA*	259	3.7 ± 2.1	0.93 ± 0.1	150	2.4	10	3.9	This study
Δ*amiC*Δ*mrcB*	137	3.8 ± 1.1	0.95 ± 0.1	73	2.5	2	1.5	This study
Δ*envC*	294	7.2 ± 4.5	0.96 ± 0.1	481	2.7	110	37.4	(Boelter et al., 2022)
Δ*envC*Δ*mrcA*	143	6.6 ± 5.4	0.82 ± 0.1	144	3.3	26	18.2	This study
Δ*envC*Δ*mrcB*	ND	ND	ND	ND	ND	ND	ND	This study
Δ*nlpD*	218	4.7 ± 1.2	1.04 ± 0.1	89	1.9	0	0	(Boelter et al., 2022)
Δ*nlpD*Δ*mrcA*	180	3.4 ± 1.3	0.90 ± 0.1	61	2.6	1	0.6	This study
Δ*nlpD*Δ*mrcB*	136	3.6 ± 0.9	0.98 ± 0.1	53	2.6	1	0.7	This study
Δ*dacB*	338	4.2 ± 1.1	1.05 ± 0.1	146	2.9	4	1.2	(Jeon & Cho, 2022)
Δ*dacB*Δ*mrcA*	431	4.1 ± 1.0	0.98 ± 0.1	238	2.6	6	1.4	This study
Δ*dacB*Δ*mrcB*	261	4.2 ± 1.4	1.05 ± 0.1	123	2.8	8	3.1	This study
Δ*mepA*	243	4.4 ± 1.7	0.95 ± 0.1	170	2.7	14	5.8	(Jeon & Cho, 2022)
Δ*mepA*Δ*mrcA*	407	4.9 ± 3.4	0.77 ± 0.1	286	2.9	42	10.3	This study
Δ*mepA*Δ*mrcB*	483	6.1 ± 4.4	0.93 ± 0.1	137	4.7	62	12.8	This study
Δ*mepH*	322	3.9 ± 1.1	0.90 ± 0.1	175	2.5	2	0.6	(Jeon & Cho, 2022)
Δ*mepH*Δ*mrcA*	428	3.6 ± 1.0	0.80 ± 0.1	221	2.4	5	1.2	This study
Δ*mepH*Δ*mrcB*	509	3.8 ± 1.0	0.95 ± 0.1	207	2.7	0	0.0	This study
Δ*mepM*	332	3.7 ± 0.9	0.94 ± 0.1	169	2.4	2	0.6	(Jeon & Cho, 2022)
Δ*mepM*Δ*mrcA*	467	3.7 ± 0.9	0.85 ± 0.1	224	2.5	2	0.4	This study
Δ*mepM*Δ*mrcB*	330	4.0 ± 1.1	0.97 ± 0.1	157	2.7	1	0.3	This study
Δ*mepS*	232	4.5 ± 1.4	1.12 ± 0.1	115	3.0	3	1.3	(Banzhaf et al., 2020)
Δ*mepS*Δ*mrcA*	604	4.7 ± 2.1	1.20 ± 0.1	245	3.4	23	3.8	This study
Δ*mepS*Δ*mrcB*	231	4.1 ± 1.4	1.19 ± 0.2	89	3.0	3	1.3	This study
Δ*pbpG*	225	3.9 ± 1.0	1.10 ± 0.1	90	2.8	0	0.0	(Jeon & Cho, 2022)
Δ*pbpG*Δ*mrcA*	260	3.3 ± 0.8	0.88 ± 0.1	101	2.4	2	0.8	This study
Δ*pbpG*Δ*mrcB*	203	4.0 ± 1.0	0.98 ± 0.1	108	2.6	1	0.5	This study

Table 4. Phenotypes of Δ*mrcA,* Δ*mrcB*, amidases and endopeptidases mutants in LB.

1. All cells were considered single cells independent of the number of segments.
2. Refers to the total length/number of cells.
3. Refers to the total width/number of cells.
4. Septa are considered as any membrane constrictions or completed membrane septa in cell chains.

5. The number of cell segments refers to the number of cells plus the number of septa. The "length/segment" is the total length/total number of segments. In normal (non-chaining) cells, this measurement is similar to the average cell length (pole-pole distance), but the value is smaller because pre-divisional cells contain two segments and are counted as two cells instead of one (i.e., some pole-to-septa measurements are taken into account, as well as pole-pole measurements). In chaining cells, the length/segment measurement refers mainly to the distance between adjacent septa.
6. Cells with more than one septum are considered chaining cells.
7. Percentage of chaining cells related to the total no. of cells.

All single mutants showed wildtype-like or mild abnormal morphologies in accordance to previously published work (Banzhaf *et al.*, 2020; Boelter *et al.*, 2022) (**Figure 12**). However, some of the double mutants showed mild changes in morphology compared to their parental mutants (**Figure 12** and **Table 4**). Cells of Δ*mepS*Δ*mrcA* and Δ*mepS*Δ*mrcB* were slightly wider than Δ*mepS* (1.20 µm, 1.19 µm and 1.12 µm, respectively), and Δ*amiA*Δ*mrcB* and Δ*amiB*Δ*mrcB* cells were shorter (2.7 µm and 2.6 µm, respectively) than Δ*amiA* (5.4 µm) and Δ*amiB* (4.9 µm). In addition, Δ*mepA*Δ*mrcA* (length 4.9 µm) and Δ*mepA*Δ*mrcB* (6.1 µm) grew longer in contrast to Δ*mepA* (4.4 µm) and had an increased rate of filamentation (10.3%, 12.8% and 5.8%). These observations point to altered functionalities of the class A PBPs, but did not uncover a clear dependency of PBP1A or PBP1B on one of the tested hydrolases.

This result might not be unexpected as *E. coli* harbors an arsenal of hydrolases that are collectively able to complement each other in standard laboratory conditions (Pazos *et al.*, 2017). However, previous work showed that PBP1A and PBP1B have different pH requirements to be functional (Mueller *et al.*, 2019b), suggesting that PG enzymes might have specialized roles depending on the growth environment. Hence, we tested whether envelope targeting stresses impact fitness of the mutant panel and whether the mutants genetically interact under these conditions. Mutants were pinned on agar plates supplemented with metal chelator EDTA (ethylene diamine tetra acetic acid), SDS (sodium-dodecyl sulphate), vancomycin, 600 mM NaCl,

0 mM NaCl, at pH 4.8 or pH 8.2, and incubated for 18 hours at 37°C or, for some conditions, at 18°C, 25°C and 42°C to probe for heat stress. End point images were analyzed by the software Iris (Kritikos *et al.*, 2017) to quantify colony size as a proxy of fitness. Fitness ratios of 1.0 indicate WT fitness. Values below 1.0 represent reduced fitness, values above 1.0 indicate improved fitness of a mutant compared to WT growth in the same condition (**Figure 13**).

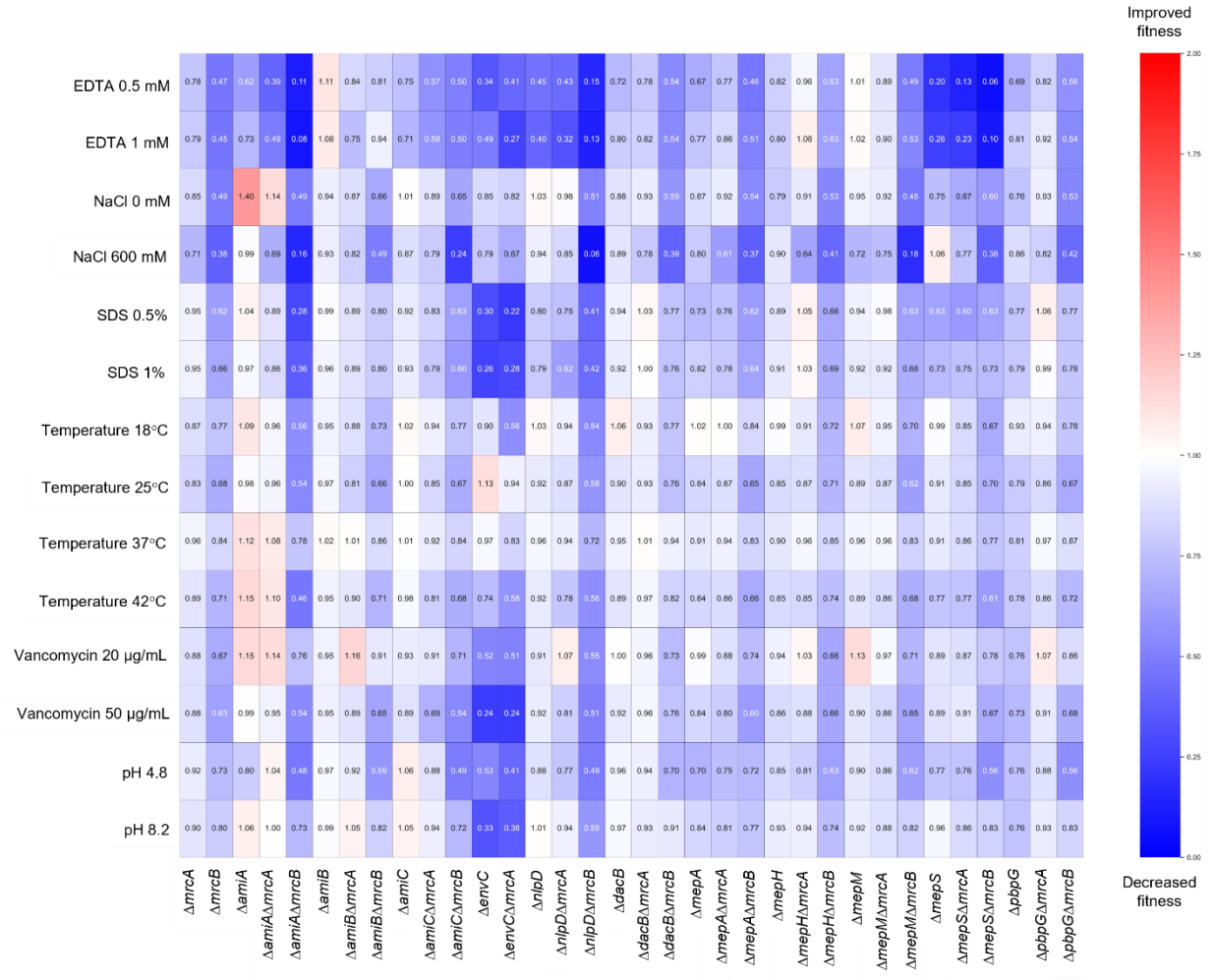

Figure 13. **Chemical genomics screening indicates high and no NaCl conditions as the harshest stress for the mutants tested causing decreased fitness**. Heatmap of chemical genomics screening generated by ChemGAPP of Δ*mrcA,* Δ*mrcB,* EPases and amidases mutants under chemical perturbations. The different colours represent the colony size compared to WT of each condition ranging from blue (smaller colony

size and decreased fitness) through white (WT size) to red (larger colony size and increased fitness). Colony size was considered as fitness readout.

Subsequently, genetic interactions were calculated by ChemGAPP GI (Doherty *et al.*, 2023). The package calculates the fitness ratio of two single mutants (ΔA and ΔB) and the double mutant ΔAΔB compared to the WT strain, and then calculates the expected double mutant fitness ratio, comparing it to the observed fitness ratio (**Figure 14**).

As anticipated, the envelope stress screen revealed multiple phenotypes for us to explore. Overall, the strongest fitness defects were observed in mutants lacking *mrcB* when exposed to acidic pH, EDTA and salt stress. This aligns with the notion that PBP1B functions more robust in cells than PBP1A (Mueller *et al.*, 2019b).

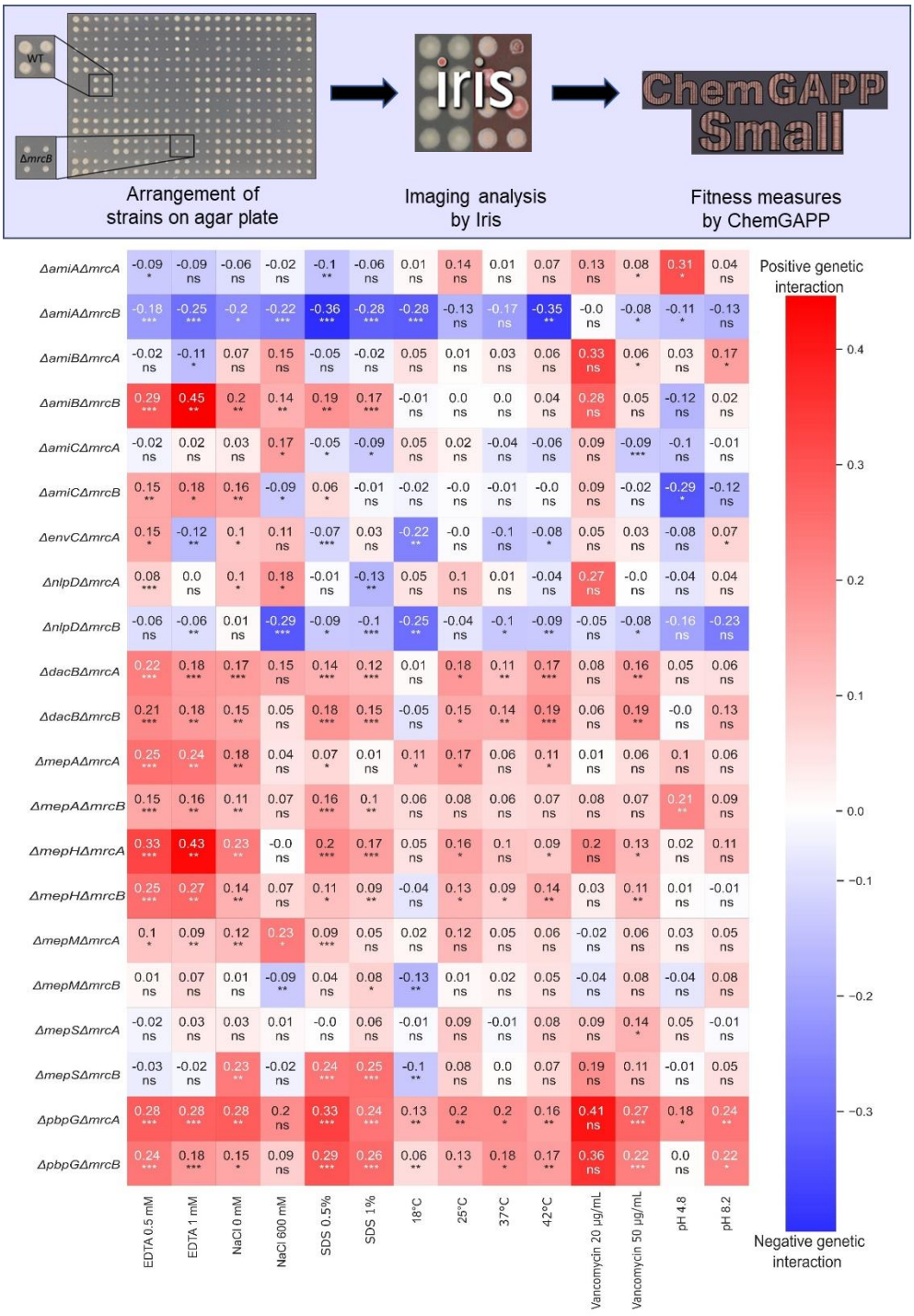

Figure 14. **Chemical genomics screening of double mutants in stress conditions**. **A** Schematic of chemical genomics screening, imaging analysis of colony size and fitness measures. In detail, 4 replicates of WT and Δ*mrcB* showing the difference of colony sizes grown on 600 mM NaCl LB agar plate. **B** Heatmap of genetic interaction generated by ChemGAPP GI after chemical genomics screening of Δ*mrcA,* Δ*mrcB* and EPases (*mepS, mepA, mepH, mepM, pbpG* and dacB) and amidases/regulators (*amiA, amiB, amiC, nlpD* and *envC*) mutants under chemical perturbations. The colony size was considered as fitness readout (see text for more details). The different colours

represent the genetic interaction ranging from blue (negative genetic interaction, negative values) to red (positive genetic interaction, positive values).

As acidic pH severely affects *mrcB* mutants, we first looked at this condition in our panel (**Figure 14B**). At pH 4.8 we found a positive genetic interaction (0.31) when deleting both, *amiA* and *mrcA*, meaning that deletion of both genes leads to increased fitness. This could be due to the previously suggested specialised function of AmiB at acidic pH (Mueller *et al.*, 2021) promoting cell growth in the absence of AmiA and PBP1A. On the opposite, we observed a negative genetic interaction between *amiC* and *mrcB,* as deleting both genes led to decreased fitness (-0.29). We also observed a negative interaction between Δ*amiA* and Δ*mrcB* (-0.11). It seems that a further deletion of *amiA* or *amiC* exacerbates the sickness of Δ*mrcB* cells at acidic pH (Mueller *et al.*, 2019a).

Addition of the metal chelator EDTA into the media affected severely the fitness (<0.2) of all strains lacking *mepS*, and the Δ*nlpD*Δ*mrcB* and Δ*amiA*Δ*mrcB* double mutants (**Figure 14**). The depletion of MepS and MepM together is synthetic lethal (Singh *et al.*, 2012a) and EDTA diminishes the function of MepM, which is a metal-dependent EPase, explaining the reduced fitness of all strains lacking *mepS*. The severe fitness loss of Δ*amiA*Δ*mrcB* is likely unrelated to MepM, as an Δ*amiA*Δ*mrcB*Δ*mepM* mutant is viable (**Figure 15**).

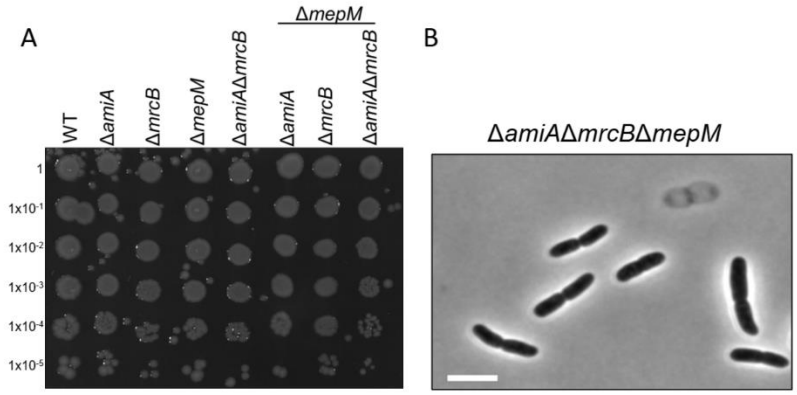

Figure 15. The triple mutation Δ*amiA*Δ*mrcB*Δ*mepM* is viable and shows a reduced lysis. A Strains WT, Δ*amiA*, Δ*mrcB*, Δ*mepM*, Δ*amiA*Δ*mrcB*, Δ*amiA*Δ*mepM,* Δ*mrcB*Δ*mepM* and Δ*amiA*Δ*mrcB*Δ*mepM* were grown overnight in LB at 37 °C. The cultures were adjusted to OD600=1 and serially diluted (10^{-1} to10^{-6}). 5 µl of each dilution was spotted on LB agar. The plates were incubated at 37 °C and photographed after ~16 h. **B** Phase contrast microscopy of Δ*amiA*Δ*mrcB*Δ*mepM* cells grown in LB at 37°C until mid-exponential phase growth (OD600=0.4). Scale bar = 5µm

We also observed a strong positive genetic interaction at both EDTA concentrations (0.5 mM and 1 mM) of Δ*amiB*Δ*mrcB* (0.29 and 0.45) indicating that inactivation of MepM is beneficial in the absence of AmiB and PBP1B. We also observed positive genetic interactions between Δ*mepH* and Δ*mrcA* (0.33 and 0.43) and, to lesser extent, between Δ*mepH* and Δ*mrcB* (0.25 and 0.27) (**Figure 14B**). In these cases, MepS may function better with either PBP in the absence of MepM and MepH. However, as EDTA causes pleiotropic effects on both cell membranes beyond the inactivation of MepM, it is difficult to draw more detailed conclusions.

Salt (NaCl) stress modulates the intracellular osmotic pressure by either decreasing it (high salt levels) or increasing it (low salt levels). Both osmotic extremes affect the envelope integrity negatively as they potentially constrain membrane fluidity, protein-protein interactions and

protein function. We noticed that the Δ*mrcB* single mutant had decreased fitness (0.49 and 0.38) at both, 0 and 600 mM NaCl (**Figure 13**), resulting in many positive and negative genetic interactions (**Figure 14B**). Most notably, in 600 mM NaCl we observed genetic interaction of *mrcB* with *amiA* (-0.22), *amiB* (0.14) *nlpD* (-0.29) and *amiC* (-0.09). As NlpD activates AmiC it is expected that both genetic interactions phenocopy each other. Interestingly, between *amiA* and *amiB* we observed an inverse fitness pattern despite both amidases sharing EnvC as their activator. This suggests that AmiB might be important for fitness at high salt.

The envelope stress screen of the PBP-hydrolase mutant panel confirmed several of the already known genetic interaction pairs in pH and EDTA stress. In addition, we observed that Δ*mrcB* had reduced fitness in salt stress indicating that PBP1A alone might not be sufficient to uphold cell growth. To test this hypothesis, we next explored how salt stress affects the morphology of some of the *mrcB*-hydrolase mutants.

3.2.2 Cells need PBP1B or AmiC-NlpD under high salt stress.

To test how salt stress affects the cell morphology we analyzed some of the most severely affected mutants: Δ*amiC*Δ*mrcB*, Δ*nlpD*Δ*mrcB,* Δ*mepS*Δ*mrcB* and the respective control strains, using phase contrast and fluorescence microscopy as described above.

As expected, Δ*mrcB* cells were sick in both salt stresses and 16% of all analysed Δ*mrcB* cells showed signs of cell lysis (**Figure 16** and **Table 6** in **Appendix**). In 600 mM NaCl, the lysis of Δ*mepS*Δ*mrcB* was increased to 40% (**Figure 16** and **Table 6** in **Appendix**).

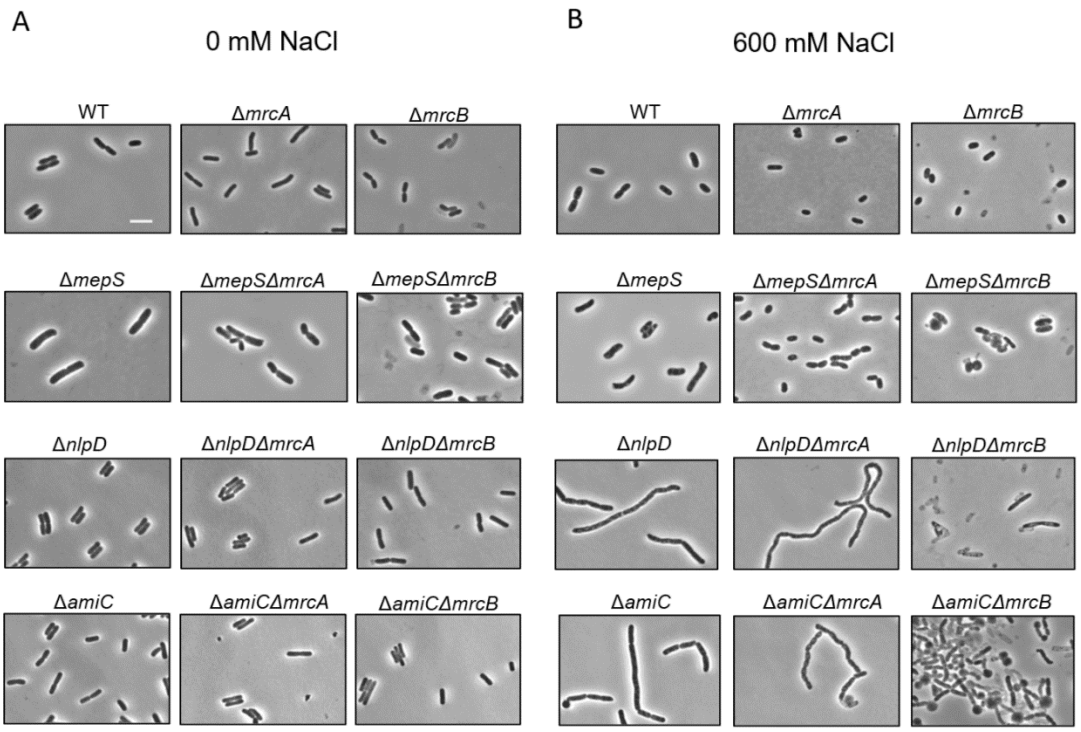

Figure 16. *mepS, nlpD* and *amiC* deletions enhance growth defect of Δ*mrcB* mutants under high salt stress. Phase contrast microscopy of WT exponential phase (OD600=~0.2), back-diluted to media altered with **A** 0 mM NaCl or **B** 600 mM NaCl and grown until OD600=~0.2. Scale bar= 5 µm. Images of fluorescence microscopy are shown in **Appendix**.

Considering the prominent role of MepS in cell elongation and its interaction with PBP1A (Banzhaf *et al.*, 2020; Singh *et al.*, 2012a) the increased lysis of Δ*mrcB*Δ*mepS* in high salt stress is not surprising. Almost all cells of Δ*amiC*Δ*mrcB* and Δ*nlpD*Δ*mrcB* showed signs of lysis confirming the observed severe negative genetic interactions (**Figure 14**). However, Δ*amiC*Δ*mrcA* and Δ*nlpD*Δ*mrcA* cells exclusively chained (>95% of all cells) compared to their controls, Δ*mrcA* (0%), Δ*amiC* (49.2%) and Δ*nlpD* (65.5%) (**Figure 16** and **Table 4** in **Appendix**). As both, Δ*amiC*Δ*mrcA* and

Δ*nlpD*Δ*mrcA* also had positive genetic interactions, this indicates that in high salt, cells need either PBP1B or NlpD-AmiC to successfully separate into daughter cells. In 0 mM NaCl we did not observe notable morphological abnormalities in the strains tested. Together, these data provide additional evidence that the observed phenotypes may be related to the inability of class A PBPs to properly function in cells growing in the presence of high concentration of NaCl.

3.2.3 The activity of class A PBPs is reduced at high salt.

Our previous efforts to identify potential hydrolases as preferred partners by class A PBPs in certain stress conditions did not show a clear dependency of PBP1A or PBP1B with one of the tested hydrolases, instead our results showed a notable impact on Δ*mrcB* cells under salt stresses. In collaboration with Prof Waldemar Vollmer, we sought to investigate this impact of salt concentration on PBP1A and PBP1B function highlighting the salt requirements for proper activity. The Vollmer laboratory conducted experiments to determine if the activities of PBP1A and PBP1B are affected by NaCl. We assayed the purified enzymes in two buffer conditions with different concentrations of NaCl: low salt (minimum NaCl concentration achievable upon dilution of proteins stock into reaction conditions, 30 mM NaCl for PBP1B and 45 mM for PBP1A) and high salt (500 mM NaCl). We used three different activity assays to monitor the glycosyltransferase (GTase) and/or transpeptidase (TPase) activities of these proteins. In every case, we measured the activity of PBP1A and PBP1B in the presence or absence of their cognate activator, LpoA and LpoB, respectively.

We first used a real-time GTase assay using dansyl-labelled lipid II which is based on the reduction in fluorescence intensity of the dansyl probe upon polymerization of glycan strands and

subsequent digestion to muropeptides by cellosyl present in the reaction (**Figure 17A**) (Egan & Vollmer, 2016). The apparent GTase rate obtained in this assay for PBP1A reactions was 60-70% lower at high salt than at low salt (**Figure 17A** and **Table 5**). LpoA mildly activated the PBP1A GTase rate at low salt and had no effect at high salt (**Figure 17A** and **Table 5**). PBP1B had ~80% lower apparent GTase activity at high salt than at low salt. LpoB strongly increased the GTase rate, as previously published (Typas et al., 2010, Egan *et al*. 2014, Lupoli *et al*. 2014), but at high salt the apparent GTase rate with activator was ~40% decreased compared to low salt (**Figure 17A** and **Table 5**). Interestingly, the apparent GTase rates obtained for PBP1B were nearly an order of magnitude higher than those for PBP1A when comparing reactions under the same buffer conditions (**Figure 17A** and **Table 5**). This observation is even more relevant considering that PBP1B reactions were performed at 25°C and PBP1A reactions at 30°C.

We next analysed the TPase function of both PBPs in the same conditions as above using an end-point assay in which the PG product from radiolabelled lipid II was digested with cellosyl and the resulting muropeptides quantified by HPLC (**Figure 17**B) (Banzhaf *et al.*, 2012a; Biboy *et al.*, 2013). The percentage of transpeptidation products decreased at high salt compared to low salt conditions for both proteins, with a higher decrease for PBP1B than for PBP1A (**Figure 17**B, left panel). LpoA and LpoB increased the proportion of transpeptidation products for their cognate enzyme in both conditions (**Figure 17**B, left panel). Interestingly, we noticed a substantial increase in DD-carboxypeptidase (CPase) products for PBP1A in the presence of LpoA at high salt compared to low salt conditions without LpoA (Fig. 4B, right panel); such an increase was not observed for PBP1B (**Figure 17**B, right panel). We noticed previously that both PBP1A and PBP1B have inherent CPase side activity, which is enhanced at acidic pH in the presence of the cognate

activator, removing the terminal D-Ala at position 5 of the donor peptide instead of performing a TPase reaction (Egan *et al*. 2015). As this is an end-point assay that shows the composition of the PG product synthesized, it was not possible to distinguish differences in the TPase rates between PBP1A and PBP1B. Nonetheless, these results show that PBP1B produced a slightly more crosslinked PG (54 ± 3% cross-linked peptides) than PBP1A (44 ± 3% cross-linked peptides) at low salt and PBP1A produced more cross-linked PG (16 ± 1% cross-linked peptides) than PBPB (13.7 ± 0.9% cross-linked peptides) at high salt (**Table 5**).

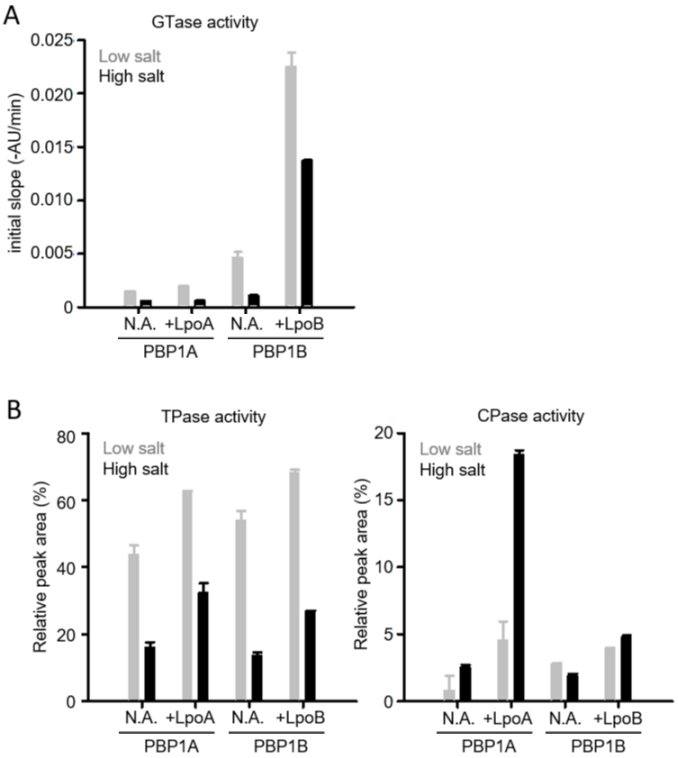

Figure 17. Gtase and TPase activties of PBP1A and PBP1B using labelled-lipid II. The activity of PBP1A and PBP1B was tested in low (30 or 45 mM NaCl for PBP1A or PBP1B, respectively) or high salt (500 mM NaCl) concentrations, and in the presence (+LpoA or +LpoB) or absence (N.A.) of activators. **A**, initial slopes of GTase assays with of 0.5 µM PBP1A or PBP1B and 10 µM dansyl-lipid II at low (grey) and high salt (black) conditions. Samples were incubated for 90 min at 30°C (PBP1A) or 30 min at 25°C (PBP1B). Error bars are SD for 3 repeats. **B**, relative areas of

the peaks for transpeptidase products (left, peaks 5-10 in Fig. VS2C-D) or carboxypeptidase products (right, peaks 2 and 5 in Fig. VS2C-D) for reactions with of 0.5 µM PBP1A or 0.7 µM PBP1B and 25 µM ^{14}C-lipid II at low (grey) and high (black) salt. Error bars are SD for 2 repeats.

Finally, we used a recently developed FRET-based assay employing two types of labelled lipid II (lipid II-Atto550 and lipid II-Atto647n) in the presence of unlabelled lipid II that can monitor both, GTase and TPase activities in real time (**Figure 18AB**) (Hernández-Rocamora *et al.*, 2021). We used this assay previously to monitor the GTase and TPase activities of PBP1B homologues from *E. coli*, *P. aeruginosa* and *A. baumannii*. In this assay, the apparent GTase rates are obtained when adding ampicillin to block the TPase. In the absence of ampicillin, the combined apparent GTase+TPase rates are obtained, as crosslinking increases the FRET by bringing more probes from different glycan strands close together. After having followed FRET over time and terminating the reaction, we recorded the spectra to measure the amount of FRET developed, which indicates the activity level, and the products were analyzed by SDS-PAGE to confirm the presence of crosslinked PG and the consumption of labelled lipid II. In order to interpret the results, it was also important to determine whether the class A PBP can polymerize labelled lipid II in the absence of unlabelled lipid II. We previously reported that only LpoB-activated PBP1B can utilize the labelled lipid II versions in the absence of unlabelled lipid II (Hernández-Rocamora *et al.*, 2021). Here we found that PBP1A was unable to polymerize labelled lipid II in the absence of unlabelled lipid II, irrespective of the presence or not of LpoA. This simplified the interpretation of FRET signals in the presence of LpoA, as any increase in FRET when LpoA is present, will be due to stimulation of GTase or TPase rates, and not due to probes being incorporated closer on the same glycan strands.

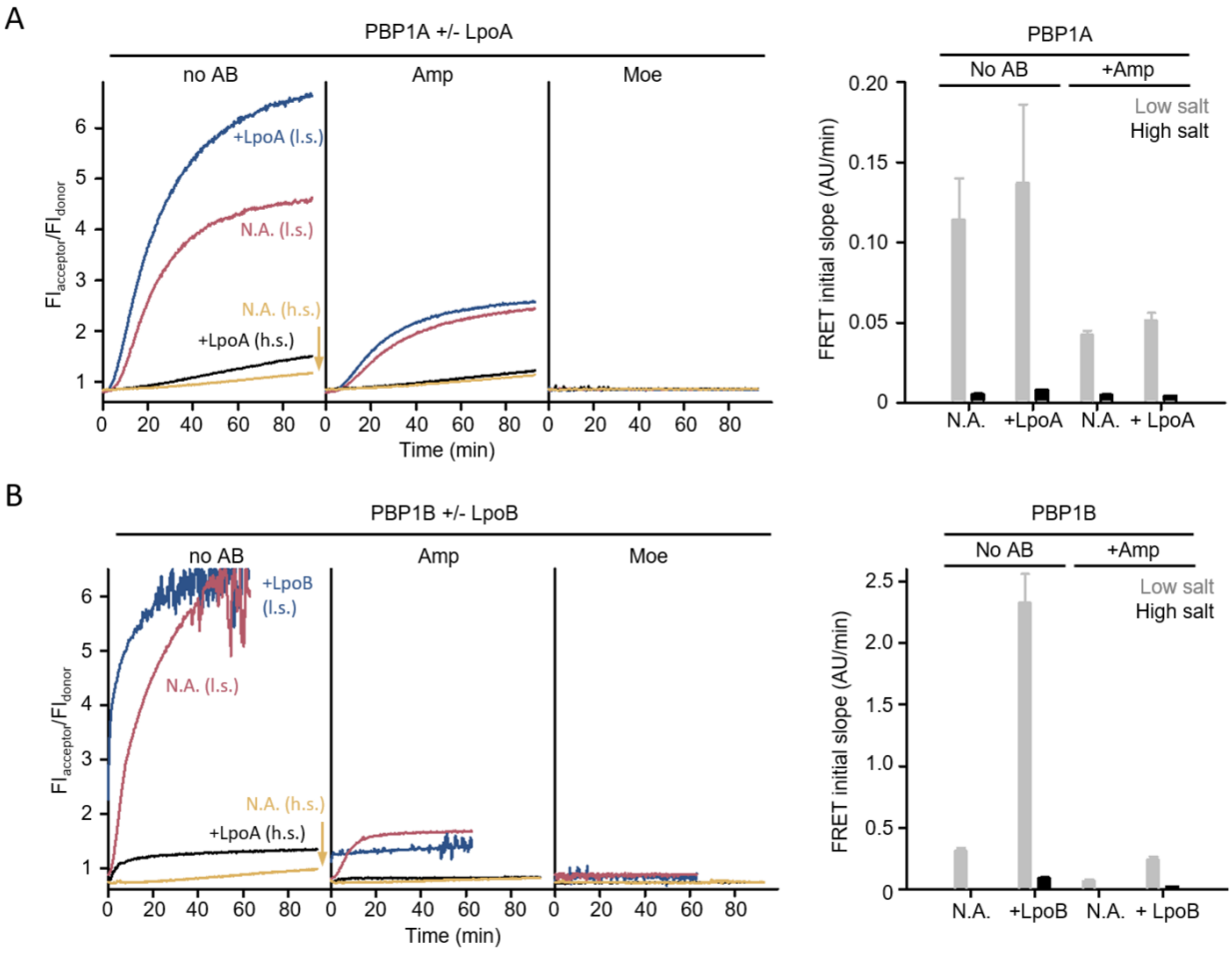

Figure 18. FRET assay of PBP1A and PBP1B GTases/TPase + GTases activities. The activity of PBP1A and PBP1B was tested in low (30 or 45 mM NaCl for PBP1A or PBP1B, respectively) or high salt (500 mM NaCl) concentrations, and in the presence (+LpoA or +LpoB) or absence (N.A.) of activators. **A**, left, representative reaction curves from FRET assays of PBP1A at low (blue with LpoA, red without activator) and high salt conditions (black with LpoA, yellow without activator), respectively. Right, initial slopes calculated from FRET curves obtained from PBP1A assays at low (grey) and high salt (black). Error bars are SD at least 2 repeats. **B**, left, representative reaction curves from FRET assays of PBP1B at low (blue with LpoB, red without activator) and high salt conditions (black with LpoB, yellow without activator), respectively. Right, initial slopes calculated from FRET curves obtained from PBP1B assays at low (grey) and high salt (black). Error bars are SD at least 2 repeats. In **A** and **B**, 1 mM ampicillin or 50 µM moenomycin were added when indicated and reactions were incubated at 30 or 25°C for PBP1A or PBP1B. The concentration of activators was 4 times the one of their cognate enzyme in all assays.

Condition	Enzyme/ Activator	GTase rate (dansyl-LII)[1]	GTase rate (FRET)[2]	GTase+TPase rate (FRET)[3]	%TPase products[4]	%CPase products[5]
low salt	*PBP1A*	32 ± 1	65 ± 5	37 ± 8	44 ± 3%	1 ± 1%
	PBP1A + LpoA	42 ± 2	78 ± 8	44 ± 16	62.3 ± 0.5%	5 ± 1%
high salt	*PBP1A*	12 ± 1	7 ± 1	1.7 ± 0.2	16 ± 1%	2.5 ± 0.2%
	PBP1A + LpoA	12 ± 3	6.1 ± 0.5	2.5 ± 0.2	32 ± 3%	18.4 ± 0.3%
low salt	*PBP1B*	100 ± 13	100 ± 22	100 ± 8	54 ± 3%	2.7 ± 0.2%
	PBP1B + LpoB	492 ± 32	365 ± 43	752 ± 76	68 ± 1%	3.9 ± 0.1%
high salt	*PBP1B*	22 ± 3	1.6 ± 0.4	0.8 ± 0.2	13.7 ± 0.9%	1.9 ± 0.2%
	PBP1B + LpoB	300 ± 2	31 ± 3	29 ± 2	26.9 ± 0.1%	4.7 ± 0.2%

Table 5. Comparison of reactions rates and transpeptidation and carboxypeptidase levels in PG products of PBP1A and PBP1B reactions. 1. GTase rates obtained from dansyl-lipid II assays (**Figure 16**), normalized to the rate of PBP1B at low salt and no activator. 2. and 3. GTase and combined GTase+TPase rates obtained from FRET assays (**Figure 17**) in the presence and absence of ampicillin, respectively. Rates are normalized to the rate of PBP1B at low salt and no activator. 4. and 5. percentage of the radioactivity signal present in transpeptidase or carboxypeptidase products, respectively, from assays with radioactive lipid II (data not shown).

When we performed FRET assays including unlabelled lipid II in high salt condition, both PBP1A and PBP1B showed a substantially smaller amount of FRET at the end of the reaction, a reduced consumption of lipid II, and less production of PG chains or crosslinked PG, compared to low salt conditions. In addition, the apparent GTase and GTase+TPase rates were ~15-20 times smaller at high salt than at low salt for both enzymes, with or without activator (**Figure 18** and **Table 5**). PBP1B consumed more lipid II, produced higher final FRET and showed higher GTase or GTase+TPase rates than PBP1A in every condition tested (data not shown), in agreement with the results from the dansyl-lipid II assay (**Figure 17A**). The addition of LpoA slightly increased the apparent GTase and GTase+TPase rates at low salt, but had no effect on the GTase rate of PBP1A

at high salt (**Figure 18A** and **Table 5**). By contrast, LpoB activated PBP1B robustly at both high and low salt conditions (**Figure 18B** and **Table 5**).

In summary, the GTase and TPase activities of both class A PBPs were considerably reduced at high salt. The real-time assays revealed that PBP1B is up to one order of magnitude more active than PBP1A in similar conditions (**Table 5**). LpoB activated both, GTase and TPase of PBP1B at low and high salt conditions, but LpoA had only a modest effect on the GTase and GTase+TPase of PBP1A at low salt conditions, and only slightly activated the GTase+TPase rate, but not the GTase rate, at high salt.

3.3 Discussion.

Research has enhanced our understanding of the redundancy among peptidoglycan (PG) hydrolases, indicating their potential specialization in specific environmental stress conditions (Hugonnet et al., 2016; Peters et al., 2016; Santin & Cascales, 2017; Morè et al., 2019; Mueller et al., 2019). This study explores the potential connections between PG hydrolases and the major Class A penicillin-binding proteins (PBPs), PBP1A and PBP1B, in various environmental conditions. While the genetic interaction network did not reveal strong PBP-hydrolase pairs linking specific hydrolases to PBP1A or PBP1B, it was observed that the fitness of ΔmrcB cells significantly decreased under salt stress. This aligns with recent findings indicating that outer membrane-anchored LpoB regulates PBP1B in response to osmotic challenges. Investigating the effects of salt on purified PBP1A and PBP1B activities, it was discovered that high salt conditions led to reduced crosslinked PG compared to low salt conditions, suggesting a link between residual Class A PBP activity and observed morphological defects in mutants lacking one of the

class A PBPs at high salt. Notably, an mrcB mutant exhibited more severe growth defects than the mrcA mutant, hinting at the critical role of PBP1B in survival. The in vitro activities of PBP1A and PBP1B, especially in high salt conditions, further emphasized PBP1B's higher efficacy. Additionally, LpoB demonstrated the ability to activate PBP1B at high salt, while LpoA did not activate PBP1A (GTase) under the same conditions. Analysis of PG composition in mutant strains lacking a class A PBP under mild salt stress revealed that cells could still produce PG with a normal composition, indicating that the main issue under high salt is insufficient PG synthesis capacity. This insufficiency led to morphological defects, such as bulging and lysis, akin to WT cells subjected to antibiotic-induced PG synthesis inhibition at standard conditions. The observed cell branching at high salt suggested a potential impact on cell division placement, possibly affecting the robustness of the septum. The study also addressed the role of LpoA in stimulating the GTase activity of PBP1A, finding a mild stimulation at low salt and no activation at high salt, affirming previous reports that LpoA primarily activates the TPase. Overall, this research underscores the intricate interplay of PG hydrolases, Class A PBPs, and environmental conditions in shaping bacterial cell morphology and growth.

Chapter 4. *In Vitro* Peptidoglycan Degradation Assay Using FITC Labelled Sacculi.

4.1 Introduction.

PG degradation assays are utilized to characterize PG lytic enzymes. The principle of all these assays is the same (using PG as substrate) but have different detection approaches of hydrolytic fragments. There are several methods to separate and quantify the hydrolytic fragments, such as high-performance-liquid-chromatography (HPLC) and mass spectrometry, respectively. Also, by labeling free amines within PG sacculi with different dyes such as Remazol Brilliant Blue R (Zhou et al., 1988) or fluorescein-5-isohtiocyanate (Maeda, 1980).

FITC dye molecules have isothiocyanate moiety (-N=C=S) that binds covalently to peptides by forming a durable thiourea bond with the available free amino group (**Figure 19**). The specificity of this reaction lies in the selective interaction of the isothiocyanate (-N=C=S) group within FITC with N-terminal amines, attributed to their increased stability. This process involves the electrophilic carbon within the isothiocyanate group being targeted by the primary amine, resulting in the formation of a thiourea linkage that connects the peptide and FITC. Proper pH management is crucial, as the potential interaction of the isothiocyanate group with secondary amines can occur under specific reaction conditions (Shah et al., 2019).

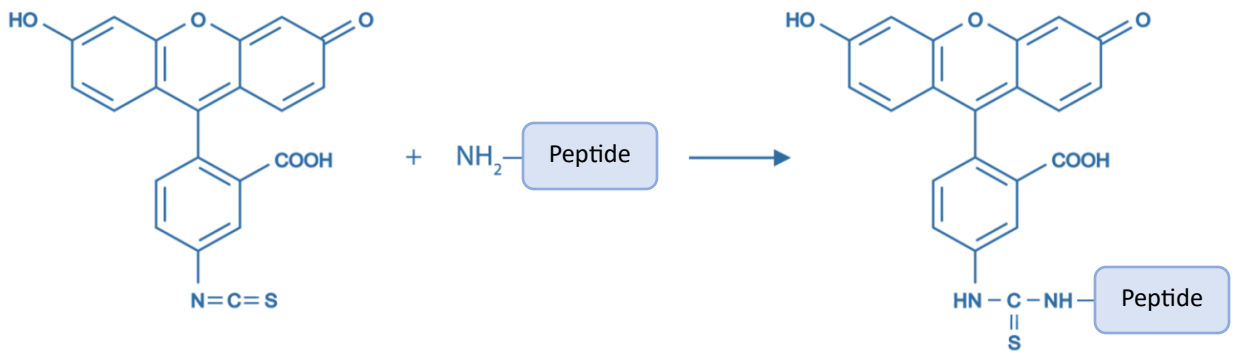

Figure 19. FITC-peptide labelling reaction. The moiety (-N=C=S) of isothiocyanate on FITC conjugates with the free amino group of peptides to form stable thiourea covalent bond. The isothiocyanate (-N=C=S) group in FITC selectively reacts with N-terminal amines due to their greater stability. The electrophilic carbon of the isothiocyanate group is attacked by the primary amine, resulting in the formation of a thiourea bond that links FITC to the peptide (Shah, 2019).

FITC dye was used to label peptidoglycan sacculi to investigate the activity of peptidoglycan hydrolases *in vitro*. Insoluble substrates are then removed by centrifugation or filtration to isolate the soluble hydrolytic fragments released by PG hydrolases and set to measure spectrophotometrically. A plate reader is then able to measure the PG hydrolase activity and compare it with a control enzyme that as activity against PG like Lysozyme. Lysozyme is universally found in different mammalian secretions (e.g. saliva, tears, egg whites… etc.). It damages bacterial cells by catalyzing hydrolysis of β-1,4-glycosidic bindings between N-acetyl-D-glucosamine and N-acetylmuramic acid residues in PG (Maeda, 1980).

First, we purified and collected PG from *Escherichia coli* according to a protocol by Glauner, (Glauner et al., 1988). For this chapter, our goal was to optimize the *in vitro* peptidoglycan

degradation assay using FITC labelled sacculi for 96 well plates format. Subsequently, I used this PG degradation assay to characterize the activity of several *E. coli* hydrolases and their respective regulators in the presence of NlpI and DolP proteins.

4.1.1. The lipoprotein NlpI.

Previous work discovered the presence of *yhbM* gene (NlpI) of unknown function, positioned between *pnp* and *deaD* at 71 min on the *E. coli* chromosome (Blattner et al., 1997). The gene *yhbM* encodes a polypeptide predicted to have 294 amino acids residues and a molecular weight of 33,619 Da. The amino acid sequence suggests that the *yhbM* product is lipoprotein. NlpI (OM-anchored new lipoprotein I) is assumed to be part of cell division. NlpI nucleates hydrolases in multienzyme complex and alters the activity of several endopeptidases (Banzhaf et al., 2019). NlpI interacts with the MepS endopeptidase and targets it for degradation via the tail-specific protease Prc. Monomers of NlpI form a homodimer while their OM-binding N-termini stay in close proximity (Wilson et al., 2005). These monomers have 14 α-helices which form four, canonical but distinct, tetratricopeptide helix-turn-helix repeats (TRP) and two non-TPR motifs (**Figure 20**), and the C-terminus is rolled-up (folded) inside the N-terminus (Wilson et al., 2005). The curvature of helices gives support to protein-protein interactions. Hence, the idea of NlpI serves as a scaffold for protein complexes (e.g. amidases) (Das et al., 1998; Wilson et al., 2005).

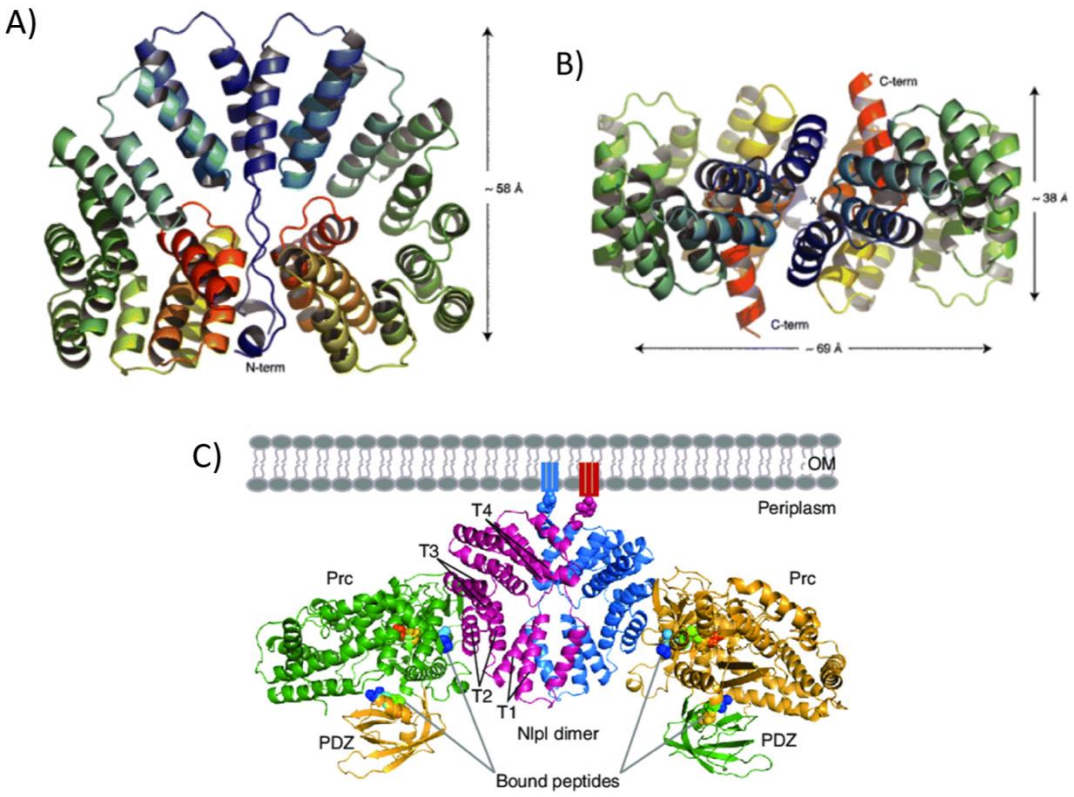

Figure 20. Structure of mature NlpI and NlpI-Prc complex (Wilson et al., 2005). A) side and B) top views of NlpI dimer. Color from dark blue chains = N- termini to orange chains = C-termini. C) dimeric NlpI (blue and purple) bound to two Prc (one green and one orange, with PDZ domain in contrasting color) ribbon diagram. The four TRPs are indicated (T1-4).

Some preliminary protein-protein interaction data discovered further (Jolanda Verheul et al., 2022) that NlpI interacts with the LytM domain of EnvC (regulator of AmiA and AmiB). We hypothesized that NlpI could affect amidases activities, as it is now known for NlpI to interacts with the fundamental component (EnvC) of amidase-activation.

4.1.2. The DolP protein.

DolP (division and OM stress-associated lipid-binding protein) is a non-essential OM-anchored protein comprising of 2 BON (Bacterial OsmY and Nodulation) domains (BON1/2) required for phospholipid binding (Morris et al., 2018; Yeats & Bateman, 2003). The C-terminal BON domain is essential for localization of DolP at cell division site by binding to anionic phospholipids (Bryant et al., 2020). To date, DolP is known to contribute to the function of BAM complex (β-barrel-assembly-machines) (Ranava et al., 2021). The β-barrel proteins form a structure that is inserted into the OM layer through a periplasmic-chaperon BAM system (Tomasek & Kahne, 2021; Wu et al., 2021). The β-barrel-assembly machinery (BAM) is required for the assembly of outer-membrane-proteins (OMPs) found in the outer membrane of Gram-negatives. OMPs is one type of integral membrane proteins, along with the α-helical membrane proteins (Onufryk et al., 2005). BAM comprises of a five-protein complex, responsible for the proper folding and accurate insertion of nascent OMPs in cell's outer membrane (Plummer et al., 2015). The first step of OMP biogenesis is the synthesis of OMP substrates in the cytoplasm (Von Heijne, 1992). Next, these substrates are translocated via the Sec translocon across the cytoplasmic membrane. With the help of chaperones, OMP substrates are escorted to the inner side of the outer membrane by BAM complex (Wu et al., 2021). The complex size is about 200 kDa in size, comprising of BamA (an integral OMP) and four lipoproteins (BamB, BamC, BamD, and BamE) (Gu et al., 2016; Han et al., 2016; Noinaj et al., 2015). Previous data (Babu et al., 2018; Carlson et al., 2019) reported that DolP plays a role with the BAM complex, suggesting that DolP could be linked to the OMP biogenesis, with yet unclear function.

4.2 Results.

I applied the *in vitro* PG degradation protocol to test the impact of two distinct proteins, NlpI and DolP, on amidases activities as part of two separate projects. First study, in collaboration with Prof Waldemar Vollmer, we sought to investigate the relationship between NlpI and amidases (AmiA, AmiB, and AmiC) by the *in vitro* PG degradation assay as part of an ongoing study. 2) In the second study, we investigated the impact of DolP on the amidases in the published study (Boelter et al., 2022) as we hypothesized that DolP could impact amidases activities and/or NlpD during cell separation. For the PG degradation assays, the purified *E. coli* sacculi was provided the Moynihan laboratory and DolP protein was provided by Dr Jack Bryant.

4.2.1 NlpI reduces AmiA and AmiC activities likely via hindering their activation by their cognate regulators EnvC and NlpD.

During cell division in *E. coli*, approximately 30% of newly-synthesized PG is removed after its formation by hydrolases (Park & Uehara, 2008), particularly the N-acetylmuramyl-L-Alanine amidases (AmiA, AmiB, and AmiC) and Lytic transglycosylases (see **1.2.3.2.1** and **1.2.3.2.3** sections, respectively). Single amidases deletion has a very minor effect on bacterial cells, but cells lacking all amidases create a septum with a defect geometry resulting in connected cells growing in long chains (Heidrich et al., 2001; Priyadarshini et al., 2007). AmiABC amidases are auto-inhibited and need to be activated by interaction partners. In *E. coli*, the two most characterized regulators are NlpD (activates AmiC) and EnvC (activates AmiA &

AmiB) (Peters et al., 2013; Tsang et al., 2017; Uehara et al., 2009; Uehara et al., 2010; Yang et al., 2012). Each activator possesses catalytically degenerated C-terminal LytM EPase domain (Lysostaphin/peptidase M23). LytM domains are found in different bacterial proteins and functions in both PG hydrolysis and division (Meisner & Moran Jr, 2011; Sabala et al., 2012). With all that in mind, we investigated the NlpI role as an amidase regulator as we expect a change in their activities.

All our purified proteins of interest (NlpI, AmiA, AmiB, AmiC, EnvC, and NlpD) (**Figure 21A**) were added in equal molarities and incubated with FITC labelled sacculi alone or combined (Maeda, 1980). Using the Omega plate reader, the omitted fluorescence yielded from amidases activity is absorbed and measured after 1 hour of incubation in 37°C and showed microplate wells in numerical form indicating level of amidase PG hydrolase activity (**Figure 21B**). For the single amidases and regulators we observed very little omitted fluorescence meaning low enzyme activity. As expected, amidases were highly active when incubated with their regulators EnvC and NlpD (Uehara et al., 2010). EnvC activated AmiA-EnvC (~75%) and AmiB-EnvC (~41%), and NlpD activated AmiC-NlpD (~70%). Addition of NlpI to amidases alone did impact their activities. Meanwhile, addition of NlpI to amidases along with EnvC and NlpD resulted in minor reduction in AmiA-EnvC-NlpI (~64%) and AmiC-NlpD-NlpI (~50%) activities.

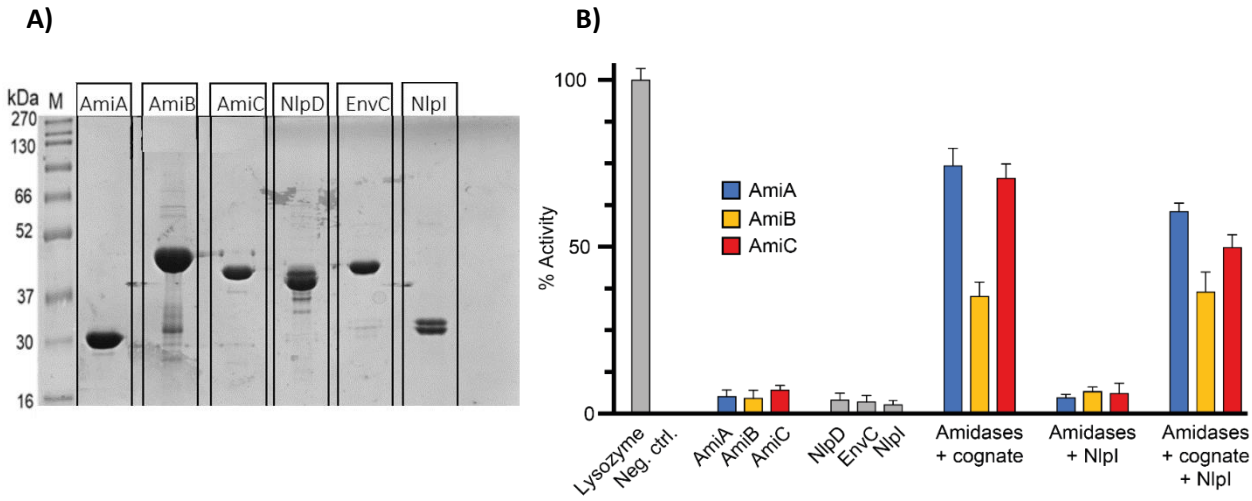

Figure 21. PG degradation of FITC-sacculi by amidases and/or their regulators in the presence of NlpI. A) SDS-PAGE gel stained with Coomassie blue to verify our proteins indicated by molecular weights. (M) marker. AmiA: 31.412 kD, AmiB: 47.985 kD, AmiC: 45.634 kD, NlpD: 40.149 kD, EnvC: 46.595 kD, NlpI: 33.619 kD. **B)** the mean of three replicas is calculated and represented in above graph of measured absorbance of released fluorescence from PG degradation as a result of amidases activity incubated alone or with their cognate activator and NlpI. FITC fluorescence intensity was measured at 485 nm excitation and 525 nm emission.

We then sought to investigate the slight reduction in AmiA-EnvC and AmiC-NlpD activities in the presence of NlpI, as this observation could identify NlpI as a potential regulator of AmiA/AmiC, directly or indirectly via EnvC and NlpD. To test if NlpI can affect amidases directly, single amidases activities (without their regulators) were investigated in the presence of various NlpI ratios. After 4 hours of incubation (**Figure 22A**), NlpI, AmiA, and AmiC alone showed little activity (~1%, ~3.8%, and ~5%, respectively). When NlpI of different concentrations were added, both AmiA (~3%) and AmiC (~4%) activities had no noticeable changes. After 24 hours of incubation (**Figure 22B**), activities showed gradual decrease until

activity plateaued at NlpI =/> 2X. According to these findings, we concluded that NlpI does not regulate amidases directly.

To test if NlpI has indirect impact on amidases via EnvC and NlpD, amidases activities were examined in combination with EnvC and NlpD after one hour of incubation in the presence of different NlpI ratios, in order to determine the amount of NlpI needed to impact amidases/regulators activities (**Figure 22C**). As expected, AmiA-EnvC and AmiC-NlpD yielded high activities (~80% and ~84%, respectively), but the addition of NlpI gradually reduced amidases activity until NlpI = 2X (AmiA-EnvC-NlpI= ~60% / AmiC-NlpD-NlpI= ~56%) and then saturate after NlpI > 2X. Using t test to determine significance, the impact of NlpI on AmiA and AmiC activities was statistically significant (P value = 0.0130 and 0.0010, respectively).

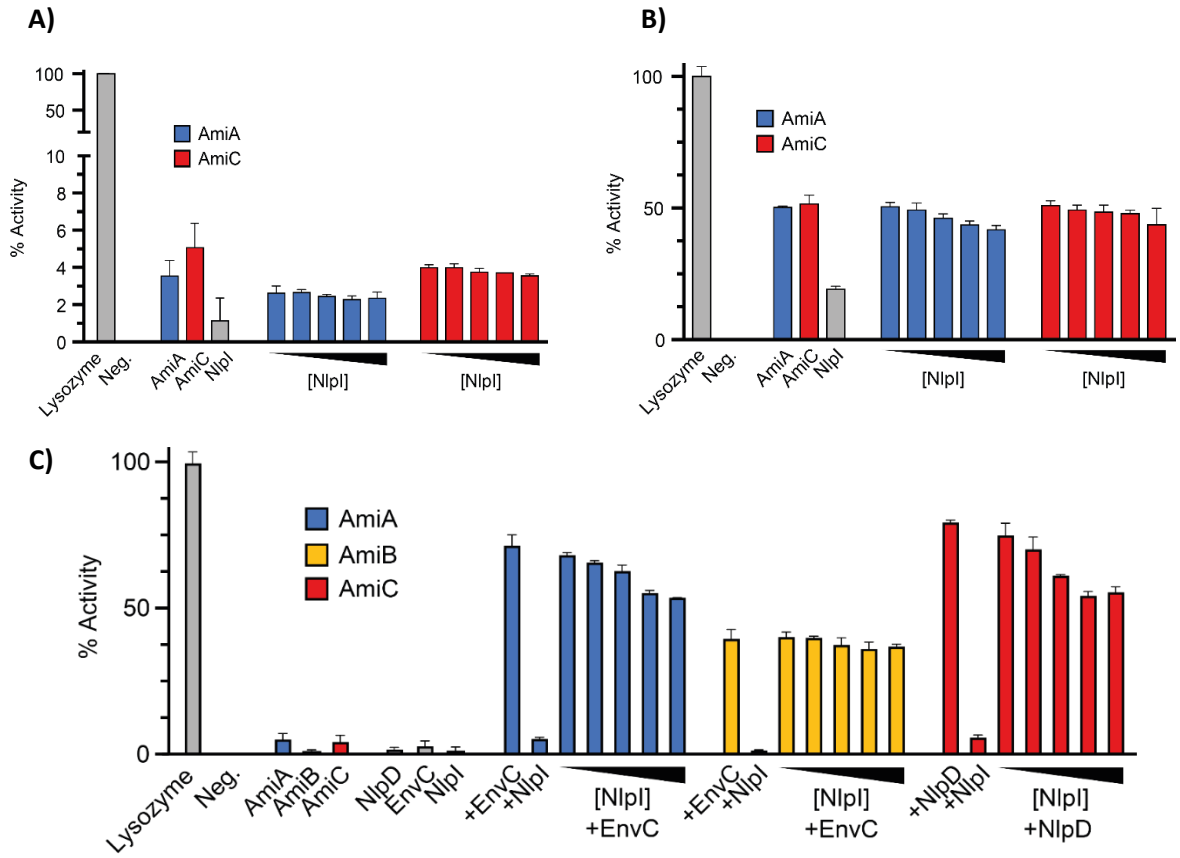

Figure 22. PG degradation of FITC-sacculi by AmiA/C - NlpI. *In vitro* PG degradation assay measuring fluorescence released by AmiA and AmiC with different NlpI ratios (0.25X, 0.5X, 1.0X, 2.0X, 4.0X) with (**C**) or without (**A** & **B**) their activators EnvC and NlpD. Concentrations were calculated following the same approach explained in section **2.7.2** (Maeda, 1980; Uehara et al., 2010). Graph summarizes the average of two replicas of PG degradation assay of proteins incubated for **A)** 4-, **B)** 24-, and **C)** 1- hours**,** at 37°C heat-block with maximum speed agitation. FITC fluorescence intensity was measured at 485 nm excitation and 525 nm emission.

Even though the reduction is statistically significant, it may not translate as biologically relevant to amidases activity. We concluded that NlpI is not a direct regulator to AmiA/AmiC activities, rather it might have an affect via amidases cognate regulators EnvC and NlpD, suggesting that NlpI indirectly impact AmiA/AmiC activation.

4.2.2 DolP is likely not an amidases activity regulator.

It was reported that DolP contributes during cell division and might regulate amidases either directly or indirectly. DolP was identified by Tsang and collaborators (Tsang et al., 2017) as a potential direct activator of AmiC, or indirect activation via NlpD. In a *ΔenvC* genetic background, Tsang and collaborators generated a transposon-inserting library aiming to identify mutants with chaining phenotype during EnvC pathway inactivation. They reported that *ΔdolPΔenvC* double mutant share a similar chaining phenotype as *ΔnlpDΔenvC* mutant. The screen showed cell elongation defects in *ΔdolPΔenvC* cells, implicating role of DolP in cell division process. Microscopically, *ΔdolPΔenvC* cells showed major chaining phenotype as observed in *ΔnlpDΔenvC* cells, suggesting that DolP might be in the same NlpD pathway and required for NlpD activation, as EnvC requires FtsEX for AmiA and AmiB activation (Cook et al., 2020; Tsang et al., 2017).

In our published study (Boelter et al., 2022). We tested our hypothesis of a potential impact by DolP on amidases activities and/or NlpD during cell separation using *in vitro* PG degradation assay expecting a change in amidases activities in the presence of DolP. I performed *in vitro* PG degradation assay (**Figure 23**) where DolP was incubated with FITC-sacculi and amidaseABC alone or with their activators EnvC/NlpD, and the released fluorescence was measured. Single-incubated proteins showed low enzyme activity. As expected, amidase-regulator yielded high activities (AmiA-EnvC= ~90%, AmiB-EnvC= ~50%, AmiC-NlpD= ~80%).

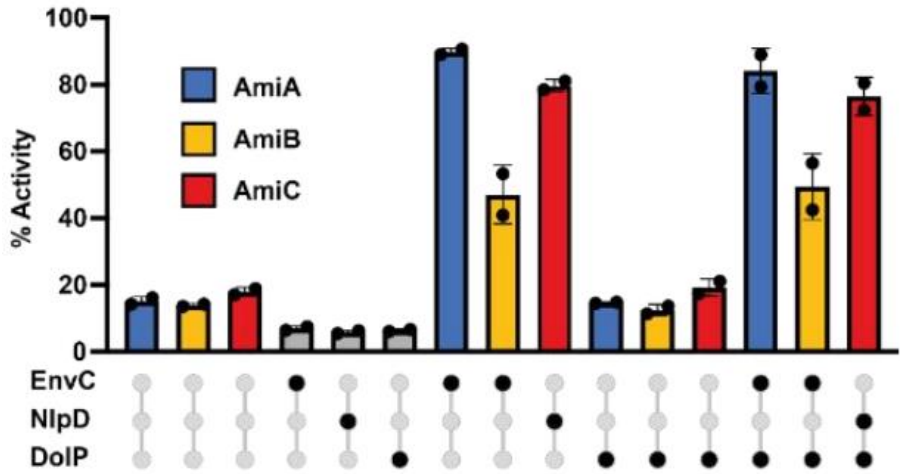

Figure 23. FITC-sacculi degradation by amidases-regulators activity (Boelter et al., 2022). All proteins were incubated in 37°C heat-block with maximum speed agitation. The % Activity of amidases and/or regulators readouts were normalized to lysozyme control. The graph summarizes the average of two replicates. FITC fluorescence intensity was measured at 485 nm excitation and 525 nm emission.

DolP did not cause any changes in amidases activities, nor alteration in PG degradation when combined with EnvC/NlpD (AmiA-EnvC-DolP= ~89%, AmiB-EnvC-DolP= ~51%, AmiC-NlpD= ~77%). This result lead to the conclusion that DolP is likely not an amidase activity modulator.

4.3 Discussion.

NlpI forms a binding cleft when bound to monomers with curved helices. This binding cleft gives support to protein-protein interactions (Das et al., 1998; Wilson et al., 2005). Hence, we questioned if NlpI might serve as a scaffold and/or regulator for amidases. Attempting to test amidases activities against various ratios of NlpI without the activators EnvC and NlpD showed no drastic impact on AmiA and AmiC activities (**Figure 22A & B**), making NlpI unlikely

to be a direct amidases regulator. On the other hand, when we tested the indirect impact of different ratios of NlpI on amidases via EnvC and NlpD, amidases activities were reduced in AmiA-EnvC-NlpI and AmiC-NlpD-NlpI by ~20% and ~28%, respectively (**Figure 22C**). Some preliminary protein-protein interaction data (Jolanda Verheul et al., 2022) revealed that NlpI interacts with the LytM domain of the fundamental amidase-activation component EnvC. Also, another study (Banzhaf et al., 2020) utilized *in vitro* and *in vivo* proteomics-based assays reporting NlpI binding to amidases and their activators (AmiA and EnvC), LTs (MltA and MltC), and some Epases (PBP4 and PBP7). Collectively, the reported findings suggest a role part for NlpI as an indirect contributor in amidase activation via EnvC and NlpD (Jolanda Verheul et al., 2022) or through undiscovered mechanism. The results obtained from PG degradation assay of NlpI-amidases motivated us to test their relationship even further in collaboration with Prof Waldemar Vollmer, where we aim to utilize different approaches to confirm the NlpI role in amidases activation and explain its function during cell division in future works.

In our published study (Boelter et al., 2022) tested the hypothesis of DolP acts as an activator for amidases and/or it is required for NlpD to activate AmiC using *in vitro* PG degradation assay monitoring amidases activity (**Figure 23**). DolP did not show AmiC activation, nor alteration in PG degradation when combined with NlpD. Even though the absence or presence of DolP did not change amidases/regulators activities *in vitro* PG degradation assay, alternatively, we carried out exploring DolP possibilities during cell division using different techniques (microscale thermophoresis (MST), pull-down, and colony-fitness assays) and collective evidence suggests

that DolP is likely not to be NlpD upstream regulator (Boelter et al., 2022), but might functions indirectly through undiscovered mechanism.

Chapter 5. General discussion.

Two decades ago, Höltje proposed a hypothesis suggesting that the expansion of the PG sacculus requires the collaborative action of both synthases and hydrolases, ensuring a controlled and secure growth process. For the murein layer to undergo seamless growth (Höltje, 1998), the addition and insertion of material need to be minimal. Structural considerations indicate that the smallest patch of murein added to a single glycan strand, the structural attachment point, consists of three cross-linked glycan strands, not two. In a relaxed state, a murein triplet can be anchored beneath a specific strand, termed a docking strand, when the murein layer is under stress. Transpeptidation of the peptide moieties of the outer strands in the triplet to the free epsilon amino groups of A2pm residues in the peptide cross bridges on both sides of the docking strand forms covalent links, creating trimeric cross bridges as attachment sites. This unique configuration allows for the targeted removal of the old strand without disrupting the murein network. The murein triplet's attachment sites enclose the d-Ala–(d)-m-A2pm peptide bonds, facilitating the cleavage needed for the specific removal of the docking strand. Upon the release of the old strand, the newly added triplet is automatically drawn into the tensioned layer. This process, known as the "three-for-one" growth strategy, results in the replacement of one existing strand with three new ones (Höltje, 1998). This concept, along with other works, supports the notion that PG multi-protein complexes have high dynamics driven by interactions between proteins (Pazos et al, 2017).

Contributing to studying the roles of hydrolases in PG biogenesis, recent studies have investigated their redundancy and physiological significance (Hugonnet et al., 2016; Peters et al., 2016; Santin and Cascales, 2017; More et al., 2019; Mueller et al., 2019). In this study, we hypothesized potential dependencies between PBP1A or PBP1B and selected hydrolases

growing under different stress conditions, aiming to uncover the roles they play in bacterial envelope biogenesis.

We found that *ΔmrcB*-hydrolase double mutants resulted in minor morphological changes in normal laboratory conditions, as *ΔmepSΔmrcA* and *ΔmepSΔmrcB* double mutants showed wider cells than *ΔmepS*, in agreement with (Banzhaf et al., 2020). Double mutants with amidases *ΔamiAΔmrcB* and *ΔamiBΔmrcB* showed shorter cells than both *ΔamiA* and *ΔamiB*, while double mutants *ΔmepAΔmrcA* and *ΔmepAΔmrcB* grew longer than single *ΔmepA* mutant. As morphology does not necessarily correlate with fitness, we employed a chemical genomics screen to assess the stress-related genetic interactions of mutants panel. We observed in our screen that *ΔamiAΔmrcB* showed a significant negative genetic interaction, indicating that deletion of both genes at once caused growth reduction under high salt (600 mM). We also observed a strange positive genetic interaction in *ΔmepSΔmrcA* in high salt, which later was investigated by morphology. Furthermore, genetic interaction failed to reveal a specific pair between PBP1A or PBP1B and the tested hydrolases that would suggest a strong preference to either PBPs, but also showed some observations that align with previously published projects. As bacterial cells respond to environmental challenges by changes in their PG biochemistry and cell architecture (Vollmer et al., 2008; Yao et al., 1999). Specific protein-protein interactions between synthases and hydrolases involved in PG sacculus metabolism have been documented by different studies (Romeis and Höltje, 1994; von Rechenberg et al., 1996) (**Figure 24**).

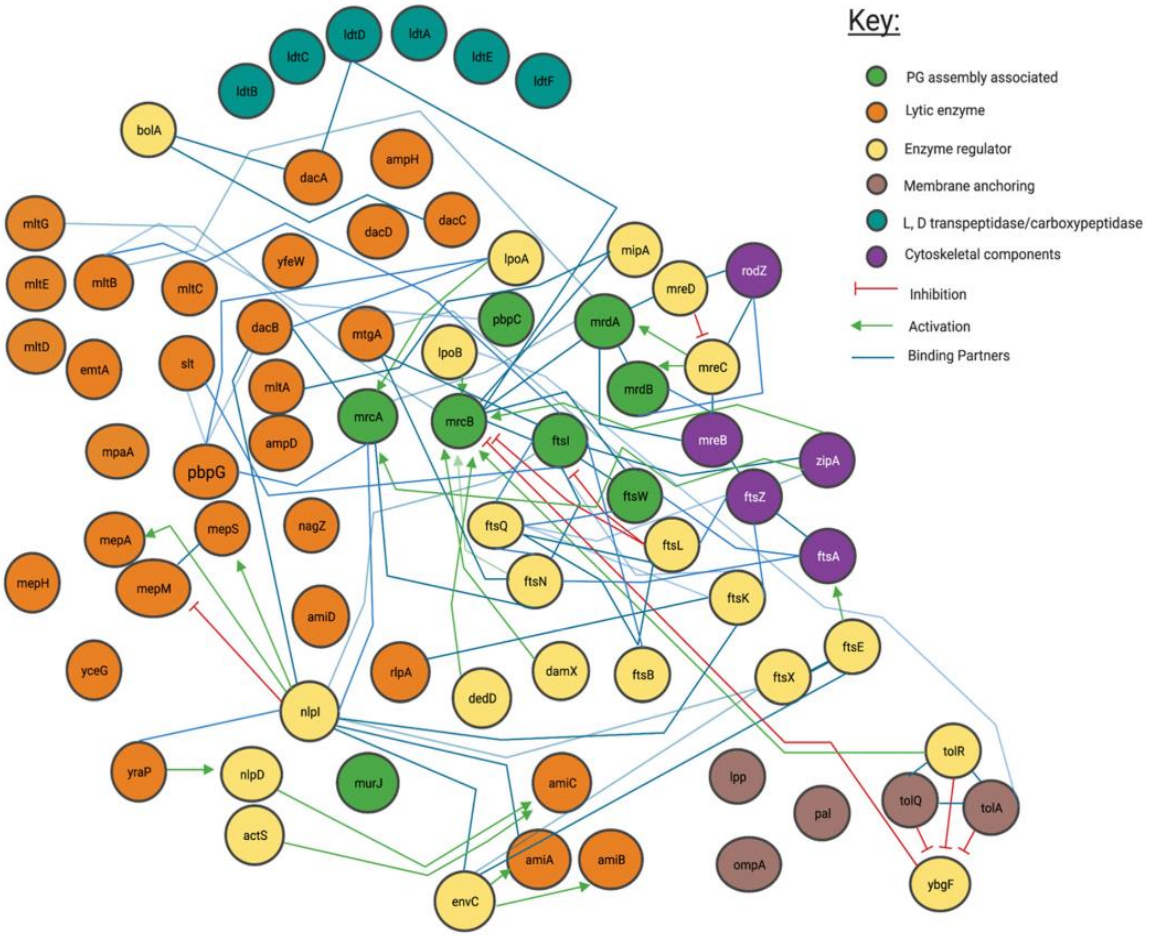

Figure 24. Network of PG enzymes interactions and their partners (Graham et al., 2021).
Interaction map of PG-associated proteins categorized by enzymatic action.

It was reported that the bifunctional class A PBPs (MrcA and MrcB), the transpeptidases PBP2 (MrdA) and PBP3 (FtsI), the endopeptidases PBP4 (DacB) and PBP7 (PbpG), and lytic transglycosylases (Slt70, MltA, and MltB) interact with one another, creating a multienzyme complex *in vivo* (Ghuysen, 1997; Ishino et al., 1980; Korat et al., 1991; Nakagawà et al., 1979; Tomasz, 1979; Weidel & Pelzer, 1964). Multienzyme complex formation ensures proper PG

sacculus growth, cell shape maintenance, and division via effective control of autolytic PG hydrolases. Both PBP2 and PBP4 associate genetically with PBP1A, for cell elongation and shape maintenance, while PBP3 and PBP7 associate genetically with PBP1B, for cell division (Nanninga, 1998); Meberg et al., 2004; Priyadarshini et al., 2006). Their association was also confirmed in our genetic interaction screen, as Δ*dacB*/Δ*pbpG* and Δ*mrcA*/Δ*mrcB* double mutants showed strong observed interactions. Another published study (Park et al., 2020) observed salt sensitivity in Δ*mrcB,* Δ*mrcA,* Δ*mepM,* Δ*lpoA,* and Δ*lpoB* mutants, and found that *mepM* genetically associates with both PBP1A and PBP1B in 750 mM NaCl, consistent with Δ*mepM*Δ*mrcA* and Δ*mepM*Δ*mrcB* genetic interactions observed in high salt. As reported (Mueller et al., 2019; Gurnani et al., 2021), AmiB is sufficient for daughter cell separation growing under acidic pH, and our genetic interaction screen in pH 4.8 showed a negative genetic interaction in Δ*amiB*Δ*mrcB*. Along with morphology assessment by phase contrast microscopy showed recovery of cell length in Δ*amiB*Δ*mrcA* in high salts, made us suggest a role for AmiB with PBP1A growing in high salt. In addition, morphology assessment concluded that MepS and MepA ensure optimal growth in Δ*mrcB* cells under high salt stress. The lysis seen in double mutants could be partially due to membrane fluidity alteration.

While PBP-hydrolases double mutation did not reveal a specific dependency to either PBPs, we thought it would be helpful to extend our initial hypothesis by testing PBP-hydrolase triple (or more) knockout mutants growing in the same stress conditions (or even combine two stresses at once) to identify or negate dependencies, but due to COVID-19 pandemic and maternity leave, I could not explore this further.

So, we had another hypothesis that class A PBPs have salt requirements for proper activity. For this, we conducted GTaes/TPase activity assays. We found that at high salt, both PBP1A and PBP1B were inhibited and produced less crosslinked PG compared to low salt conditions, where enzymes were fully active. The results suggest that a low residual class A PBP activity could be the reason for growth defects observed in mutants lacking one of the class A PBPs at high salt, whilst no growth defects are observed at low salt. Interestingly, the growth defects at high salt in Δ*mrcB* mutants more severe than in Δ*mrcA* mutants, in which higher NaCl concentration is needed to affect growth. As PBP1A showed a lower in vitro PG synthesis activity than PBP1B, including at high salt, it is possible that PBP1A on its own cannot supply the necessary class A PBP activity required for survival. In fact, PBP1B was more active *in vitro* than PBP1A in every assay and condition, in agreement with previous reports (Egan et al., 2015; Pazos et al., 2020). Importantly, PBP1B was still activated by LpoB at high salt, while LpoA did not activate PBP1A GTase at high salt.

It has been recently suggested that LpoA is necessary to stimulate the GTase activity of PBP1A as mutations that confer higher GTase activity *in vitro* allow the deletion of *lpoA in vivo* (Sardis et al., 2021). However, this study provided no direct evidence for an effect of LpoA on the GTase activity of PBP1A. Here, we observed only a mild stimulation of PBP1A's GTase by LpoA at low salt, and not activation at high salt. The TPase was activated at both conditions. Thus, our results confirm previous reports indicating that the main effect of LpoA is the activation of the TPase (T. J. Lupoli et al., 2014; J. Verheul et al., 2022).

Vollmer group sought to analyze the PG composition (data not shown) in mutant strains lacking one of the class A PBPs at conditions that affected the growth but did not cause extensive lysis.

The PG composition was similar in the mutants experiencing mild salt stress, suggesting that the growth defects are not due to structural deficiencies in the PG that is produced. Alternatively, the growth defects at high salt, which include lysis of cells reminiscent of that caused by β-lactams, with bulging and bursting, could be caused by an insufficient rate of PG synthesis whilst hydrolases are active. It has been previously reported that *E. coli* cells produce a dynamic PG triangular wedge at the lagging edge of the septum, which appears to be important for robustness of the septum and whose thickness depends on the balance between PG synthesis and hydrolysis rates (Navarro et al., 2022). The most likely candidate for producing the PG in this wedge were identified as class A PBPs (Navarro et al., 2022). At high salt, the importance of septum robustness and the balance between synthesis and hydrolysis of PG increases and the reduced activity by class A PBPs in these conditions, might reduce the ability of cells to reinforce the septum and makes cell division more fragile at high salt.

In conclusion, the relationship between redundant hydrolases and the bifunctional Class A PBPs in *E. coli* presents an interesting yet complex mystery in bacterial cell wall synthesis investigation. Although we have made substantial efforts in comprehending the functionalities of these proteins, numerous questions remain unanswered. What is the precise coordination and regulation governing these redundant hydrolases and bifunctional PBPs during cellular wall reconstruction? What are the *in vivo* factors (such as novel regulators of class A PBPs) that could account for cell's preference toward PBP1A and/or PBP1B in stress conditions? Furthermore, the functional redundancy exhibited by hydrolases raises questions regarding the extents to which each enzyme's activity is interchangeable or if they possess specialized functions exclusive to their own domains? Deciphering the convoluted interplay among these enzymes will clarify

fundamental relationships between PG hydrolases and the PBPs, as well as reveal their roles in regulating bacterial cell growth and morphology.

***In vitro* PG degradation assay as a tool for characterizing roles of bacterial proteins.**

Numerous methods have been established (e.g. Zymogram) to test whether bacterial enzymes have PG hydrolytic activities (Leclerc and Asselin, 1989; Kazemier and Keck, 1991; Lommatzsch et al., 1997; Bernadsky et al., 1994). However, these approaches have their limitations as described by Santin & Cascales (Santin & Cascales, 2017). There are other methods not subjected to the limitations above and performed in solution, such as monitoring the degradation of PG labelled with fluorescent dye indicating protein activity (Maeda, 1980; Glauner 1988; Uehara et al., 2010; Fibriansah et al., 2012). Synthetic dyes are intensively used in several sectors, as they possess great chemical structure stability, such as FITC and Remazol Brilliant Blue R (RBBR) (Maeda, 1980; Glauner 1988; Uehara et al., 2010). We used FITC to label our PG succulus, because of its conjugate stability and high quantum efficiency (The & Feltkamp, 1970). This method will have advantages for a wide spectrum of applications if an adequate measuring device is available. Among these advantages, 1) simple operation, 2) any natural protein can be employed as a substrate for any distinctive protease, 3) high sensitivity, 4) facilitates studying hydrolases activities in time-course or end-point experiments, and 5) no radioactive materials are required (Maeda, 1980).

We developed our assay to characterize different hydrolytic activities of proteins, indicating the assay flexibility for application with more other substrates.

Using PG degradation assay as a tool to investigate NlpI role as amidases regulator.

A published study (Banzhaf et al., 2020) showed multiple changes in proteins thermostability and abundance in *ΔnlpI* cells. Among these changes, the decreased abundance in amidases. Here we propose our hypothesis of a potential interaction between the lipoprotein NlpI and amidases directly or indirectly. Our results revealed no direct impact on amidases, but when combined with activators EnvC and NlpD, NlpI decreased AmiA and AmiC activities, suggesting an indirect contribution of NlpI on amidases activity via unclear mechanism. However, we further attempted to investigate the NlpI-hydrolases double mutants morphology using phase contrast and fluorescent microscopy (unpublished data). We generated single/double mutant panel of NlpI-amidases growing in normal LB, and only Δ*nlpI*Δ*amiA* and Δ*nlpI*Δ*amiC* showed altered phenotypes (42% and 0.4% filamentation, respectively). Knowing that NlpI targets MepS for proteolytic degradation, and Δ*nlpI* mutant have uncontrolled MepS levels results in formation of filaments (Singh et al., 2012; 2015, Banzhaf et al., 2020), we checked if the filamentation in Δ*nlpI*Δ*amiA* was due to uncontrolled MepS using 0.2% glucose- and 0.2% arabinose-inducible media and found that is likely unrelated to MepS (unpublished data). This project might be continued in the future by other colleagues.

Using PG degradation assay as a tool to investigate DolP role as an upstream regulator for amidases/NlpD.

In our published study (Boelter et al., 2022), we conducted *in vitro* PG degradation assay to assess amidase activity in the presence of DolP. Our findings indicated that DolP did not activate AmiC, nor did it cause any changes in PG degradation when combined with NlpD. To further explore this relationship, we employed additional methods such as MST, pull-down assays, and colony-fitness assays. The collective evidence from these approaches suggests that DolP is unlikely to function as an upstream regulator of NlpD. To date, data (Babu et al., 2018; Carlson et al., 2019) reported that DolP plays a role with the BAM complex, suggesting that DolP could be linked to the OMP biogenesis, exerts its effects indirectly through an undiscovered mechanism.

References.

Ago, R., & Shiomi, D. (2019). RodZ: a key-player in cell elongation and cell division in Escherichia coli. *AIMS microbiology*, *5*(4), 358.

Alcorlo, M., Martínez-Caballero, S., Molina, R., & Hermoso, J. A. (2017). Carbohydrate recognition and lysis by bacterial peptidoglycan hydrolases. *Current opinion in structural biology*, *44*, 87-100.

Alva, A., Sabido-Ramos, A., Escalante, A., & Bolívar, F. (2020). New insights into transport capability of sugars and its impact on growth from novel mutants of Escherichia coli. *Applied microbiology and biotechnology*, *104*, 1463-1479.

Amir, A., Männik, J., Woldringh, C. L., & Zaritsky, A. (2019). the bacterial cell: coupling between growth, nucleoid replication, cell division, and shape volume 2. In (Vol. 10, pp. 2056): Frontiers Media SA.

Auclair, S. M., Bhanu, M. K., & Kendall, D. A. (2012). Signal peptidase I: cleaving the way to mature proteins. *Protein Science*, *21*(1), 13-25.

Babu, M., Bundalovic-Torma, C., Calmettes, C., Phanse, S., Zhang, Q., Jiang, Y., Minic, Z., Kim, S., Mehla, J., & Gagarinova, A. (2018). Global landscape of cell envelope protein complexes in Escherichia coli. *Nature biotechnology*, *36*(1), 103-112.

Banzhaf, M., van den Berg van Saparoea, B., Terrak, M., Fraipont, C., Egan, A., Philippe, J., Zapun, A., Breukink, E., Nguyen-Distèche, M., & den Blaauwen, T. (2012). Cooperativity of peptidoglycan synthases active in bacterial cell elongation. *Molecular microbiology*, *85*(1), 179-194.

Banzhaf, M., Yau, H. C., Verheul, J., Lodge, A., Kritikos, G., Mateus, A., Cordier, B., Hov, A. K., Stein, F., & Wartel, M. (2020). Outer membrane lipoprotein NlpI scaffolds peptidoglycan hydrolases within multi-enzyme complexes in Escherichia coli. *The EMBO journal*, *39*(5), e102246.

Banzhaf, M., Yau, H. C., Verheul, J., Lodge, A., Kritikos, G., Mateus, A., Hov, A. K., Stein, F., Wartel, M., & Pazos, M. (2019). The outer membrane lipoprotein NlpI nucleates hydrolases within peptidoglycan multi-enzyme complexes in Escherichia coli. *BioRxiv*, 609503.

Benz, R. (2006). *Bacterial and eukaryotic porins: structure, function, mechanism*. John Wiley & Sons.

Betzner, A., Ferreira, L., Höltje, J.-V., & Keck, W. (1990). Control of the activity of the soluble lytic transglycosylase by the stringent response in Escherichia coli. *FEMS microbiology letters*, *67*(1-2), 161-164.

Bi, E., & Lutkenhaus, J. (1991). FtsZ ring structure associated with division in Escherichia coli. *Nature*, *354*(6349), 161-164.

Blattner, F. R., Plunkett III, G., Bloch, C. A., Perna, N. T., Burland, V., Riley, M., Collado-Vides, J., Glasner, J. D., Rode, C. K., & Mayhew, G. F. (1997). The complete genome sequence of Escherichia coli K-12. *Science*, *277*(5331), 1453-1462.

Boelter, G., Bryant, J. A., Doherty, H., Wotherspoon, P., Alodaini, D., Ma, X., Alao, M. B., Moynihan, P. J., Moradigaravand, D., & Glinkowska, M. (2022). The lipoprotein DolP affects cell separation in Escherichia coli, but not as an upstream regulator of NlpD. *Microbiology*, *168*(5), 001197.

Boelter, G., Bryant, J. A., Doherty, H., Wotherspoon, P., Alodaini, D., Ma, X., Alao, M. B., Moynihan, P. J., Moradigaravand, D., Glinkowska, M., Knowles, T. J., Henderson, I. R., & Banzhaf, M. (2022). The lipoprotein DolP affects cell separation in Escherichia coli, but not as an upstream regulator of NlpD. *Microbiology*, *168*(5).

Booth, W. T., Clodfelter, J. E., Leone-Kabler, S., Hughes, E. K., Eldeeb, K., Howlett, A. C., & Lowther, W. T. (2021). Cannabinoid receptor interacting protein 1a interacts with myristoylated Gαi N terminus via a unique gapped β-barrel structure. *Journal of Biological Chemistry*, *297*(3).

Born, P., Breukink, E., & Vollmer, W. (2006). In vitro synthesis of cross-linked murein and its attachment to sacculi by PBP1A from Escherichia coli. *Journal of Biological Chemistry*, *281*(37), 26985-26993.

Bryant, J. A., Morris, F. C., Knowles, T. J., Maderbocus, R., Heinz, E., Boelter, G., Alodaini, D., Colyer, A., Wotherspoon, P. J., & Staunton, K. A. (2020). Structure of dual BON-domain protein DolP identifies phospholipid binding as a new mechanism for protein localisation. *Elife*, *9*, e62614.

Buist, G., Steen, A., Kok, J., & Kuipers, O. P. (2008). LysM, a widely distributed protein motif for binding to (peptido) glycans. *Molecular microbiology*, *68*(4), 838-847.

Bush, K., & Bradford, P. A. (2016). β-Lactams and β-Lactamase Inhibitors: An Overview. *Cold Spring Harb Perspect Med*, *6*(8).

Busiek, K. K., & Margolin, W. (2015). Bacterial actin and tubulin homologs in cell growth and division. *Current Biology*, *25*(6), R243-R254.

Cabeen, M. T., & Jacobs-Wagner, C. (2007). Skin and bones: the bacterial cytoskeleton, cell wall, and cell morphogenesis. *The Journal of Cell Biology*, *179*(3), 381.

Carlson, M. L., Stacey, R. G., Young, J. W., Wason, I. S., Zhao, Z., Rattray, D. G., Scott, N., Kerr, C. H., Babu, M., & Foster, L. J. (2019). Profiling the Escherichia coli membrane protein interactome captured in peptidisc libraries. *Elife*, *8*, e46615.

Celler, K., Koning, R. I., Koster, A. J., & van Wezel, G. P. (2013). Multidimensional view of the bacterial cytoskeleton. *Journal of bacteriology*, *195*(8), 1627-1636.

Chipman, D. M., Grisaro, V., & Sharon, N. (1967). The binding of oligosaccharides containing n-acetylglucosamine and n-acetylmuramic acid to lysozyme: the specificity of binding subsites. *Journal of Biological Chemistry*, *242*(19), 4388-4394.

Cho, H., Uehara, T., & Bernhardt, T. G. (2014). Beta-lactam antibiotics induce a lethal malfunctioning of the bacterial cell wall synthesis machinery. *Cell*, *159*(6), 1300-1311.

Chodisetti, P. K., & Reddy, M. (2019). Peptidoglycan hydrolase of an unusual cross-link cleavage specificity contributes to bacterial cell wall synthesis. *Proceedings of the National Academy of Sciences*, *116*(16), 7825-7830.

Chung, H. S., Yao, Z., Goehring, N. W., Kishony, R., Beckwith, J., & Kahne, D. (2009). Rapid β-lactam-induced lysis requires successful assembly of the cell division machinery. *Proceedings of the National Academy of Sciences*, *106*(51), 21872-21877.

Cook, J., Baverstock, T. C., McAndrew, M. B., Roper, D. I., Stansfeld, P. J., & Crow, A. (2023). Activator-induced conformational changes regulate division-associated peptidoglycan amidases. *Proceedings of the National Academy of Sciences*, *120*(24), e2302580120.

Cook, J., Baverstock, T. C., McAndrew, M. B., Stansfeld, P. J., Roper, D. I., & Crow, A. (2020). Insights into bacterial cell division from a structure of EnvC bound to the FtsX periplasmic domain. *Proceedings of the National Academy of Sciences*, *117*(45), 28355-28365.

Cooper, G. M. (2000). The Cell: A Molecular Approach. Sunderland (MA) Sinauer Associates. *Structure and Organization of Actin Filaments*.

Corey, R. A., Song, W., Duncan, A. L., Ansell, T. B., Sansom, M. S., & Stansfeld, P. J. (2021). Identification and assessment of cardiolipin interactions with E. coli inner membrane proteins. *Science advances*, *7*(34), eabh2217.

Crane, J. M., & Randall, L. L. (2017). The Sec system: protein export in Escherichia coli. *EcoSal Plus*, *7*(2), 10.1128/ecosalplus. ESP-0002-2017.

Danese, P. N., & Silhavy, T. J. (1998). CpxP, a stress-combative member of the Cpx regulon. *Journal of bacteriology*, *180*(4), 831-839.

Das, A. K., Cohen, P. T., & Barford, D. (1998). The structure of the tetratricopeptide repeats of protein phosphatase 5: implications for TPR-mediated protein–protein interactions. *The EMBO journal*, *17*(5), 1192-1199.

Datsenko, K. A., & Wanner, B. L. (2000). One-step inactivation of chromosomal genes in Escherichia coli K-12 using PCR products. *Proceedings of the National Academy of Sciences*, *97*(12), 6640-6645.

De Boer, P., Crossley, R., & Rothfield, L. (1992). The essential bacterial cell-division protein FtsZ is a GTPase. *Nature*, *359*(6392), 254-256.
De Gier, J. W., & Luirink, J. (2001). Biogenesis of inner membrane proteins in Escherichia coli. *Molecular microbiology*, *40*(2), 314-322.
de Jong, I. G., Beilharz, K., Kuipers, O. P., & Veening, J.-W. (2011). Live cell imaging of Bacillus subtilis and Streptococcus pneumoniae using automated time-lapse microscopy. *JoVE (Journal of Visualized Experiments)*(53), e3145.
Delhaye, A., Collet, J.-F., & Laloux, G. (2019). A fly on the wall: how stress response systems can sense and respond to damage to peptidoglycan. *Frontiers in Cellular and Infection Microbiology*, *9*, 380.
Den Blaauwen, T., De Pedro, M. A., Nguyen-Disteche, M., & Ayala, J. A. (2008). Morphogenesis of rod-shaped sacculi. *FEMS microbiology reviews*, *32*(2), 321-344.
Denome, S. A., Elf, P. K., Henderson, T. A., Nelson, D. E., & Young, K. D. (1999). Escherichia coli mutants lacking all possible combinations of eight penicillin binding proteins: viability, characteristics, and implications for peptidoglycan synthesis. *Journal of bacteriology*, *181*(13), 3981-3993.
Derouaux, A., Wolf, B., Fraipont, C., Breukink, E., Nguyen-Distèche, M., & Terrak, M. (2008). The monofunctional glycosyltransferase of Escherichia coli localizes to the cell division site and interacts with penicillin-binding protein 3, FtsW, and FtsN. *J Bacteriol*, *190*(5), 1831-1834.
Dik, D. A., Marous, D. R., Fisher, J. F., & Mobashery, S. (2017). Lytic transglycosylases: concinnity in concision of the bacterial cell wall. *Critical Reviews in Biochemistry and Molecular Biology*, *52*(5), 503-542.
Doherty, H. M., Kritikos, G., Galardini, M., Banzhaf, M., & Moradigaravand, D. (2023). ChemGAPP: a tool for chemical genomics analysis and phenotypic profiling. *Bioinformatics*, *39*(4), btad171.
Doherty, H. M., Kritikos, G., Galardini, M., Banzhaf, M., & Moradigaravand, D. (2023). ChemGAPP: a tool for chemical genomics analysis and phenotypic profiling. *Bioinformatics*, *39*(4).
Dramsi, S., Magnet, S., Davison, S., & Arthur, M. (2008). Covalent attachment of proteins to peptidoglycan. *FEMS Microbiol Rev*, *32*(2), 307-320.
Du, S., Pichoff, S., Kruse, K., & Lutkenhaus, J. (2018). FtsZ filaments have the opposite kinetic polarity of microtubules. *Proceedings of the National Academy of Sciences*, *115*(42), 10768-10773.
Dubarry, N., Possoz, C., & Barre, F. X. (2010). Multiple regions along the Escherichia coli FtsK protein are implicated in cell division. *Molecular microbiology*, *78*(5), 1088-1100.
Ducret, A., Quardokus, E. M., & Brun, Y. V. (2016). MicrobeJ, a tool for high throughput bacterial cell detection and quantitative analysis. *Nature microbiology*, *1*(7), 1-7.
Egan, A. J., Biboy, J., van't Veer, I., Breukink, E., & Vollmer, W. (2015). Activities and regulation of peptidoglycan synthases. *Philosophical Transactions of the Royal Society B: Biological Sciences*, *370*(1679), 20150031.
Egan, A. J., Biboy, J., van't Veer, I., Breukink, E., & Vollmer, W. (2015). Activities and regulation of peptidoglycan synthases. *Philos Trans R Soc Lond B Biol Sci*, *370*(1679).
Emami, K., Guyet, A., Kawai, Y., Devi, J., Wu, L. J., Allenby, N., Daniel, R. A., & Errington, J. (2017). RodA as the missing glycosyltransferase in Bacillus subtilis and antibiotic discovery for the peptidoglycan polymerase pathway. *Nature microbiology*, *2*(3), 1-9.
Fenton, M., McAuliffe, O., O'Mahony, J., & Coffey, A. (2010). Recombinant bacteriophage lysins as antibacterials. *Bioengineered bugs*, *1*(1), 9-16.
Fivenson, E. M., Rohs, P. D. A., Vettiger, A., Sardis, M. F., Torres, G., Forchoh, A., & Bernhardt, T. G. (2023). A role for the Gram-negative outer membrane in bacterial shape determination. *Proc Natl Acad Sci U S A*, *120*(35), e2301987120.
Fleming, A. (1929). On the antibacterial action of cultures of a penicillium, with special reference to their use in the isolation of B. influenzae. *British journal of experimental pathology*, *10*(3), 226.

Fleming, K. G. (2015). A combined kinetic push and thermodynamic pull as driving forces for outer membrane protein sorting and folding in bacteria. *Philosophical Transactions of the Royal Society B: Biological Sciences*, *370*(1679), 20150026.

Fraipont, C., Alexeeva, S., Wolf, B., van der Ploeg, R., Schloesser, M., den Blaauwen, T., & Nguyen-Disteche, M. (2011). The integral membrane FtsW protein and peptidoglycan synthase PBP3 form a subcomplex in Escherichia coli. *Microbiology*, *157*(1), 251-259.

Fuda, C., Suvorov, M., Vakulenko, S. B., & Mobashery, S. (2004). The basis for resistance to β-lactam antibiotics by penicillin-binding protein 2a of methicillin-resistant Staphylococcus aureus. *Journal of Biological Chemistry*, *279*(39), 40802-40806.

Ghuysen, J.-M. (1997). Penicillin-binding proteins. Wall peptidoglycan assembly and resistance to penicillin: facts, doubts and hopes. *International journal of antimicrobial agents*, *8*(1), 45-60.

Glauner, B., Höltje, J., & Schwarz, U. (1988). The composition of the murein of Escherichia coli. *Journal of Biological Chemistry*, *263*(21), 10088-10095.

Godino, E., Doerr, A., & Danelon, C. (2022). Min waves without MinC can pattern FtsA-anchored FtsZ filaments on model membranes. *Commun Biol*, *5*(1), 675.

Goffin, C., & Ghuysen, J.-M. (1998). Multimodular penicillin-binding proteins: an enigmatic family of orthologs and paralogs. *Microbiology and molecular biology reviews*, *62*(4), 1079-1093.

González-Leiza, S. M., de Pedro, M. A., & Ayala, J. A. (2011). AmpH, a bifunctional DD-endopeptidase and DD-carboxypeptidase of Escherichia coli. *Journal of bacteriology*, *193*(24), 6887-6894.

Goodall, E. C., Robinson, A., Johnston, I. G., Jabbari, S., Turner, K. A., Cunningham, A. F., Lund, P. A., Cole, J. A., & Henderson, I. R. (2018). The essential genome of Escherichia coli K-12. *MBio*, *9*(1), 10.1128/mbio. 02096-02017.

Graham, C. L., Newman, H., Gillett, F. N., Smart, K., Briggs, N., Banzhaf, M., & Roper, D. I. (2021). A dynamic network of proteins facilitate cell envelope biogenesis in gram-negative bacteria. *International Journal of Molecular Sciences*, *22*(23), 12831.

Gram, C. (1884). The differential staining of Schizomycetes in tissue sections and in dried preparations. *Fortschitte der Medicin*, *2*(6), 185-189.

Gray, A. N., Egan, A. J., Van't Veer, I. L., Verheul, J., Colavin, A., Koumoutsi, A., Biboy, J., Altelaar, A. M., Damen, M. J., & Huang, K. C. (2015). Coordination of peptidoglycan synthesis and outer membrane constriction during Escherichia coli cell division. *Elife*, *4*, e07118.

Gu, Y., Li, H., Dong, H., Zeng, Y., Zhang, Z., Paterson, N. G., Stansfeld, P. J., Wang, Z., Zhang, Y., & Wang, W. (2016). Structural basis of outer membrane protein insertion by the BAM complex. *Nature*, *531*(7592), 64-69.

Gurnani Serrano, C. K., Winkle, M., Martorana, A. M., Biboy, J., Morè, N., Moynihan, P., Banzhaf, M., Vollmer, W., & Polissi, A. (2021). ActS activates peptidoglycan amidases during outer membrane stress in Escherichia coli. *Molecular microbiology*, *116*(1), 329-342.

Hale, C. A., Persons, L., & de Boer, P. A. (2022). Recruitment of the TolA protein to cell constriction sites in Escherichia coli via three separate mechanisms, and a critical role for FtsWI activity in recruitment of both TolA and TolQ. *Journal of bacteriology*, *204*(1), e00464-00421.

Han, L., Zheng, J., Wang, Y., Yang, X., Liu, Y., Sun, C., Cao, B., Zhou, H., Ni, D., & Lou, J. (2016). Structure of the BAM complex and its implications for biogenesis of outer-membrane proteins. *Nature structural & molecular biology*, *23*(3), 192-196.

Hara, H., Narita, S., Karibian, D., Park, J. T., Yamamoto, Y., & Nishimura, Y. (2002). Identification and characterization of the Escherichia coli envC gene encoding a periplasmic coiled-coil protein with putative peptidase activity. *FEMS microbiology letters*, *212*(2), 229-236.

Harold, F. M. (2007). Bacterial morphogenesis: learning how cells make cells. *Current opinion in microbiology*, *10*(6), 591-595.

Hedge, P. J., & Spratt, B. G. (1985). Resistance to β-lactam antibiotics by re-modelling the active site of an E. coli penicillin-binding protein. *Nature*, *318*(6045), 478-480.
Heidrich, C., Templin, M. F., Ursinus, A., Merdanovic, M., Berger, J., Schwarz, H., De Pedro, M. A., & Höltje, J. V. (2001). Involvement of N-acetylmuramyl-L-alanine amidases in cell separation and antibiotic-induced autolysis of Escherichia coli. *Molecular microbiology*, *41*(1), 167-178.
Henderson, T. A., Young, K. D., Denome, S. A., & Elf, P. K. (1997). AmpC and AmpH, proteins related to the class C beta-lactamases, bind penicillin and contribute to the normal morphology of Escherichia coli. *Journal of bacteriology*, *179*(19), 6112-6121.
Hershey, A. (1939). Factors limiting bacterial growth: IV. The age of the parent culture and the rate of growth of transplants of Escherichia coli. *Journal of bacteriology*, *37*(3), 285-299.
Höltje, J.-V. (1995). From growth to autolysis: the murein hydrolases in Escherichia coli. *Archives of microbiology*, *164*, 243-254.
Höltje, J.-V. (1998). Growth of the stress-bearing and shape-maintaining murein sacculus of Escherichia coli. *Microbiology and molecular biology reviews*, *62*(1), 181-203.
Höltje, J.-V., & Schwarz, U. (1985). Biosynthesis and growth of the murein sacculus.
Höltje, J.-V., & Tuomanen, E. I. (1991). The murein hydrolases of Escherichia coli: properties, functions and impact on the course of infections in vivo. *Microbiology*, *137*(3), 441-454.
Höltje, J., Mirelman, D., Sharon, N., & Schwarz, U. (1975). Novel type of murein transglycosylase in Escherichia coli. *Journal of bacteriology*, *124*(3), 1067-1076.
Hughes, G. W., Hall, S. C., Laxton, C. S., Sridhar, P., Mahadi, A. H., Hatton, C., Piggot, T. J., Wotherspoon, P. J., Leney, A. C., & Ward, D. G. (2019). Evidence for phospholipid export from the bacterial inner membrane by the Mla ABC transport system. *Nature microbiology*, *4*(10), 1692-1705.
Ishino, F., Mitsui, K., Tamaki, S., & Matsuhashi, M. (1980). Dual enzyme activities of cell wall peptidoglycan synthesis, peptidoglycan transglycosylase and penicillin-sensitive transpeptidase, in purified preparations of Escherichia coli penicillin-binding protein 1A. *Biochemical and biophysical research communications*, *97*(1), 287-293.
Jacoby, G. A. (2009). AmpC β-lactamases. *Clinical microbiology reviews*, *22*(1), 161-182.
Jacoby, G. A., & Munoz-Price, L. S. (2005). The new β-lactamases. *New England Journal of Medicine*, *352*(4), 380-391.
Jean, N. L., Bougault, C. M., Lodge, A., Derouaux, A., Callens, G., Egan, A. J., Ayala, I., Lewis, R. J., Vollmer, W., & Simorre, J.-P. (2014). Elongated structure of the outer-membrane activator of peptidoglycan synthesis LpoA: implications for PBP1A stimulation. *Structure*, *22*(7), 1047-1054.
Jeon, W.-J., & Cho, H. (2022). A cell wall hydrolase MepH is negatively regulated by proteolysis involving Prc and NlpI in Escherichia coli. *Frontiers in microbiology*, *13*, 878049.
Jiang, Y., Wang, Y., Pang, W., Chen, L., Sun, H., Liang, Y., & Blanzieri, E. (2015). Essential protein identification based on essential protein–protein interaction prediction by integrated edge weights. *Methods*, *83*, 51-62.
Jorgenson, M. A., Chen, Y., Yahashiri, A., Popham, D. L., & Weiss, D. S. (2014). The bacterial septal ring protein RlpA is a lytic transglycosylase that contributes to rod shape and daughter cell separation in P seudomonas aeruginosa. *Molecular microbiology*, *93*(1), 113-128.
Jorgenson, M. A., MacCain, W. J., Meberg, B. M., Kannan, S., Bryant, J. C., & Young, K. D. (2019). Simultaneously inhibiting undecaprenyl phosphate production and peptidoglycan synthases promotes rapid lysis in Escherichia coli. *Molecular microbiology*, *112*(1), 233-248.
Käshammer, L., van den Ent, F., Jeffery, M., Jean, N. L., Hale, V. L., & Löwe, J. (2023). Cryo-EM structure of the bacterial divisome core complex and antibiotic target FtsWIQBL. *Nat Microbiol*, *8*(6), 1149-1159.

Kitano, K., Tuomanen, E., & Tomasz, A. (1986). Transglycosylase and endopeptidase participate in the degradation of murein during autolysis of Escherichia coli. *Journal of bacteriology*, *167*(3), 759-765.

Kleckner, N., Fisher, J. K., Stouf, M., White, M. A., Bates, D., & Witz, G. (2014). The bacterial nucleoid: nature, dynamics and sister segregation. *Curr Opin Microbiol*, *22*, 127-137.

Köhler, T., Michea-Hamzehpour, M., Epp, S. F., & Pechere, J.-C. (1999). Carbapenem activities against Pseudomonas aeruginosa: respective contributions of OprD and efflux systems. *Antimicrobial agents and chemotherapy*, *43*(2), 424-427.

Kohlrausch, U., & Höltje, J. (1991). Analysis of murein and murein precursors during antibiotic-induced lysis of Escherichia coli. *Journal of bacteriology*, *173*(11), 3425-3431.

Korat, B., Mottl, H., & Keck, W. (1991). Penicillin-binding protein 4 of Escherichia coli: molecular cloning of the dacB gene, controlled overexpression, and alterations in murein composition. *Molecular microbiology*, *5*(3), 675-684.

Laddomada, F., Miyachiro, M. M., & Dessen, A. (2016). Structural insights into protein-protein interactions involved in bacterial cell wall biogenesis. *Antibiotics*, *5*(2), 14.

Lam, H., Oh, D.-C., Cava, F., Takacs, C. N., Clardy, J., de Pedro, M. A., & Waldor, M. K. (2009). D-amino acids govern stationary phase cell wall remodeling in bacteria. *Science*, *325*(5947), 1552-1555.

Li, Y., Boes, A., Cui, Y., Zhao, S., Liao, Q., Gong, H., Breukink, E., Lutkenhaus, J., Terrak, M., & Du, S. (2022). Identification of the potential active site of the septal peptidoglycan polymerase FtsW. *PLoS genetics*, *18*(1), e1009993.

Liu, C., Luo, G., Liu, H., Yang, Z., Angelidaki, I., Sompong, O., Liu, G., Zhang, S., & Wang, W. (2020). CO as electron donor for efficient medium chain carboxylate production by chain elongation: Microbial and thermodynamic insights. *Chemical Engineering Journal*, *390*, 124577.

Lugtenberg, B., Meijers, J., Peters, R., Hoek, P. v. d., & Alphen, L. v. (1975). Electrophoretic resolution of the 'major outer membrane protein'of Escherichia coli K12 into four bands. *FEBS letters*, *58*(12), 254-258.

Luirink, J., Heijne, G. v., Houben, E., & Gier, J.-W. d. (2005). Biogenesis of inner membrane proteins in Escherichia coli. *Annu. Rev. Microbiol.*, *59*, 329-355.

Lupoli, T. J., Lebar, M. D., Markovski, M., Bernhardt, T., Kahne, D., & Walker, S. (2014). Lipoprotein activators stimulate *Escherichia coli* penicillin-binding proteins by different mechanisms. *Journal of the American Chemical Society*, *136*(1), 52-55.

Lupoli, T. J., Lebar, M. D., Markovski, M., Bernhardt, T., Kahne, D., & Walker, S. (2014). Lipoprotein activators stimulate Escherichia coli penicillin-binding proteins by different mechanisms. *Journal of the American Chemical Society*, *136*(1), 52-55.

Lutkenhaus, J., Pichoff, S., & Du, S. (2012). Bacterial cytokinesis: from Z ring to divisome. *Cytoskeleton*, *69*(10), 778-790.

Maeda, H. (1980). A new lysozyme assay based on fluorescence polarization or fluorescence intensity utilizing a fluorescent peptidoglycan substrate. *The Journal of Biochemistry*, *88*(4), 1185-1191.

Magnet, S., Bellais, S., Dubost, L., Fourgeaud, M., Mainardi, J.-L., Petit-Frère, S., Marie, A., Mengin-Lecreulx, D., Arthur, M., & Gutmann, L. (2007). Identification of the L, D-transpeptidases responsible for attachment of the Braun lipoprotein to Escherichia coli peptidoglycan. *Journal of bacteriology*, *189*(10), 3927-3931.

Mainardi, J.-L., Fourgeaud, M., Hugonnet, J.-E., Dubost, L., Brouard, J.-P., Ouazzani, J., Rice, L. B., Gutmann, L., & Arthur, M. (2005). A novel peptidoglycan cross-linking enzyme for a β-lactam-resistant transpeptidation pathway. *Journal of Biological Chemistry*, *280*(46), 38146-38152.

Mamou, G., Inns, P. G., Sun, D., Kaminska, R., Housden, N. G., Cohen-Khait, R., Miller, H., Storek, K. M., Rutherford, S. T., & Payandeh, J. (2021). Spatiotemporal organization of BamA governs the

pattern of outer membrane protein distribution in growing Escherichia coli cells. *BioRxiv*, 2021.2001. 2027.428258.
Marcyjaniak, M., Odintsov, S. G., Sabala, I., & Bochtler, M. (2004). Peptidoglycan amidase MepA is a LAS metallopeptidase. *Journal of Biological Chemistry*, *279*(42), 43982-43989.
Matteï, P.-J., Neves, D., & Dessen, A. (2010). Bridging cell wall biosynthesis and bacterial morphogenesis. *Current opinion in structural biology*, *20*(6), 749-755.
Meberg, B. M., Sailer, F. C., Nelson, D. E., & Young, K. D. (2001). Reconstruction of Escherichia coli mrcA (PBP 1a) mutants lacking multiple combinations of penicillin binding proteins. *Journal of bacteriology*, *183*(20), 6148-6149.
Meeske, A. J., Riley, E. P., Robins, W. P., Uehara, T., Mekalanos, J. J., Kahne, D., Walker, S., Kruse, A. C., Bernhardt, T. G., & Rudner, D. Z. (2016). SEDS proteins are a widespread family of bacterial cell wall polymerases. *Nature*, *537*(7622), 634-638.
Meisner, J., & Moran Jr, C. P. (2011). A LytM domain dictates the localization of proteins to the mother cell-forespore interface during bacterial endospore formation. *Journal of bacteriology*, *193*(3), 591-598.
Mercer, K. L., & Weiss, D. S. (2002). The Escherichia coli cell division protein FtsW is required to recruit its cognate transpeptidase, FtsI (PBP3), to the division site. *Journal of bacteriology*, *184*(4), 904-912.
Mesnage, S., Dellarole, M., Baxter, N. J., Rouget, J.-B., Dimitrov, J. D., Wang, N., Fujimoto, Y., Hounslow, A. M., Lacroix-Desmazes, S., & Fukase, K. (2014). Molecular basis for bacterial peptidoglycan recognition by LysM domains. *Nature communications*, *5*(1), 4269.
Mingorance, J., Tamames, J., & Vicente, M. (2004). Genomic channeling in bacterial cell division. *Journal of molecular recognition*, *17*(5), 481-487.
Monod, J. (1958). Recherches sur la croissance des cultures bacteriennes. *(No Title)*.
Morris, F. C., Wells, T. J., Bryant, J. A., Schager, A. E., Sevastsyanovich, Y. R., Squire, D. J., Marshall, J., Isom, G. L., Rooke, J., & Maderbocus, R. (2018). YraP contributes to cell envelope integrity and virulence of Salmonella enterica serovar Typhimurium. *Infection and immunity*, *86*(11), 10.1128/iai. 00829-00817.
Mueller, E. A., Egan, A. J., Breukink, E., Vollmer, W., & Levin, P. A. (2019). Plasticity of Escherichia coli cell wall metabolism promotes fitness and antibiotic resistance across environmental conditions. *Elife*, *8*, e40754.
Mueller, E. A., Iken, A. G., Ali Öztürk, M., Winkle, M., Schmitz, M., Vollmer, W., Di Ventura, B., & Levin, P. A. (2021). The active repertoire of Escherichia coli peptidoglycan amidases varies with physiochemical environment. *Molecular microbiology*, *116*(1), 311-328.
Nakagawà, J.-i., Tamaki, S., & Matsuhashi, M. (1979). Purified penicillin binding proteins 1Bs from Escherichia coli membrane showing activities of both peptidoglycan polymerase and peptidoglycan crosslinking enzyme. *Agricultural and Biological Chemistry*, *43*(6), 1379-1380.
Nanninga, N. (1998). Morphogenesis of Escherichia coli. *Microbiology and molecular biology reviews*, *62*(1), 110-129.
Navarro, P. P., Vettiger, A., Ananda, V. Y., Llopis, P. M., Allolio, C., Bernhardt, T. G., & Chao, L. H. (2022). Cell wall synthesis and remodelling dynamics determine division site architecture and cell shape in Escherichia coli. *Nature Microbiology*, *7*(10), 1621-1634.
Nelson, D. E., & Young, K. D. (2000). Penicillin binding protein 5 affects cell diameter, contour, and morphology of Escherichia coli. *Journal of bacteriology*, *182*(6), 1714-1721.
Neuhaus, F. C., & Baddiley, J. (2003). A continuum of anionic charge: structures and functions of D-alanyl-teichoic acids in gram-positive bacteria. *Microbiol Mol Biol Rev*, *67*(4), 686-723.
Noinaj, N., Rollauer, S. E., & Buchanan, S. K. (2015). The β-barrel membrane protein insertase machinery from Gram-negative bacteria. *Current opinion in structural biology*, *31*, 35-42.

Onufryk, C., Crouch, M.-L., Fang, F. C., & Gross, C. A. (2005). Characterization of six lipoproteins in the σE regulon. *Journal of bacteriology*, *187*(13), 4552-4561.

Paradis-Bleau, C., Markovski, M., Uehara, T., Lupoli, T. J., Walker, S., Kahne, D. E., & Bernhardt, T. G. (2010). Lipoprotein cofactors located in the outer membrane activate bacterial cell wall polymerases. *Cell*, *143*(7), 1110-1120.

Park, J. T., & Uehara, T. (2008). How bacteria consume their own exoskeletons (turnover and recycling of cell wall peptidoglycan). *Microbiology and molecular biology reviews*, *72*(2), 211-227.

Park, S. H., Kim, Y. J., Lee, H. B., Seok, Y.-J., & Lee, C.-R. (2020). Genetic evidence for distinct functions of peptidoglycan endopeptidases in Escherichia coli. *Frontiers in microbiology*, *11*, 565767.

Pazos, M., Peters, K., Boes, A., Safaei, Y., Kenward, C., Caveney Nathanael, A., Laguri, C., Breukink, E., Strynadka Natalie, C. J., Simorre, J.-P., Terrak, M., & Vollmer, W. (2020). SPOR Proteins Are Required for Functionality of Class A Penicillin-Binding Proteins in Escherichia coli. *MBio*, *11*(6), e02796-02720.

Peters, N. T., Morlot, C., Yang, D. C., Uehara, T., Vernet, T., & Bernhardt, T. G. (2013). Structure–function analysis of the LytM domain of EnvC, an activator of cell wall remodelling at the E scherichia coli division site. *Molecular microbiology*, *89*(4), 690-701.

Petiti, M., Serrano, B., Faure, L., Lloubes, R., Mignot, T., & Duché, D. (2019). Tol energy-driven localization of Pal and anchoring to the peptidoglycan promote outer-membrane constriction. *Journal of molecular biology*, *431*(17), 3275-3288.

Pichoff, S., Du, S., & Lutkenhaus, J. (2019). Roles of FtsEX in cell division. *Research in microbiology*, *170*(8), 374-380.

Pilhofer, M., & Jensen, G. J. (2013). The bacterial cytoskeleton: more than twisted filaments. *Current opinion in cell biology*, *25*(1), 125-133.

Plummer, A. M., Gessmann, D., & Fleming, K. G. (2015). The role of a destabilized membrane for OMP insertion. *The BAM Complex: Methods and Protocols*, 57-65.

Priyadarshini, R., de Pedro, M. A., & Young, K. D. (2007). Role of peptidoglycan amidases in the development and morphology of the division septum in Escherichia coli. *Journal of bacteriology*, *189*(14), 5334-5347.

Ranava, D., Yang, Y., Orenday-Tapia, L., Rousset, F., Turlan, C., Morales, V., Cui, L., Moulin, C., Froment, C., & Munoz, G. (2021). Lipoprotein DolP supports proper folding of BamA in the bacterial outer membrane promoting fitness upon envelope stress. *Elife*, *10*, e67817.

Rigden, D. J., Jedrzejas, M. J., & Galperin, M. Y. (2003). Amidase domains from bacterial and phage autolysins define a family of γ-d, l-glutamate-specific amidohydrolases. *Trends in biochemical sciences*, *28*(5), 230-234.

Rios-Szwed, D. O., Garcia-Wilson, E., Sanchez-Pulido, L., Alvarez, V., Jiang, H., Bandau, S., Lamond, A., Ponting, C. P., & Alabert, C. (2020). FAM111A regulates replication origin activation and cell fitness. *BioRxiv*, 2020.2004. 2022.055574.

Rocaboy, M., Herman, R., Sauvage, E., Remaut, H., Moonens, K., Terrak, M., Charlier, P., & Kerff, F. (2013). The crystal structure of the cell division amidase AmiC reveals the fold of the AMIN domain, a new peptidoglycan binding domain. *Molecular microbiology*, *90*(2), 267-277.

Rohs, P. D., Buss, J., Sim, S. I., Squyres, G. R., Srisuknimit, V., Smith, M., Cho, H., Sjodt, M., Kruse, A. C., & Garner, E. C. (2018). A central role for PBP2 in the activation of peptidoglycan polymerization by the bacterial cell elongation machinery. *PLoS genetics*, *14*(10), e1007726.

Rothfield, L., Taghbalout, A., & Shih, Y.-L. (2005). Spatial control of bacterial division-site placement. *Nature Reviews Microbiology*, *3*(12), 959-968.

Sabala, I., Jonsson, I.-M., Tarkowski, A., & Bochtler, M. (2012). Anti-staphylococcal activities of lysostaphin and LytM catalytic domain. *BMC microbiology*, *12*(1), 1-11.

Sanganna Gari, R. R., Chattrakun, K., Marsh, B. P., Mao, C., Chada, N., Randall, L. L., & King, G. M. (2019). Direct visualization of the E. coli Sec translocase engaging precursor proteins in lipid bilayers. *Science advances*, *5*(6), eaav9404.

Sardis, M. F., Bohrhunter, J. L., Greene, N. G., & Bernhardt, T. G. (2021). The LpoA activator is required to stimulate the peptidoglycan polymerase activity of its cognate cell wall synthase PBP1a. *Proceedings of the National Academy of Sciences*, *118*(35), e2108894118.

Sauvage, E., Kerff, F., Terrak, M., Ayala, J. A., & Charlier, P. (2008). The penicillin-binding proteins: structure and role in peptidoglycan biosynthesis. *FEMS microbiology reviews*, *32*(2), 234-258.

Schaechter, M. (2015). A brief history of bacterial growth physiology. *Front Microbiol*, *6*, 289.

Scheurwater, E., Reid, C. W., & Clarke, A. J. (2008). Lytic transglycosylases: bacterial space-making autolysins. *The international journal of biochemistry & cell biology*, *40*(4), 586-591.

Schleifer, K. H., & Kandler, O. (1972). Peptidoglycan types of bacterial cell walls and their taxonomic implications. *Bacteriological reviews*, *36*(4), 407-477.

Schmit, A.-C., & Nick, P. (2008). Microtubules and the evolution of mitosis. In *Plant Microtubules: Development and Flexibility* (pp. 233-266). Springer.

Shah, D., Guo, Y., Ocando, J., & Shao, J. (2019). FITC labeling of human insulin and transport of FITC-insulin conjugates through MDCK cell monolayer. *Journal of Pharmaceutical Analysis*, *9*(6), 400-405.

Shih, Y.-L., & Rothfield, L. (2006). The bacterial cytoskeleton. *Microbiology and molecular biology reviews*, *70*(3), 729-754.

Silhavy, T. J., Kahne, D., & Walker, S. (2010). The bacterial cell envelope. *Cold Spring Harbor perspectives in biology*, *2*(5), a000414.

Singh, S. K., Parveen, S., SaiSree, L., & Reddy, M. (2015). Regulated proteolysis of a cross-link–specific peptidoglycan hydrolase contributes to bacterial morphogenesis. *Proceedings of the National Academy of Sciences*, *112*(35), 10956-10961.

Singh, S. K., SaiSree, L., Amrutha, R. N., & Reddy, M. (2012). Three redundant murein endopeptidases catalyse an essential cleavage step in peptidoglycan synthesis of E scherichia coli K 12. *Molecular microbiology*, *86*(5), 1036-1051.

Smith, M., Espiner, E., Yandle, T., Charles, C., & Richards, A. (2000). Delayed metabolism of human brain natriuretic peptide reflects resistance to neutral endopeptidase. *Journal of endocrinology*, *167*(2), 239-246.

Spratt, B. G. (1975). Distinct penicillin binding proteins involved in the division, elongation, and shape of Escherichia coli K12. *Proceedings of the National Academy of Sciences*, *72*(8), 2999-3003.

Spratt, B. G. (1977). Temperature-sensitive cell division mutants of Escherichia coli with thermolabile penicillin-binding proteins. *Journal of bacteriology*, *131*(1), 293-305.

Spratt, B. G., & Strominger, J. L. (1976). Identification of the major penicillin-binding proteins of Escherichia coli as D-alanine carboxypeptidase IA. *Journal of bacteriology*, *127*(1), 660-663.

Su, M.-Y., Som, N., Wu, C.-Y., Su, S.-C., Kuo, Y.-T., Ke, L.-C., Ho, M.-R., Tzeng, S.-R., Teng, C.-H., & Mengin-Lecreulx, D. (2017). Structural basis of adaptor-mediated protein degradation by the tail-specific PDZ-protease Prc. *Nature communications*, *8*(1), 1516.

Sung, M.-T., Lai, Y.-T., Huang, C.-Y., Chou, L.-Y., Shih, H.-W., Cheng, W.-C., Wong, C.-H., & Ma, C. (2009). Crystal structure of the membrane-bound bifunctional transglycosylase PBP1b from Escherichia coli. *Proceedings of the National Academy of Sciences*, *106*(22), 8824-8829.

Suzuki, H., Nishimura, Y., & Hirota, Y. (1978). On the process of cellular division in Escherichia coli: a series of mutants of E. coli altered in the penicillin-binding proteins. *Proceedings of the National Academy of Sciences*, *75*(2), 664-668.

Taguchi, A., Welsh, M. A., Marmont, L. S., Lee, W., Sjodt, M., Kruse, A. C., Kahne, D., Bernhardt, T. G., & Walker, S. (2019). FtsW is a peptidoglycan polymerase that is functional only in complex with its cognate penicillin-binding protein. *Nature microbiology*, *4*(4), 587-594.

Terrak, M., & Nguyen-Disteche, M. (2006). Kinetic characterization of the monofunctional glycosyltransferase from Staphylococcus aureus. *Journal of bacteriology*, *188*(7), 2528-2532.

The, T. H., & Feltkamp, T. E. (1970). Conjugation of fluorescein isothiocyanate to antibodies. I. Experiments on the conditions of conjugation. *Immunology*, *18*(6), 865-873.

Tipper, D. J., & Strominger, J. L. (1965). Mechanism of action of penicillins: a proposal based on their structural similarity to acyl-D-alanyl-D-alanine. *Proceedings of the National Academy of Sciences*, *54*(4), 1133-1141.

Tomasek, D., & Kahne, D. (2021). The assembly of β-barrel outer membrane proteins. *Current opinion in microbiology*, *60*, 16-23.

Tomasz, A. (1979). The mechanism of the irreversible antimicrobial effects of penicillins: how the beta-lactam antibiotics kill and lyse bacteria. *Annual Reviews in Microbiology*, *33*(1), 113-137.

Truong, T. T. (2020). *The Cell Elongation Activity of Peptidoglycan Endopeptidases Antagonizes Cell Division in Escherichia coli* Harvard University].

Tsang, M.-J., Yakhnina, A. A., & Bernhardt, T. G. (2017). NlpD links cell wall remodeling and outer membrane invagination during cytokinesis in Escherichia coli. *PLoS genetics*, *13*(7), e1006888.

Typas, A., Banzhaf, M., Gross, C. A., & Vollmer, W. (2012). From the regulation of peptidoglycan synthesis to bacterial growth and morphology. *Nature Reviews Microbiology*, *10*(2), 123-136.

Typas, A., Banzhaf, M., van Saparoea, B. v. d. B., Verheul, J., Biboy, J., Nichols, R. J., Zietek, M., Beilharz, K., Kannenberg, K., & von Rechenberg, M. (2010). Regulation of peptidoglycan synthesis by outer-membrane proteins. *Cell*, *143*(7), 1097-1109.

Uehara, T., Dinh, T., & Bernhardt, T. G. (2009). LytM-domain factors are required for daughter cell separation and rapid ampicillin-induced lysis in Escherichia coli. *Journal of bacteriology*, *191*(16), 5094-5107.

Uehara, T., Parzych, K. R., Dinh, T., & Bernhardt, T. G. (2010). Daughter cell separation is controlled by cytokinetic ring-activated cell wall hydrolysis. *The EMBO journal*, *29*(8), 1412-1422.

van den Ent, F., Amos, L. A., & Löwe, J. (2001). Prokaryotic origin of the actin cytoskeleton. *Nature*, *413*(6851), 39-44.

Van der Ploeg, R., Verheul, J., Vischer, N. O., Alexeeva, S., Hoogendoorn, E., Postma, M., Banzhaf, M., Vollmer, W., & Den Blaauwen, T. (2013). Colocalization and interaction between elongasome and divisome during a preparative cell division phase in E scherichia coli. *Molecular microbiology*, *87*(5), 1074-1087.

van Heijenoort, J. (2011). Peptidoglycan hydrolases of Escherichia coli. *Microbiology and molecular biology reviews*, *75*(4), 636-663.

Van Teeffelen, S., & Gitai, Z. (2011). Rotate into shape: MreB and bacterial morphogenesis. *The EMBO journal*, *30*(24), 4856-4857.

Vega, D., & Ayala, J. A. (2006). The DD-carboxypeptidase activity encoded by pbp4B is not essential for the cell growth of Escherichia coli. *Archives of microbiology*, *185*, 23-27.

Vejborg, R. M., & Klemm, P. (2009). Cellular chain formation in Escherichia coli biofilms. *Microbiology*, *155*(5), 1407-1417.

Verheul, J., Lodge, A., Yau, H. C., Liu, X., Boelter, G., Liu, X., Solovyova, A. S., Typas, A., Banzhaf, M., & Vollmer, W. (2022). Early midcell localization of Escherichia coli PBP4 supports the function of peptidoglycan amidases. *PLoS genetics*, *18*(5), e1010222.

Verheul, J., Lodge, A., Yau, H. C. L., Liu, X., Boelter, G., Liu, X., Solovyova, A. S., Typas, A., Banzhaf, M., Vollmer, W., & den Blaauwen, T. (2022). Early midcell localization of Escherichia coli PBP4 supports the function of peptidoglycan amidases. *PLoS Genet*, *18*(5), e1010222.

Vermassen, A., Leroy, S., Talon, R., Provot, C., Popowska, M., & Desvaux, M. (2019). Cell wall hydrolases in bacteria: insight on the diversity of cell wall amidases, glycosidases and peptidases toward peptidoglycan. *Frontiers in microbiology*, *10*, 331.

Voedts, H., Dorchêne, D., Lodge, A., Vollmer, W., Arthur, M., & Hugonnet, J. E. (2021). Role of endopeptidases in peptidoglycan synthesis mediated by alternative cross-linking enzymes in Escherichia coli. *The EMBO journal*, *40*(19), e108126.

Vollmer, W., & Bertsche, U. (2008). Murein (peptidoglycan) structure, architecture and biosynthesis in Escherichia coli. *Biochimica et Biophysica Acta (BBA)-Biomembranes*, *1778*(9), 1714-1734.

Vollmer, W., Blanot, D., & De Pedro, M. A. (2008). Peptidoglycan structure and architecture. *FEMS microbiology reviews*, *32*(2), 149-167.

Vollmer, W., & Holtje, J.-V. (2004). The architecture of the murein (peptidoglycan) in gram-negative bacteria: vertical scaffold or horizontal layer (s)? *Journal of bacteriology*, *186*(18), 5978-5987.

Von Heijne, G. (1992). Membrane protein structure prediction: hydrophobicity analysis and the positive-inside rule. *Journal of molecular biology*, *225*(2), 487-494.

Waxman, D. J., & Strominger, J. L. (1983). Penicillin-binding proteins and the mechanism of action of beta-lactam antibiotics. *Annual review of biochemistry*, *52*(1), 825-869.

Wehrens, M., Ershov, D., Rozendaal, R., Walker, N., Schultz, D., Kishony, R., Levin, P. A., & Tans, S. J. (2018). Size laws and division ring dynamics in filamentous Escherichia coli cells. *Current Biology*, *28*(6), 972-979. e975.

Weidel, W., & Pelzer, H. (1964). BAGSHAPED MACROMOLECULES--A NEW OUTLOOK ON BACTERIAL CELL WALLS. *Adv Enzymol Relat Areas Mol Biol*, *26*, 193-232.

Weiss, D. S., Pogliano, K., Carson, M., Guzman, L. M., Fraipont, C., Nguyen-Distèche, M., Losick, R., & Beckwith, J. (1997). Localization of the Escherichia coli cell division protein FtsI (PBP3) to the division site and cell pole. *Molecular microbiology*, *25*(4), 671-681.

White, C. L., Kitich, A., & Gober, J. W. (2010). Positioning cell wall synthetic complexes by the bacterial morphogenetic proteins MreB and MreD. *Molecular microbiology*, *76*(3), 616-633.

Wilson, C. G., Kajander, T., & Regan, L. (2005). The crystal structure of NlpI: A prokaryotic tetratricopeptide repeat protein with a globular fold. *The FEBS Journal*, *272*(1), 166-179.

Wu, R. (2022). *STRUCTURAL STUDIES ON THE BIOGENESIS OF OMPS BY THE β-BARREL ASSEMBLY MACHINERY IN E. COLI* Purdue University Graduate School].

Wu, R., Bakelar, J. W., Lundquist, K., Zhang, Z., Kuo, K. M., Ryoo, D., Pang, Y. T., Sun, C., White, T., & Klose, T. (2021). Plasticity within the barrel domain of BamA mediates a hybrid-barrel mechanism by BAM. *Nature communications*, *12*(1), 7131.

Wu, T., Malinverni, J., Ruiz, N., Kim, S., Silhavy, T. J., & Kahne, D. (2005). Identification of a multicomponent complex required for outer membrane biogenesis in Escherichia coli. *Cell*, *121*(2), 235-245.

Xu, X., Zhang, H., Huang, Y., Zhang, Y., Wu, C., Gao, P., Teng, Z., Luo, X., Peng, X., & Wang, X. (2019). Beyond a ribosomal RNA methyltransferase, the wider role of MraW in DNA methylation, motility and colonization in Escherichia coli O157: H7. *Frontiers in microbiology*, *10*, 2520.

Yang, D. C., Tan, K., Joachimiak, A., & Bernhardt, T. G. (2012). A conformational switch controls cell wall-remodelling enzymes required for bacterial cell division. *Molecular microbiology*, *85*(4), 768-781.

Yao, X., Jericho, M., Pink, D., & Beveridge, T. (1999). Thickness and elasticity of gram-negative murein sacculi measured by atomic force microscopy. *Journal of bacteriology*, *181*(22), 6865-6875.

Yeats, C., & Bateman, A. (2003). The BON domain: a putative membrane-binding domain. *Trends in biochemical sciences*, *28*(7), 352-355.

Zervosen, A., Lu, W. P., Chen, Z., White, R. E., Demuth, T. P., Jr., & Frere, J. M. (2004). Interactions between penicillin-binding proteins (PBPs) and two novel classes of PBP inhibitors, arylalkylidene

rhodanines and arylalkylidene iminothiazolidin-4-ones. *Antimicrob Agents Chemother*, *48*(3), 961-969.

Zhou, R., Chen, S., & Recsei, P. (1988). A dye release assay for determination of lysostaphin activity. *Analytical biochemistry*, *171*(1), 141-144.

Appendix.

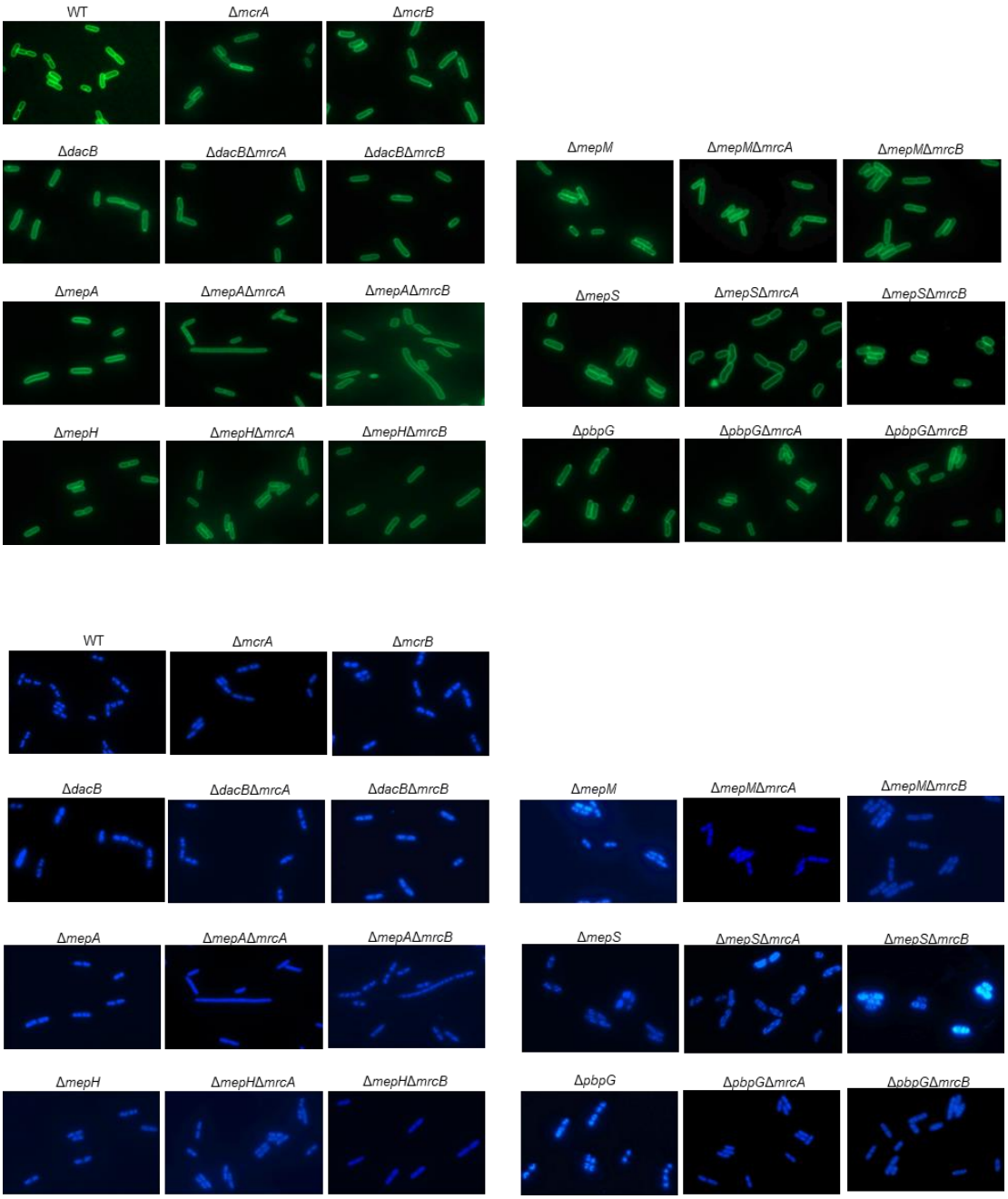

Figure ①. Absence of EPases DacB, MepM, MepA, MepS, MepH and PbpG and amidases/regulators AmiA, AmiB, AmiC, NlpD and EnvC on Δ*mrcA* and Δ*mrcB* cells causes mild changes on morphology. Fluorescence microscopy of the WT, Δ*mrcA,* Δ*mrcB,* Δ*dacB,* Δ*dacB*Δ*mrcA,* Δ*dacB*Δ*mrcB,* Δ*mepM,* Δ*mepM*Δ*mrcA,* Δ*mepM*Δ*mrcB,* Δ*mepA,* Δ*mepA*Δ*mrcA,* Δ*mepA*Δ*mrcB,* Δ*mepS,* Δ*mepS*Δ*mrcA,* Δ*mepS*Δ*mrcB,* Δ*mepH,* Δ*mepH*Δ*mrcA,* Δ*mepH*Δ*mrcB,* Δ*pbpG,* Δ*pbpG*Δ*mrcA* and Δ*pbpG*Δ*mrcB* cells. Cells were grown to mid-exponential phase (OD600 = 0.4) in LB at 37°C, stained with the membrane dye FM1-43-FX (A), fixed, and stained with DAPI (B). The cells were visualised by fluorescence microscopy.

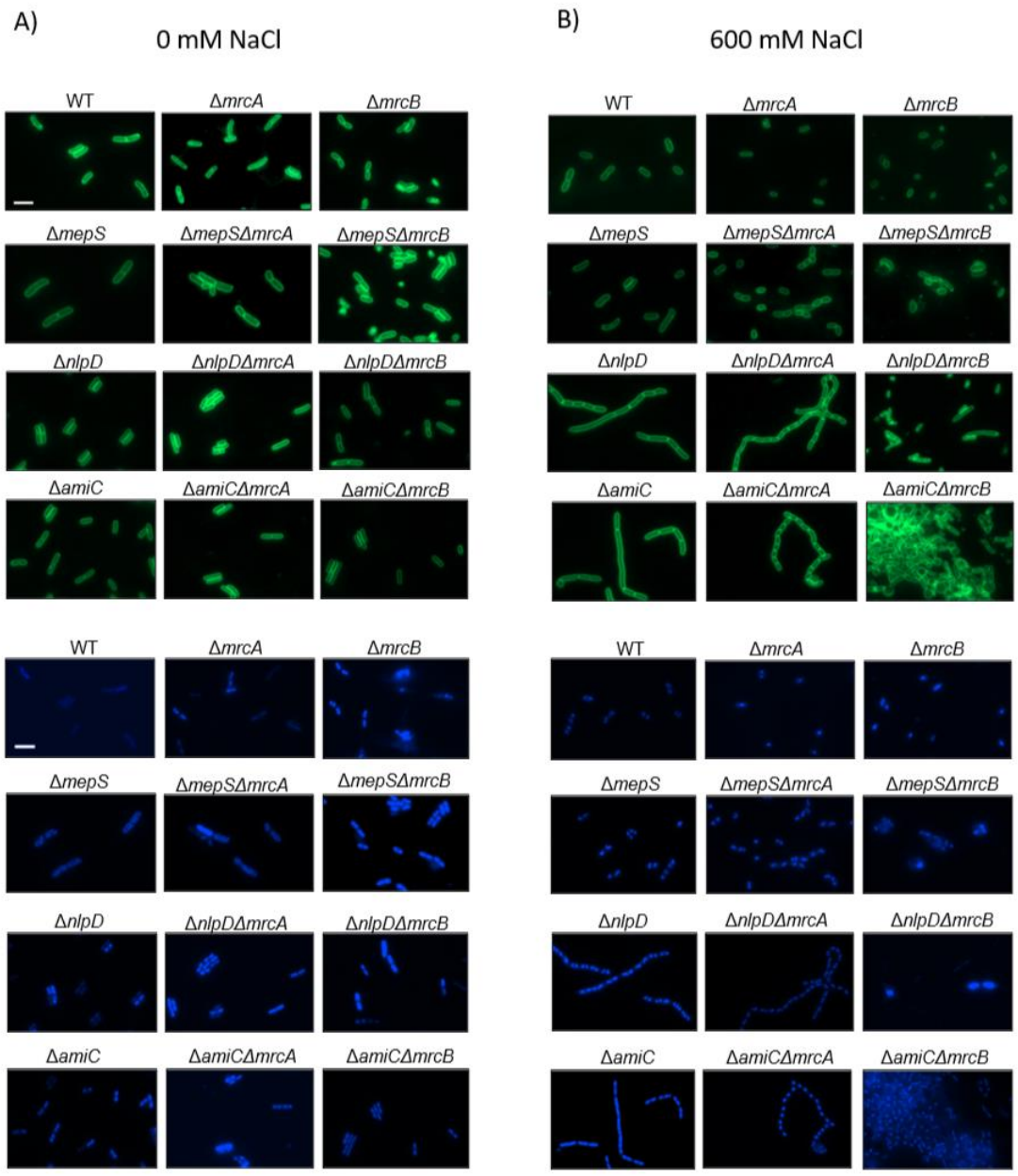

Figure ②. Fluorescence microscopy of WT, *ΔmrcA, ΔmrcB, ΔmepS, ΔnlpD, ΔamiC* and respective *ΔmrcA and ΔmrcB* double mutants cells. The cell cultures were grown at 37°C in LB medium to early exponential phase (OD600=~0.2), back-diluted to media altered with A 0 mM NaCl or B 600 mM NaCl and grown until OD600=~0.2, stained with the membrane dye FM1-43-FX, fixed, and stained with DAPI. The cells were visualised by fluorescence microscopy. Scale bar = 5 µm.

Table 6. Phenotypes of *mrcA*, *mrcB*, amidases and regulators mutants in LB with 600 mM or 0 mM NaCl.

Condition	Relevant genotype	Total cells[1]	No. of viable cells[2]	Avg length (µm)[4]	Avg width (µm)[6]	Length/ septum (µm)[8]	Length/ segment (µm)[9]	No. of septa/cell[10]	No. of chaining cells[11]	% of chaining cells[12]
600 mM NaCl										
	WT	315	315	3.5 ± 1.3	1.10 ± 0.2	8.8	2.5	0.4	10	3.2
	Δ*mrcA*	357	357	2.2 ± 0.8	0.97 ± 0.3	13.0	1.9	0.2	26	7.3
	Δ*mrcB*	501	421	2.8 ± 0.8	1.16 ± 0.2	6.6	2.0	0.4	102	24.2
	Δ*amiA*	413	413	8.7 ± 7.5	0.99 ± 0.2	5.8	3.5	1.5	102	24.7
	Δ*amiA*Δ*mrcA*	413	197	8.6 ± 6.5	0.95 ± 0.1	3.9	2.7	2.2	168	85.3
	Δ*amiA*Δ*mrcB*	ND	ND	ND	ND	ND	ND	ND	ND	ND
	Δ*amiB*	469	469	6.2 ± 4.2	0.98 ± 0.1	5.9	3.0	1.1	100	21.3
	Δ*amiB*Δ*mrcA*	323	323	5.1 ± 2.8	0.99 ± 0.1	4.9	2.5	1.0	220	68.1
	Δ*amiB*Δ*mrcB*	ND	ND	ND	ND	ND	ND	ND	ND	ND
	Δ*amiC*	258	258	12.2 ± 8.5	1.01 ± 0.1	5.9	4.0	2.1	127	49.2
	Δ*amiC*Δ*mrcA*	160	131	10.0 ± 6.5	0.95 ± 0.3	3.0	2.3	3.4	126	96.2
	Δ*amiC*Δ*mrcB*	ND	ND	ND	ND	ND	ND	ND	ND	ND
	Δ*envC*	130	130	16.8 ± 13.9	1.12 ± 0.6	4.7	3.7	3.6	78	60
	Δ*envC*Δ*mrcA*	105	105	20.2 ± 13.1	1.05 ± 0.9	3.3	2.8	6.1	94	89.5
	Δ*envC*Δ*mrcB*	ND	ND	ND	ND	ND	ND	ND	ND	ND
	Δ*nlpD*	165	165	15.7 ± 12.1	0.99 ± 0.1	4.6	3.5	3.4	108	65.5
	Δ*nlpD*Δ*mrcA*	108	108	16.2 ± 9.5	1.06 ± 0.7	2.8	2.4	5.7	103	95.4
	Δ*nlpD*Δ*mrcB*	ND	ND	ND	ND	ND	ND	ND	ND	ND
0 mM NaCl										
	WT	288	288	4.2 ± 1.3	0.99 ± 0.2	7.98	2.76	0.53	4	1.4
	Δ*mrcA*	458	458	3.93 ± 1.2	0.94 ± 0.2	8.22	2.66	0.48	9	2.0
	Δ*mrcB*	346	298	3.79 ± 0.9	1.00 ± 0.1	7.33	2.50	0.52	4	1.3
	Δ*amiA*	499	499	4.5 ± 1.2	0.94 ± 0.1	7.4	2.8	0.6	0	0
	Δ*amiA*Δ*mrcA*	484	484	4.4 ± 1.4	0.89 ± 0.1	7.8	2.8	0.6	5	1.0
	Δ*amiA*Δ*mrcB*	234	234	4.8 ± 1.2	0.92 ± 0.1	7.1	2.9	0.7	12	5.1
	Δ*amiB*	404	404	3.7 ± 0.9	0.98 ± 0.1	7.9	2.5	0.5	0	0
	Δ*amiB*Δ*mrcA*	401	401	3.5 ± 1.0	0.92 ±0.1	9.0	2.5	0.4	1	0.2
	Δ*amiB*Δ*mrcB*	653	492	3.8 ± 1.4	0.98 ± 0.1	8.0	2.6	0.5	4	0.8
	Δ*amiC*	284	284	3.9 ± 1.1	0.96 ± 0.1	8.4	2.7	0.5	0	0
	Δ*amiC*Δ*mrcA*	269	269	3.7 ± 0.9	0.92 ± 0.1	7.2	2.5	0.5	0	0
	Δ*amiC*Δ*mrcB*	398	398	4.0 ± 1.1	0.96 ± 0.1	6.3	2.4	0.6	27	6.8
	Δ*envC*	234	234	7.7 ± 4.7	0.93 ± 0.1	5.9	3.3	1.3	57	24.4
	Δ*envC*Δ*mrcA*	202	202	7.6 ± 4.3	0.89 ± 0.1	6.2	3.4	1.2	54	26.7
	Δ*envC*Δ*mrcB*	ND	ND	ND	ND	ND	ND	ND	ND	ND
	Δ*nlpD*	317	317	4.0 ± 1.0	0.95 ± 0.1	7.2	2.6	0.5	0	0
	Δ*nlpD*Δ*mrcA*	223	223	3.8 ± 0.9	0.89 ± 0.1	7.7	2.5	0.5	5	2.2
	Δ*nlpD*Δ*mrcB*	429	389	4.6 ± 1.9	0.98 ± 0.1	7.2	2.8	0.6	8	2.1

1. Total number refers to the sum of viable cells and lysed cells.
2. Viable cells were considered non-lysed cells.
3. Total length means cumulative length of all cells measured.
4. Refers to the total length/number of cells.
5. Total width means cumulative width of all cells measured.
6. Refers to the total width/number of cells.
7. Cells longer than 5 µm are considered filaments.
8. Percentage of filaments related to the total number of cells.

Publications.

Duo to COVID-19 pandemic and my pregnancy, I could not participate in more projects.

- Boelter G, Bryant JA, Doherty H, Wotherspoon P, Alodaini D, Ma X, Alao MB, Moynihan PJ, Moradigaravand D, Glinkowska M, Knowles TJ, Henderson IR, Banzhaf M. The lipoprotein DolP affects cell separation in Escherichia coli, but not as an upstream regulator of NlpD. Microbiology. 2022; 168.

- Bryant, J. A., Morris, F. C., Knowles, T. J., Maderbocus, R., Heinz, E., Boelter, G., Alodaini, D... & Henderson, I. R. (2020). Structure of dual BON-domain protein DolP identifies phospholipid binding as a new mechanism for protein localisation. *Elife*, *9*, e62614.